Master Thesis

Master's degree in Automatic Control and Robotics

FPGA-based control of fuel-cell based energy management systems

REPORT

Autor: Luis Romero Ben
Director: Ramón Costa Castelló
Convocatòria: 07/2018

Escola Tècnica Superior
d'Enginyeria Industrial de Barcelona

Abstract

For years, several researchers all over the world have been working on the study and development of alternative energetic sources which do not depend on fossil fuels like oil or coal.
Numerous options have arisen to replace them: wind, solar, hydraulic, biomass... One of the renewable energy sources which is making remarkable steps among the others is the fuel cells. They convert chemical energy directly to electric energy, by using CO and H_2, so one of its most interesting point is the utilization this hydrogen as fuel, due to its abundance. Indeed, fuel cells have been used in the space race for more than 40 years [25].
However, they are not such extended at their usage in Earth, because their efficiency is limited. This is the main reason why it is important to research about fuel cells, enhancing their capabilities, effectiveness and durability, as well as studying the electronic circuits employed to make the most of the energy obtained from the cells.
In this project, one of the most extended kinds of fuel cells, the Proton-Exchange-Membrane Fuel Cells or PEMFCs, is considered and a new control design is developed for the DC-DC converters that allow to manage the voltage at a DC bus, as well as other involved electrical variables; together with a bank of supercapacitors which provides energy to compensate fast changes in the bus current due to disturbances, optimizing the PEMFC usage and hence lengthening its lifetime. Therefore, by controlling the voltage at the bus and at the supercapacitors, the system effectiveness can be increased, fulfilling the initial objective.
These controllers, alongside others necessary for the utilized control structure, have been successfully designed and validated in simulation, from simple models to more complex ones whose resemblance to the real system is quite high. They have been also tested into the real plant, achieving quite good results.
By persevering in the research of new clean energies and the enhancement of the existing ones, in the future, the current dependency on fossil fuels will be seen as a mistake from the past.

Contents

ETSEIB

List of Figures

ETSEIB

List of Tables

Chapter 1

Introduction

This project consist in the design, validation in simulation and, as far as it is possible, validation in the real plant, of a complete control system for the management of a energy production station based on hydrogen-based Proton-Exchange Membrane Fuel Cells [17] (PEM Fuel Cells or PEMFCs). These devices generate electrical current from chemical reactions between air and hydrogen. The energy produced in this process needs to be transformed for its usage, and the conditions for this reconditioning come from the current inputs or outputs that affect the system. In the system studied for this project, there is a DC bus, which receives external current or it is requested to supply it. Apart from the PEMFCs, there is a supercapacitors set too, which when charged can provide part of this requested current, and when there is a input flow of current on the bus, they are able to use this extra current to get charged. These capacitors have a huge capacitance value, allowing to stabilize currents and voltages.

1.1 Project objectives

The objective of the project is, therefore, achieve a control system capable of maintaining a approximately constant voltage at the DC bus by managing the PWM signals that feed the two DC-DC converters.
This main aim can be splitted into different subobjectives:

- Management of the current at the PEMFC subsystem by controlling its corresponding DC-DC converter.
- Handling of the current at the supercapacitors subsystem by controlling its corresponding DC-DC converter.

- Control of the bus voltage by means of the previous currents

A second objective would be to include a control over the supercapacitors voltage, so that the charge of these capacitors could be managed in function of the necessities of the system at each moment.

1.2 Project scope

Regarding the scope of the project, the control system will be designed and validated by using MATLAB® and Simulink®, and as far as it is possible, the achieved controllers will be implemented in the real system by programming the FPGA which governs the system management.
In this way, the different chapters of this project arise naturally, starting with a presentation of the previous work in the PEMFC control field at Chapter 2; continuing with the analysis and control of the PEMFC and supercapactitors subsystems at Chapters 3 and 4 respectively; and ending the technical development of the project with the analysis and control of the complete model in Chapter 5, as well as the real system implementation in Chapter 6.
To finish the project, a report of the scheduling and planning for the different tasks is presented in Chapter 7; a budget about the project realization is provided at Chapter 8; and the impact in the environment of this realization is presented in Chapter 9.

Chapter 2

State-of-the-art

The control and management of the energy produced by PEMFCs has been widely studied through the years.

There are interesting works like [38] and [27], covering the analysis and control of hybrid systems in an extensive way, being useful to achieve a proper insight about these kind of systems, their capabilities, limitations...

It is also worth to mention the project of [28], as it consisted in a base for the work carried out in my project, that is, the working methodology of this work has been employed as a reference in the field of the power electronics and PEMFCs, although new control approaches and strategies have been employed to develop the whole project.

2.1 Hardware settings

Among the most part of the literature related to PEMFCs, similar hybrid stations are used to test the designed control strategies.

Regarding the previously mentioned works, all of them employ a system based on the Nexa^{TM} Power Module, which generates unregulated DC power from air and hydrogen. There is one located at the IRI (Institut de Robòtica Industrial). Its main scheme is presented in Figure 2.1. In this hybrid station, two DC-DC converters are employed to control the systems described in the introductory chapter. A general overview of the system to study can be found in Figure 2.2: Those PEMFCs produce a unidirectional current, reconditioned in the first DC-DC converter, so that the current is compatible with the DC bus. In the same way, the current provided by or addressed to the supercapacitors would be processed by the second DC-DC converter, with the

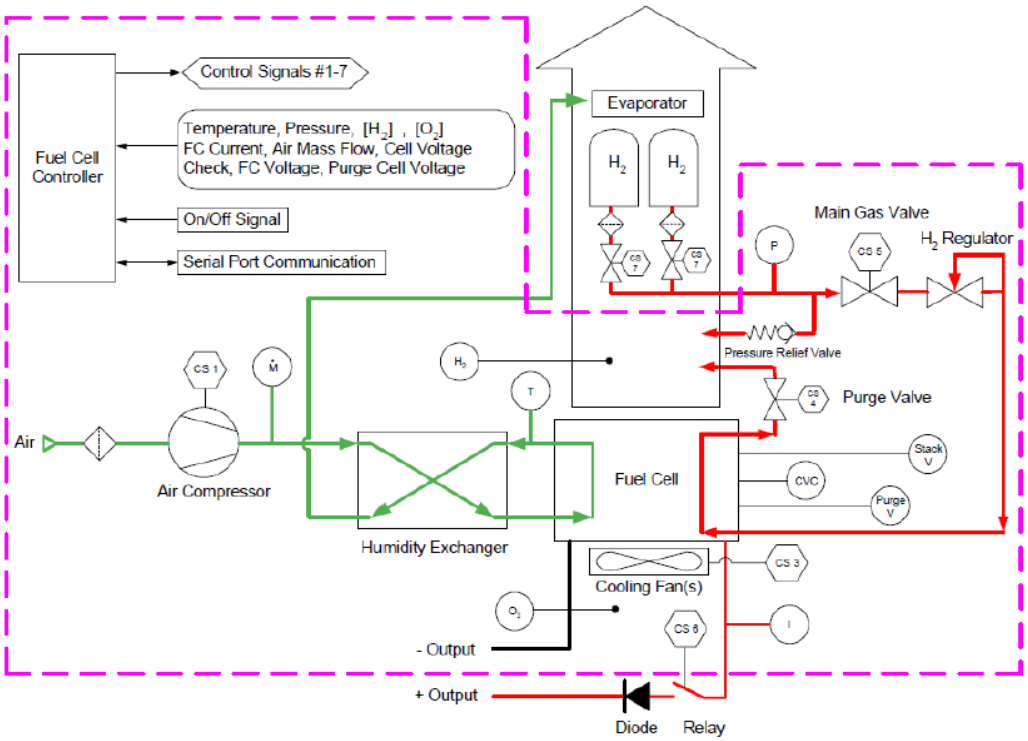

Figure 2.1: Nexa^{TM} Power Module [18]

same aim than the first case. Moreover, external current sinks or sources can demand or supply current to the system, so these outlet or inlet currents effects need to be managed.

2.2 Control methodology

Regarding the control strategies employed to manage the system in question, several different approaches have been studied during the years.

Some like [38] or [28] employs classical control structures (PIs or PIDs in the case of the second) to manage the hybrid energy system control requirements.

There are more advanced methods implemented, as it can be found at [27], due to its usage of a set of different techniques as sliding control or MIMO control designs, among others; and at [22], in which MPC, NNC or fuzzy logic control are reviewed.

In my project, all the designs have been carried out by using a state-feedback approach, alongside different robust control techniques, as Linear Parameters Varying (LPV) [33], quadratic Schur stabilization problem for discrete LMIs [23]...

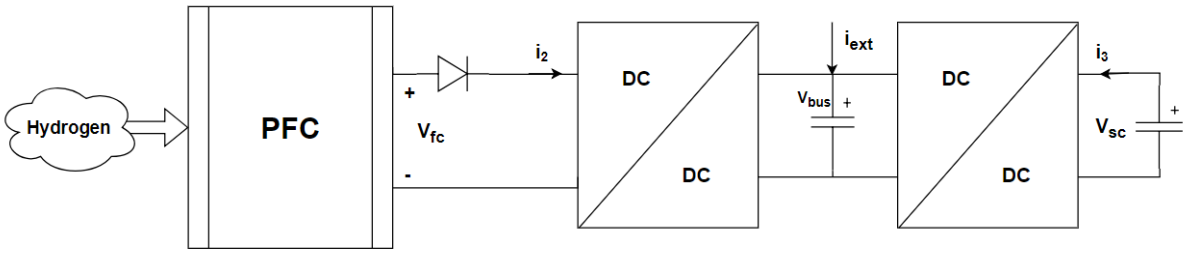

Figure 2.2: Complete system schematic diagram

Before entering the explanation of the different controllers individually, it is important to provide the reasons for selecting the control structure (for example, [28] employs a similar one). This will be done by carrying out a brief but clarifying analysis of the steady-state behaviour of the system while controlled. This means that the suppositions at Equation 2.1 are made.

$$\begin{cases} i_2 \approx i_2^{ref} \\ i_3 \approx i_3^{ref} \\ V_{bus} \approx V_{bus}^{ref} \end{cases} \tag{2.1}$$

It is also necessary to keep in mind that the currents values are different at the bus side than at their respective sources. This is represented with the approximations made at Equation 2.2

$$\begin{cases} V_{bus} i_2^{bus} \approx V_{fc} i_2 \\ V_{bus} i_3^{bus} \approx V_{sc} i_3 \end{cases} \tag{2.2}$$

From the detailed representation of the bus related variables at Figure 2.3 (extracted from Figure 2.2), and using the first Kirchhoff law about the currents at a node, Equation 2.3 is achieved:

$$i_2^{ref^{bus}} + i_3^{ref^{bus}} + i_{ext} = i_{bus} \tag{2.3}$$

And transforming it by using Equation 2.2, the expression leads to Equation 2.4:

$$\frac{V_{fc}}{V_{bus}} i_2^{ref} + \frac{V_{sc}}{V_{bus}} i_3^{ref} + i_{ext} = i_{bus} \tag{2.4}$$

Finally, manipulating it, Equation 2.5 is achieved:

$$V_{fc}i_2^{ref} + V_{sc}i_3^{ref} = V_{bus}(i_{bus} - i_{ext}) \tag{2.5}$$

Hence, from this expression, regarding that the i_{ext} comes from external sources (it is supposed that we don't manage them) and i_{bus} is the result whose value will determine the bus voltage, which is our control goal, it becomes clearer why by controlling i_2 and i_3 in a proper manner, the value of V_{bus} can be controlled. This is the reason for using a control loop for the bus voltage which generates the references for both currents control structures.

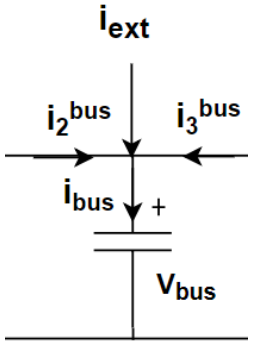

Figure 2.3: Detailed representation of the bus variables

Regarding V_{fc} and V_{sc}, which are also present in Equation 2.5, their value is also measured, so the designed control structure will take them into account for the managing of the control variables.

Alongside with the V_{bus} control system, a new feature with respect to other works like [28] is the inclusion of a way to have some control over the supercapacitors voltage.

By using the formula of the current passing through a capacitor and applying it to the supercapacitors at the right side of Figure 2.2 (we are still developing a steady-state analysis), the expression at Equation 2.6 is obtained:

$$\frac{dV_{sc}}{dt} = -\frac{i_3^{ref}}{C_{sc}} \tag{2.6}$$

From this equation, it results that to manage the voltage at the supercapacitors, it would be necessary to control i_3 in a certain manner, which does not need to be the same way than the one for controlling the bus voltage. Hence, it is understood why V_{bus} and V_{sc} can not be controlled without making a trade-off.

To handle this situation, both control structures are computed simultaneously, getting two different values for the reference of the current, and the final setpoint value provided to the current control system is a proportion of these two references, managing the distribution using a value called α.

At Chapter 5, it will be explained that only one current reference value is computed for both i_2

and i_3 from the V_{bus} control system (it is divided into the PEMFC and supercapacitor subsystems by means of filters), so the previous distribution operation would be the one represented by Equation 2.7:

$$i^{ref} = \alpha i^{ref}_{V_{bus}} + (1 - \alpha) i^{ref}_{V_{sc}}. \tag{2.7}$$

Chapter 3

PEMFC DC-DC Converter analysis and control design

3.1 Subsystem description

The first case study is carried out about the converter which connects the PEM fuel cell, or PEMFC, and the DC bus; so that a control system is designed to be capable of obtaining the necessary current from the PEMFC to feed the payload.
Regarding this, the electrical circuit is studied and analysed to understand the dynamics that it presents, obtaining the dynamical equations which represent the behaviour of the system.
Moreover, a preliminary study about the system performance is carried out, so that different insights for the controller design are achieved.
A simplified diagram of the PEMFC subsystem can be found in Figure 3.1.
The electrical variables involved in this circuit are the following:

- $\boldsymbol{i_1}$ → current at the first inductor.
- $\boldsymbol{i_2}$ → current at the second inductor.
- $\boldsymbol{i_c}$ → current at the capacitor.
- $\boldsymbol{V_{L1}}$ → voltage at the second inductor.
- $\boldsymbol{V_{L2}}$ → voltage at the first inductor.
- $\boldsymbol{V_1}$ → voltage at the capacitor.
- $\boldsymbol{V_{fc}}$ → voltage of the PEMFC.
- $\boldsymbol{V_{bus}}$ → voltage at the bus.
- $\boldsymbol{V_{u1}}$ → voltage of the IGBT, and also the control variable.

Regarding the electrical parameters, their values are shown in Table 3.1.

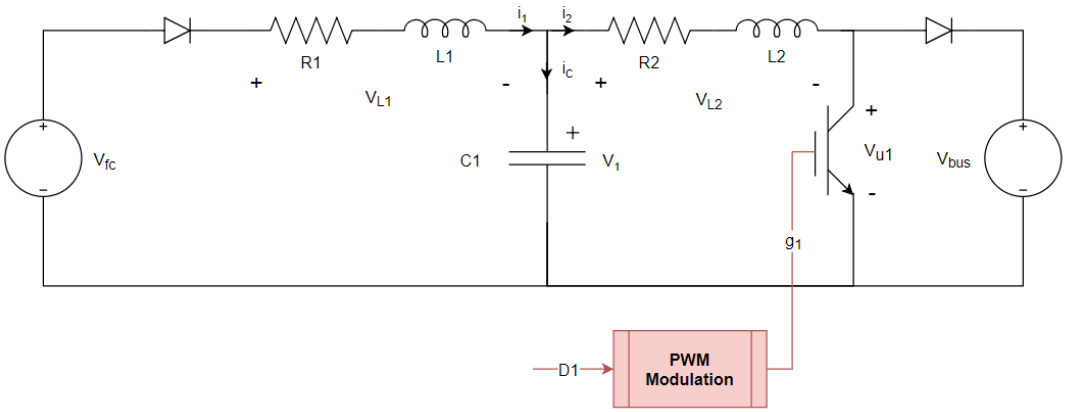

Figure 3.1: PEMFC subsystem electrical diagram

Parameter	Value	Units
L_1	140	μH
L_2	34.3	μH
R_2	0	Ω
R_2	0.0426	Ω
C_1	2200	μF

Table 3.1: PEMFC subsystem electrical components parameters

About other considerations which must be taken into account:

- The IGBT transistor used at the laboratory is the SEMiX 251GD126HDs [31], alongside the SKHI 20opA driver [32] and the SEMISTACK - IGBT three-phase inverter [30].
- The voltages of the PEMFC and bus have been fixed for this tests to their nominal values, 32.5 V and 80 V respectively, as the desired behaviour for the system consists in maintaining these values as constant as possible.
- The resistors located in series with the inductors are parasitic and must be taken into account.
- The transistor is controlled using PWM modulation [20].

Analysis of the dynamical system

From the circuit at Figure 3.1, applying the Kirchoff laws, the following system of equations is derived:

$$\begin{cases} V_{L_1} = V_{fc} - V_1 \\ V_{L_2} = V_1 - V_{u1} \\ i_c = i_1 - i_2 \end{cases} \tag{3.1}$$

Employing the equations of the voltage at an inductor, and the current of a capacitor; as well as splitting V_{L1} and V_{L2} into the voltage at the inductor and resistor, the system can be transformed into:

$$\begin{cases} L_1 \frac{di_1}{dt} + R_1 i_1 = V_{fc} - V_1 \\ L_2 \frac{di_2}{dt} + R_2 i_2 = V_1 - V_{u1} \\ C_1 \frac{dV_1}{dt} = i_1 - i_2 \end{cases} \tag{3.2}$$

This dynamical system will be used later to obtain the state-space model that represents the system behaviour.

Considering an ideal transistor, the IGBT voltage V_{u1} can be modelled as:

$$V_{u1} = (1 - D_1) V_{bus} \tag{3.3}$$

The importance of the value of D_1 can be observed by carrying out a simulation in Simulink®, so that the electrical circuit showed at Figure 3.1 must be converted to a block diagram at this software:

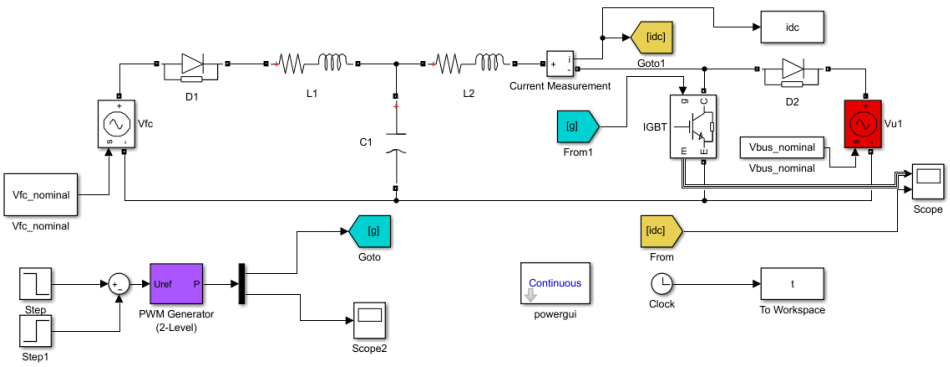

Figure 3.2: PEMFC subsystem

The input profile used to feed the PWM consists of a first section in which the value of D_1 is 1, that is to have the transistor always in conduction mode; then it is reduced to 0.6, so that the IGBT is conducting the current a 60 % of the time, and then it is reduced to 0, so that the transistor is always in cut-off mode. The response of the system can be found in Figure 3.3.

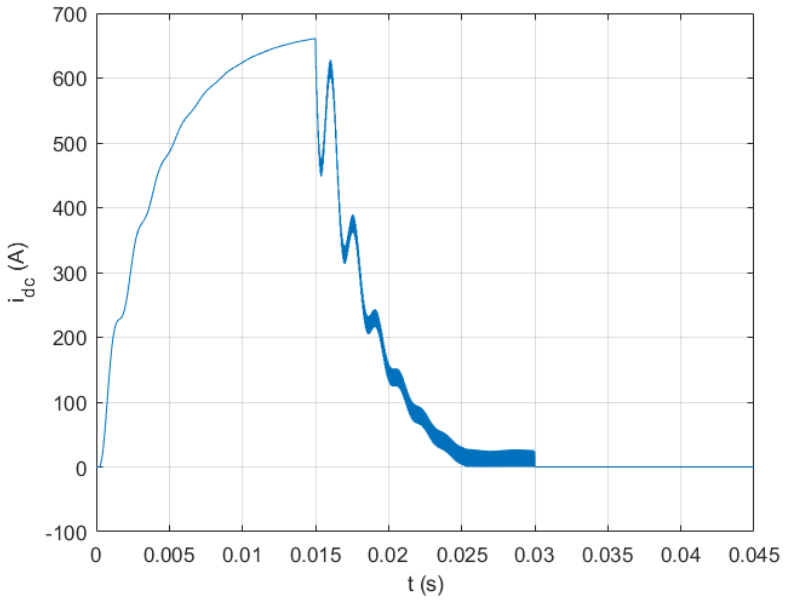

Figure 3.3: i_2 response ($t \in [0, 0.015) \rightarrow D_1 = 1$, $t \in [0.015, 0.03) \rightarrow D_1 = 0.6$, $t \in [0.03, 0.045) \rightarrow D_1 = 0$)

This result was expectable if the system equations are analysed. From Equation 3.2, by adding the first two equations and neglecting the parasitic resistances for the analysis, the following is obtained:

$$L_1 \frac{di_1}{dt} + L_2 \frac{di_2}{dt} = V_{fc} - (1 - D_1) V_{bus} \tag{3.4}$$

When $D_1 = 1$, the sum of both derivatives of the currents is positive, so they will grow until the equilibrium value of the maximum energy in the system is reached. When $D_1 = 0.6$ (every value between 0 and 1 is valid for this explanation), the transistor is commuting, the current is decreasing its value until it reaches an equilibrium point. Finally, when $D_1 = 0$, again from the equation it is observed how the derivative of the current becomes negative, so the current is decreased until its value is 0.

3.2 Control system design

3.2.1 State-space model generation

For the design of state feedback [36] controllers/observers, first, the system state-space model is needed, so that its matrices become available. Besides, this state-space model must be transformed from a continuous-time form to discrete-time one, so that the resultant controllers are directly and easily implemented in a real application.
From Equation 3.2, the system physical equations are:

$$\begin{cases} L_1 \frac{di_1}{dt} + R_1 i_1 = V_{fc} - V_1 \\ L_2 \frac{di_2}{dt} + R_2 i_2 = V_1 - V_{u1} \\ C_1 \frac{dV_1}{dt} = i_1 - i_2 \end{cases} \tag{3.5}$$

For the control design, this system will be manipulated. Two variable changes are carried out:

- A new variable V' is created as $V' = V_{fc} - V_{u1}$, so that the term V_{u1} disappears from the equations. Hence, the input of the state-space model will be V' (see Equation 3.6).

$$\begin{cases} L_1 \frac{di_1}{dt} + R_1 i_1 = V_{fc} - V_1 \\ L_2 \frac{di_2}{dt} + R_2 i_2 = V_1 - V_{fc} + V' \\ C_1 \frac{dV_1}{dt} = i_1 - i_2 \end{cases} \tag{3.6}$$

- Finally, another variable V_{dif} is generated as $V_{dif} = V_{fc} - V_1$. This is carried out because the constant term V_{fc} (it is supposed to be constant for the design) must not be present to generate a suitable state-space representation. Using this change, the state variable V_1 also disappears from the equations, and it is substituted as state variable by V_{dif}.

$$\begin{cases} L_1 \frac{di_1}{dt} + R_1 i_1 = V_{dif} \\ L_2 \frac{di_2}{dt} + R_2 i_2 = V' - V_{dif} \\ C_1 \frac{d(V_{fc} - V_{dif})}{dt} = C_1 \cancelto{0}{\frac{dV_{fc}}{dt}} - C_1 \frac{dV_{dif}}{dt} = i_1 - i_2 \end{cases} \tag{3.7}$$

  As the voltage at the PEMFC is supposed to be constant, its derivative can be neglected from Equation 3.7.

These two variable changes produce the system at Equation 3.8, which has the suitable form to be translated into a state-space model.

$$\begin{cases} L_1 \frac{di_1}{dt} + R_1 i_1 = V_{dif} \\ L_2 \frac{di_2}{dt} + R_2 i_2 = V' - V_{dif} \\ -C \frac{dV_{dif}}{dt} = i_1 - i_2 \end{cases} \tag{3.8}$$

From this system of equations, the continuous state-space model [29] at Equation 3.9 and 3.10 can be extracted (considering that the system output y is i_2):

$$\begin{bmatrix} \dot{i_2} \\ \dot{i_1} \\ \dot{V_{dif}} \end{bmatrix} = \underbrace{\begin{bmatrix} -R_2/L_2 & 0 & -1/L_2 \\ 0 & 0 & 1/L_1 \\ 1/C_1 & -1/C_1 & 0 \end{bmatrix}}_{A_1} \begin{bmatrix} i_2 \\ i_1 \\ V_{dif} \end{bmatrix} + \underbrace{\begin{bmatrix} 1/L_2 \\ 0 \\ 0 \end{bmatrix}}_{B_1} V' \tag{3.9}$$

$$y = \underbrace{\begin{bmatrix} 1 & 0 & 0 \end{bmatrix}}_{C_1} \begin{bmatrix} i_2 \\ i_1 \\ V_{dif} \end{bmatrix} + \underbrace{\begin{bmatrix} 0 \end{bmatrix}}_{D_1} V' \tag{3.10}$$

By discretizing the continuous-time model, the corresponding discrete state-space model (for a sample time of 0.05 ms) is derived using the Forward-Euler [39] approach ($\dot{x} = \frac{x_{k+1} - x_k}{T_s}$). This discretization technique is chosen over others due to its simplicity and because it carries out a linear transformation of the continuous system, so it gets easier to deal with parametric uncertainties (for example, if a exact discretization had been selected, the exponential term would have increased the difficulty to work with this kind of uncertainties).

The discrete state-space model is conformed by Equation 3.11 and Equation 3.12.

$$\begin{bmatrix} i_{2_{k+1}} \\ i_{1_{k+1}} \\ V_{dif_{k+1}} \end{bmatrix} = \underbrace{\begin{bmatrix} 1 - Ts \cdot R_2/L_2 & 0 & -Ts/L_2 \\ 0 & 1 & Ts/L_1 \\ Ts/C_1 & -Ts/C_1 & 1 \end{bmatrix}}_{A_{k1}} \begin{bmatrix} i_{2_k} \\ i_{1_k} \\ V_{dif_k} \end{bmatrix} + \underbrace{\begin{bmatrix} Ts/L_2 \\ 0 \\ 0 \end{bmatrix}}_{B_{k1}} V'_k \tag{3.11}$$

$$y_k = \underbrace{\begin{bmatrix} 1 & 0 & 0 \end{bmatrix}}_{C_{k1}} \begin{bmatrix} i_{2_k} \\ i_{1_k} \\ V_{dif_k} \end{bmatrix} + \underbrace{\begin{bmatrix} 0 \end{bmatrix}}_{D_{k1}} V'_k \tag{3.12}$$

3.2.2 Controller design

Theoretical framework

Once the state-space matrices of the model are obtained, a LMI [19] approach can be utilized to derive a state-feedback controller capable of making the system output follow the provided reference (with null steady-state error for the linear system).
It is demonstrated that, for a given discrete state-space model of the following form:

$$x_{k+1} = Ax_k + Bu_k \tag{3.13}$$

A state feedback controller is $u_k = Kx_k$ (taking care of the sign of the controller gain K), so that the closed-loop system becomes:

$$x_{k+1} = Ax_k + BKx_k = (A + BK)x_k \tag{3.14}$$

As it is a linear system, a Lyapunov function can have the form $V(x_K) = \frac{1}{2}x_k^T P x_k > 0$, where P is a symmetric positive definite matrix. The discrete derivative of this expression leads to:

$$\Delta V(x_k) = x_k^T[(K^T B^T + A^T)P(A + BK) - P]x_k \tag{3.15}$$

Reaching the conclusion that, for the closed-loop system to be stable, the following inequalities must hold:

$$\begin{aligned} &(K^T B^T + A^T)P(A + BK) - P < 0 \\ &P > 0 \end{aligned} \tag{3.16}$$

However, the LMI formed by these two equations is a non-linear problem, as it must be solved for P and K. Manipulating the inequalities and doing some variable changes, a solution to the problem can be reached for the following LMI:

$$\begin{bmatrix} -P & AP+BW \\ PA^T+W^TB^T & -P \end{bmatrix} < 0 \tag{3.17}$$

And as the realized variable change is $W = KP$, the controller gain K can be found as $K = WP^{-1}$.

For the design of our controller, a $\mathbb{D}$-stabilization problem of the following form will be solved alongside the previous LMI:

$$\mathbb{D}_{q,r} = \{x + jy | (x-q)^2 + y^2 < r^2\} \tag{3.18}$$

So that the discrete closed-loop poles of the controlled system can be assured to be placed inside a circle of radius r and center q, leading after some derivations (similar to the previous ones) to the following LMI:

$$\begin{bmatrix} -rP & qP+AP+BW \\ qP+PA^T+W^TB^T & -rP \end{bmatrix} < 0 \tag{3.19}$$

Regarding that also $P > 0$, the solution for K can be found in the same way than before.

Moreover, so that our control system is assured to deal with uncertainties (in a defined range or interval) at the system parameters (mainly resistance, capacitance and inductance values), the problem is treated as a case of quadratic Schur stabilization for interval systems, and the uncertainties are defined as:

$$\Delta_I = \{\delta_k | \delta_{i_k} \in [\delta_{i_k}^-, \delta_{i_k}^+], \quad i = 1, 2, ..., n\} \tag{3.20}$$

Considering this, and that these uncertainties affect the A and B state-space matrices, it is demonstrated in [23] that the quadratic Schur stabilization problem has a solution regarding that there exists a symmetric matrix P and another matrix W satisfying the next set of LMIs (here, the aforementioned $\mathbb{D}$-stabilization is also included):

$$\begin{bmatrix} -rP & qP+A(\delta_k)P+B(\delta_k)W \\ qP+PA(\delta_k)^T+W^TB(\delta_k)^T & -rP \end{bmatrix} < 0, \quad \delta_{i_k} = \delta_{i_k}^- or \delta_{i_k}^+ \tag{3.21}$$

And again, regarding that $P > 0$, the controller gain K can be obtained.
Finally, as state feedback will be used as control technique, to follow the proper reference, a transformation from the output to the reference units is necessary, and it is fulfilled using the k^*, obtained as the inverse steady-state gain of the closed-loop system:

$$k^* = (-C[A - BK]^{-1}B + D)^{-1} \tag{3.22}$$

Application to design

For the case of the PEMFC subsystem, recalling Equation 3.11 (there is only uncertainty in A and B), and regarding the considered uncertainty (Equation 3.20), the matrices can be expressed as in Equation 3.23 (R_1 is not neglected as in previous sections for the treatment of uncertainty).

$$A_{k1} = \begin{bmatrix} 1 - Ts \cdot \frac{R_2+\delta_{R_2}}{L_2+\delta_{L_2}} & 0 & -\frac{Ts}{L_2+\delta_{L_2}} \\ 0 & 1 - Ts \cdot \frac{R_1+\delta_{R_1}}{L_1+\delta_{L_1}} & \frac{Ts}{L_1+\delta_{L_1}} \\ \frac{Ts}{C_1+\delta_{C_1}} & -\frac{Ts}{C_1+\delta_{C_1}} & 1 \end{bmatrix} \quad B_{k1} = \begin{bmatrix} \frac{Ts}{L_2\delta_{L_2}} \\ 0 \\ 0 \end{bmatrix} \tag{3.23}$$

Considering that: $\delta_{R_1} \in [0, 0.01]\Omega$, $\delta_{R_2} \in [0.0326, 0.0526]\Omega$, $\delta_{L_1} \in [126, 152]\mu H$, $\delta_{L_2} \in [31.3, 37.3]\mu H$ and $\delta_{C_1} \in [1980, 2420]\mu F$.
By using the previously explained theoretical concepts, the controller gain K is obtained. The $\mathbb{D}_{q,r}$ - LMI parameters r and q are set to 0.09 and -0.9 respectively, so that the closed-loop poles end located inside the unitary circle and, concretely, inside a region near this unitary circle, so that the controlled system dynamics are not too fast.
By means of the utilization of MATLAB® and a couple parser-solver (YALMIP [24] and SeDuMi [11]), the aforementioned LMI is solved, and K is obtained as:

$$K = \begin{bmatrix} 0.0973 & -0.1115 & -0.8271 \end{bmatrix} \tag{3.24}$$

Due to the quadratic Schur stability problem previously solved, for this case, there are 32 different systems and, therefore, 32 distinct combinations of closed-loop poles, but the stability can be checked computing the maximum value among the their absolute values. For this control system, it is 0.9821, so the design requirements are fulfilled.
For our case, the k^* value is: $k^* = 0.0292$.

Simulation

Once the controller parameters have been computed, some simulations are carried out in an averaged Simulink® model, so that the closed-loop system behaviour is confirmed to be proper:

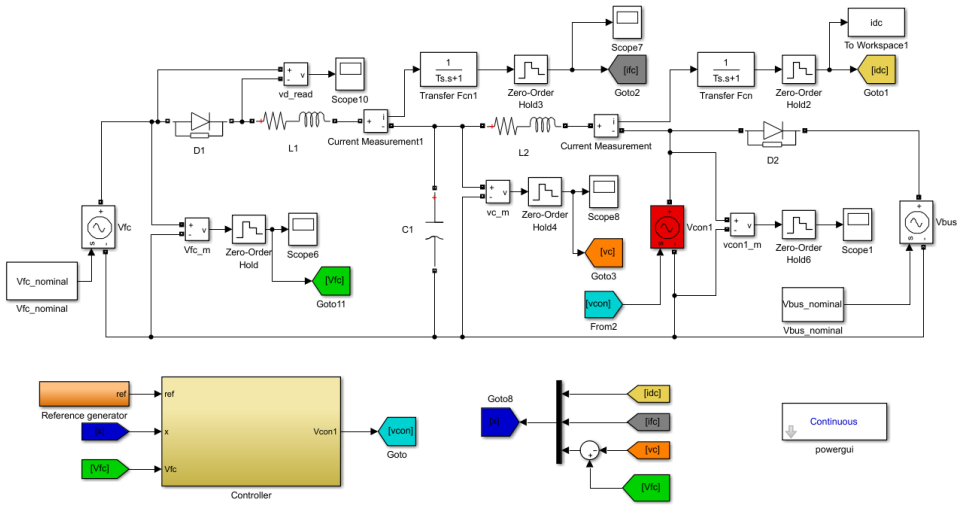

Figure 3.4: PEMFC controlled system (only controller)

The different Simscape [12] blocks parameters are the ones specified in the Section 3.1 About the controller subsystem, it would be as follows:

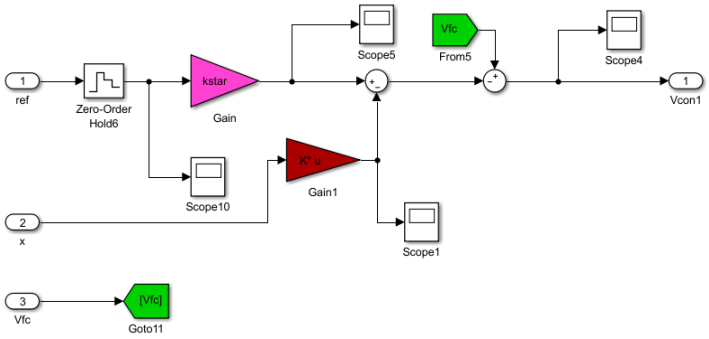

Figure 3.5: PEMFC controlled system (only controller) - Controller Subsystem

The parameters **kstar** and **K** have the aforementioned values. For a reference signal with two steps (40 and 30 V), the closed-loop system response is the following:
It can be appreciated how there is a steady state error, and it can be associated to the voltage drop in the diode adjacent to the PEMFC, which has not been modelled.

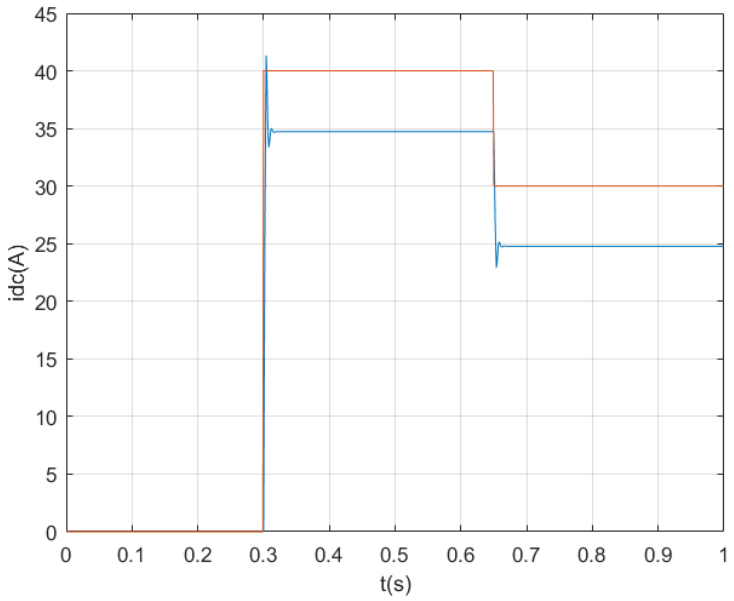

Figure 3.6: PEMFC controlled system (only controller) - i_2 output

To prove this statement, this voltage drop can be included in the variable changes explained in Section 3.2.1, so $V' = V_{fc} - V_{u1} - V_d$ and $V_{dif} = V_{fc} - V_1 - V_d$:

$$\begin{cases} L_1 \frac{di_1}{dt} + R_1 i_1 = V_{fc} - V_1 - V_d = V_{dif} \\ L_2 \frac{di_2}{dt} + R_2 i_2 = V_1 - V_{fc} + V' + V_d = V' - V_{dif} \\ C_1 \frac{d(V_{fc} - V_{dif} - V_d)}{dt} = C_1 \cancelto{0}{\frac{dV_{fc}}{dt}} - C_1 \frac{dV_{dif}}{dt} - C_1 \cancelto{0}{\frac{dV_d}{dt}} = i_1 - i_2 \end{cases} \tag{3.25}$$

The derivative of the diode voltage is neglected, as it doesn't vary significantly. The state space system remains the same, but the Simulink® needs to reflect the changed equations.

The system output could be found in the Figure 3.7. As it can be appreciated, the steady state error is nullified. However, as this design would imply to measure the diode voltage drop and it won't be interesting, the diode voltage will be considered a disturbance, which will be rejected using the observer.

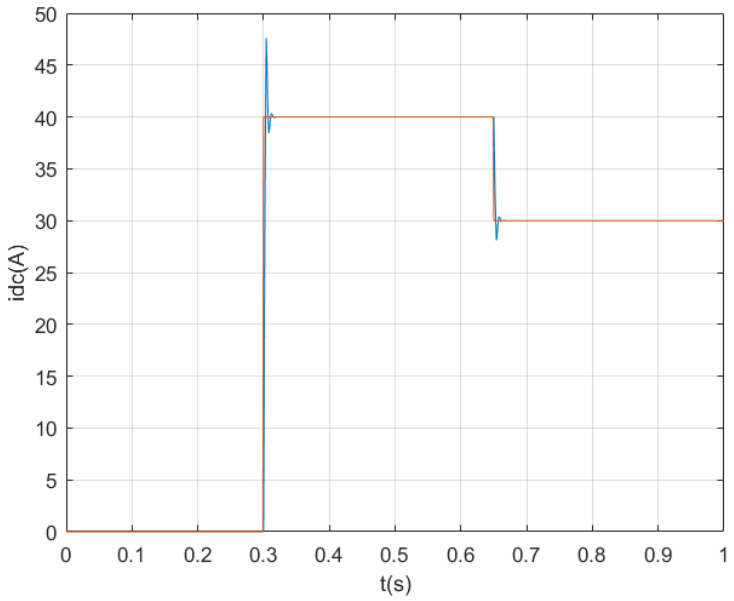

Figure 3.7: PEMFC controlled system (only controller) - i_2 output - With diode voltage

The tests using a more realistic simulation environment, which includes some non-linearities and reflects an analogue behaviour regarding the inclusion of an IGBT transistor, will be carried out when the control system becomes complete in the next subsections.

3.2.3 Observer design

Theoretical framework

In order to design a state observer [13] in an analogue way to the one previously used to obtain the controller, it is necessary to consider the **controller-observer equivalence**. Therefore, from the point of view of the related LMIs, all the previous theoretical framework can be reutilised, but considering that $\boldsymbol{A - BK \Leftrightarrow A^T - LC^T}$ [37].

Apart from this, as it was stated in the previous subsection, one of the aims for designing the observer results to be the rejection of perturbations, so that the steady-state error becomes null (it will also help to construct a robust system to some system uncertainties). To implement this, the actual state-space model is extended with a model of the perturbation, so that it becomes a state of the extended system and its value is estimated. By subtracting it to the previous control signal, the disturbance can be rejected (as all the mathematical demonstrations are necessary in Chapter 5 for the complete system construction process comprehension, they are not developed

here).

By employing the extended system to include the perturbation, the LMI to design the observer gain would be the following (in this case, the quadratic Schur stabilization is also considered, but there are not uncertain parameters at the C matrix; and it should be taken into consideration that the extended system including the perturbation model has state-space matrices with the subscript **tot**)):

$$\begin{bmatrix} -rP & qP + A_{tot}^T(\delta_k)P + C_{tot}^T W \\ qP + PA_{tot}^T(\delta_k)^T + W^T C_{tot} & -rP \end{bmatrix} < 0, \quad \delta_{i_k} = \delta_{i_k}^- or \delta_{i_k}^+ \tag{3.26}$$

And the observer gain L would be obtained as previously the controller gain K, regarding that for its use, it will be transposed and negated: $L = WP^{-1}$.

Again, the k^* needs to be computed. However, it can not be found as in the previous subsection due to the observers inclusion. The simplest way to obtain it would be to set up the complete system, and obtain the k^* as the as the inverse steady-state gain of this system.

To compute this system, the previously obtained controller gain K must be extended too, to include the perturbation rejection: $K_{tot} = [1 \quad K]$.

The complete system would have the following general form (regarding the aforementioned conversions carried out to K and L):

$$\begin{gathered} A_t = \begin{bmatrix} A_{tot} & -B_{tot}K_{tot} \\ LC_{tot} & A_{tot} - LC_{tot} - B_{tot}K_{tot} - LD_{tot}K_{tot} \end{bmatrix} \\ B_t = \begin{bmatrix} B_{tot} \\ B_{tot} + LD_{tot} \end{bmatrix} \quad C_t = \begin{bmatrix} C_{tot} & -D_{tot}K_{tot} \end{bmatrix} \quad D_t = \begin{bmatrix} D_{tot} \end{bmatrix} \end{gathered} \tag{3.27}$$

Application to design

In this way, to find the required observer gain, the LMI $\mathbb{D}$-stabilization parameters r and q are set to 0.02 and -0.92 respectively, so that the observer dynamics are faster than the ones of the previously constructed system. By using these settings, the observer gain reaches the following value:

$$L^T = \begin{bmatrix} 0.0042 & 0.2398 & -0.0092 & 0.0031 \end{bmatrix} \tag{3.28}$$

The observer poles have the same issue than the closed-loop system ones, regarding their number due to the quadratic Schur stabilization problem. However, applying the same criteria than the one it was used in the aforementioned case, the maximum absolute value among all the poles is 0.9323, so the design requirements are fulfilled.

Again, k^* value is computed as explained before, obtaining that: $k^* = 0.0401$.

Simulation

Once again, to test the controlled-observed system performance, Simulink® will be employed, as well as an averaged model of the real system.

The Simulink® can be found in Figure 3.8, where it can be appreciated how, by using the observer, the states measurements are not employed.

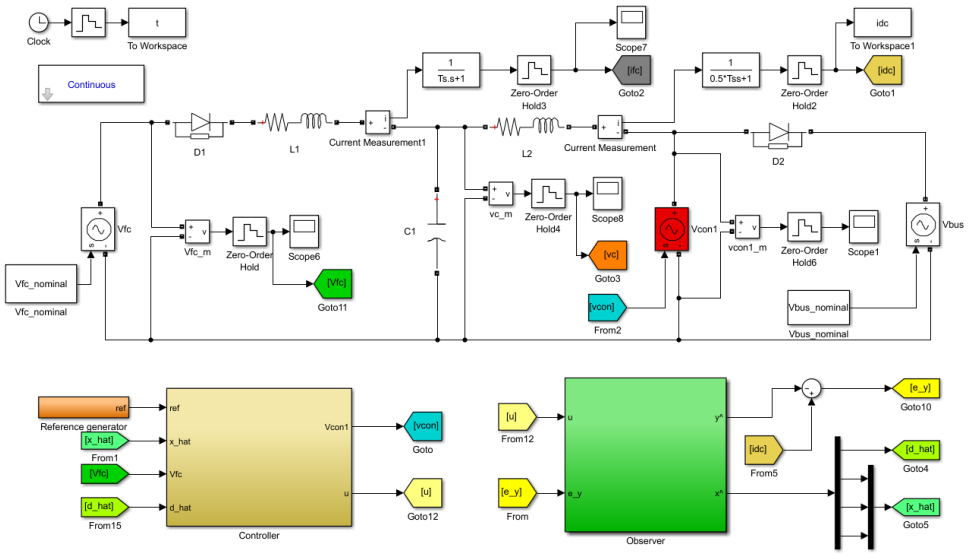

Figure 3.8: PEMFC controlled system (controller/observer)

For this model, the controller and observer subsystems would be the ones in Figure 3.9.

And again, the reference signal is set as a double step, first from a 0 value to 40 A and then from this value to 30 A. The controlled system performance can be found in Figure 3.10.

The results are as expected: the steady-state error produced by the diode voltage drop is ne-

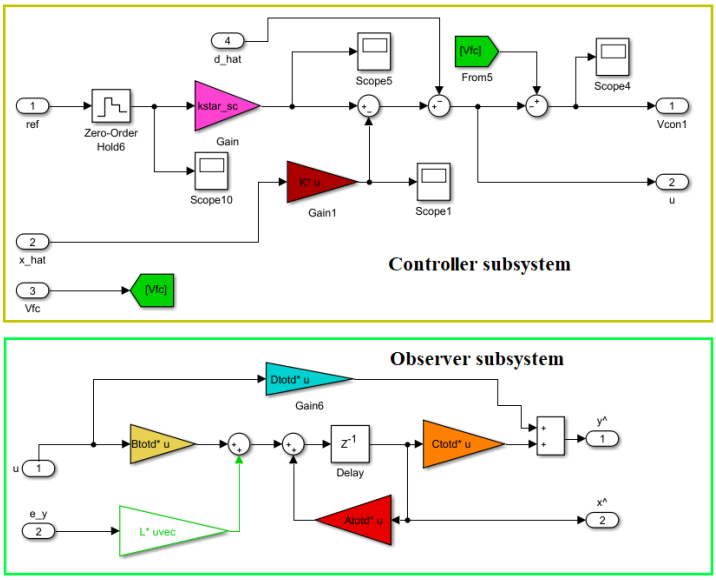

Figure 3.9: PEMFC controlled system (controller and observer subsystems)

glected by the disturbance rejection, obtaining an output that follows the reference without error.

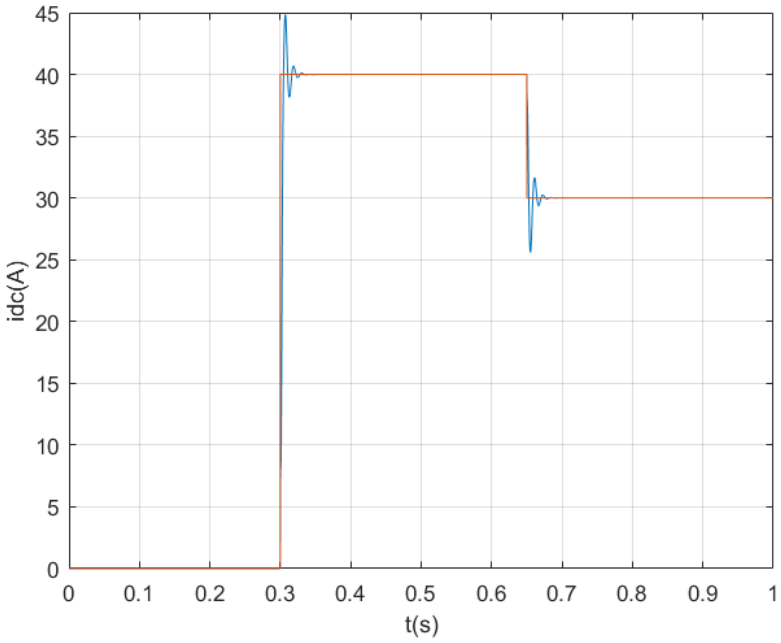

Figure 3.10: PEMFC controlled system (controller/observer) - i_2 output

3.2.4 Testing with the switched system

Once the control system goodness has been proven using the averaged model, it is important to double-check this performance in the switched model, which consists in a more precise approximation of the real behaviour of the plant.

As it was stated in previous subsections, the main difference between the averaged and switched models consists on the presence of an IGBT transistor at the last one, substituting the voltage source whose value was set to V_{u1}.

In this case, that voltage needs to be converted to the duty cycle, and as it was defined as $V_{u1} = (1 - D)V_{bus}$, the value of D is obtained as $D = 1 - \frac{V_{u1}}{V_{bus}}$ (it can be appreciated in Figure 3.12). The bus voltage remains constant for these simulations (it will be variable for the complete system, as the objective would be to control this voltage).

Finally, a PWM signal of 20 KHz is generated with this duty cycle (PWM-generator subsystem), being it the input to control the on/off state of the IGBT transistor.

The Simulink® model that implements all this features can be found in Figure 3.11, along with the two different subsystems with respect to the averaged model: the controller, which implements the conversion from V_{u1} to D, and the PWM-generator, which was not necessary before. The observer subsystem remains the same, so it is not included again.

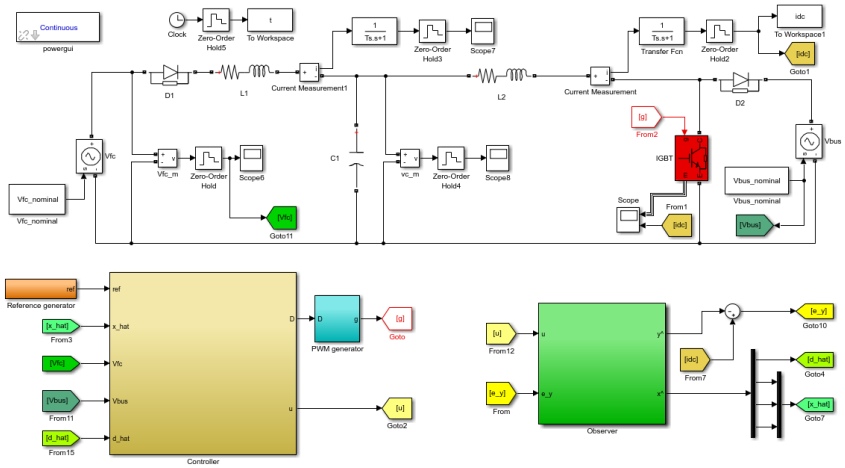

Figure 3.11: PEMFC controlled system (switched model)

Finally, a new reference pattern is used to feed the system: initially, a current of 20 A is asked, but it is changed at 0.35 s to 30 A. Then, at time $t = 1$ s, the current reference is increased to 40 A, and ends changing to 20 A at 1.5 s. The performance can be found in Figure 3.13.

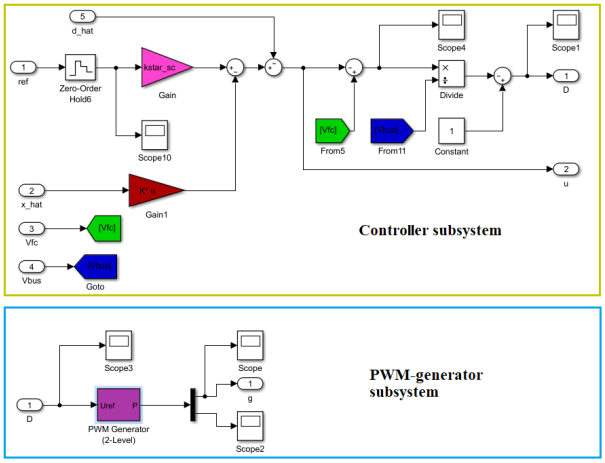

Figure 3.12: PEMFC controlled system (switched - controller and PWM-generator subsystems)

It can be appreciated how the disturbance rejection is working properly, as the perturbations associated to the starting-up phase of the system are neglected, so that after them the output remains being equal to the given reference.

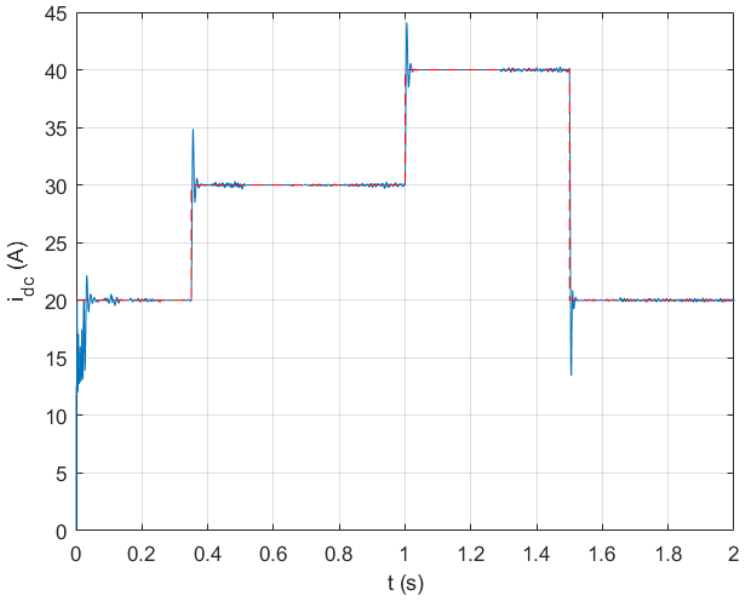

Figure 3.13: PEMFC controlled system (switched) - i_2 output

3.3 In Closing

In this chapter, the design of a control structure for the DC-DC converter of the PEMFC subsystem has been covered, from its initial steps only implementing a state-feedback proportional controller, to the final stage, including robustness to uncertainty in the controller and observer design, being the last constructed to allow the rejection of disturbances.
The performance obtained using this control design has been proven employing a precise model of the real plant, reaching a quite good result.

Chapter 4

SC DC-DC Converter analysis and control design

4.1 Subsystem description

The second study is made about the converter which connects the supercapacitors, SC from now, and the DC bus. In this case, control system is designed to manage the energy transfer from the bus to the SC and vice versa. Therefore, and opposite to the first system in which the current was only allowed to go from the PEMFC to the bus, the current will be bidirectional.
Again, the electrical circuit is analysed to understand the dynamics that it presents, and the equations that represent the behaviour of the system are achieved.
A simplified diagram of the SC subsystem can be found in Figure 4.1.
The electrical variables involved in this circuit are the following:

- i_3 → current at the supercapacitor.
- V_{L3} → voltage at the inductor.
- V_{sc} → voltage at the capacitor.
- V_{bus} → voltage at the bus.
- V_{u2} → voltage of the IGBT, and also the control variable.

Regarding the electrical parameters, their values are shown in Table 4.1.
About other considerations which must be taken into account:

- The IGBT transistor used at the laboratory is the SEMiX 251GD126HDs [31], alongside the SKHI 20opA driver [32] and the SEMISTACK - IGBT three-phase inverter [30].

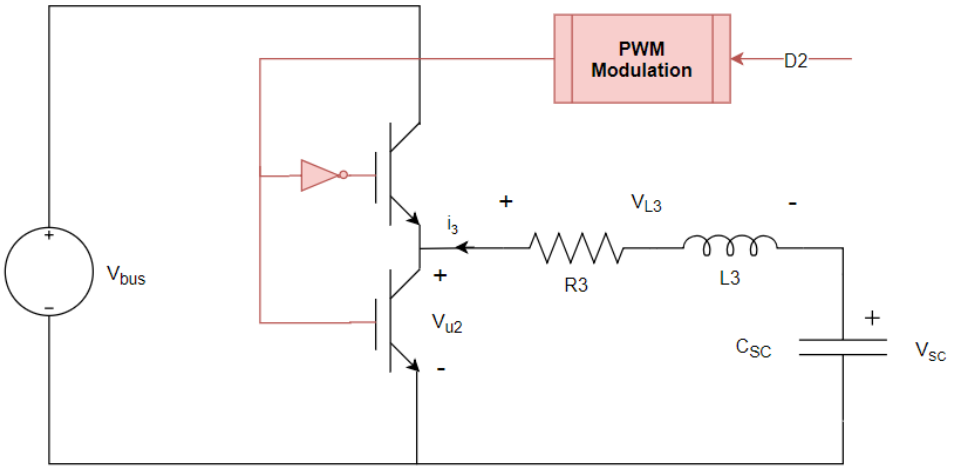

Figure 4.1: SC subsystem electrical diagram

Parameter	Value	Units
L_3	34.3	μH
R_3	0.0426	Ω
C_{sc}	165	F

Table 4.1: SC subsystem electrical components parameters

- The voltages of the bus have been fixed for this tests to its nominal value, 80 V, as the desired behaviour for the system consists in maintaining this value as constant as possible.
- The resistors located in series with the inductors are parasitic and must be taken into account.
- The transistor is controlled using PWM [20] modulation.

Analysis of the dynamical system

From the circuit at Figure 4.1, applying the Kirchoff laws, the following system of equations is derived:

$$\begin{cases} V_{L_3} = V_{u2} - V_{sc} \\ i_3 = -C_{sc}\frac{dV_{sc}}{dt} \end{cases} \tag{4.1}$$

Employing the equations of the voltage at an inductor, and the current of a capacitor; as well as

splitting V_{L3} into the voltage at the inductor and resistor; and taking into account the change of sign due to the direction chosen for the current, the system can be transformed into:

$$\begin{cases} L_3 \frac{di_3}{dt} = -R_3 i_3 + V_{sc} - V_{u2} \\ C_{sc} \frac{dV_{sc}}{dt} = -i_3 \end{cases} \tag{4.2}$$

The transistor voltage V_{u2} can be modelled as:

$$V_{u2} = (1 - D_2) V_{bus} \tag{4.3}$$

Again, to remark the importance of the value of D_2, a simulation is run in Simulink®, so that the electrical circuit showed at Figure 4.1 must be converted to a block diagram at this software, presented at Figure 4.2.

The input profile used to feed the PWM consists of a first section in which the value of D_2 is 0, that is to have the transistors always in cut-off mode; then it is increased to 1, so that the IGBTs are always conducting, and then it is reduced to 0.6, so that the transistors current reaches an equilibrium. The response of the system can be found in Figure 4.3.

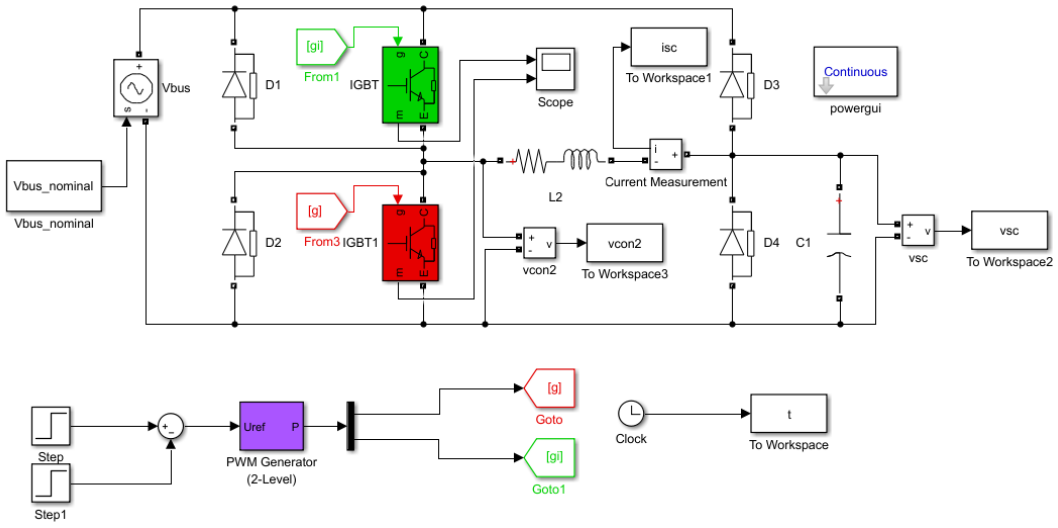

Figure 4.2: SC subsystem

This result was expectable if the system equations are analysed. Recalling the first equation of Equation 4.2:

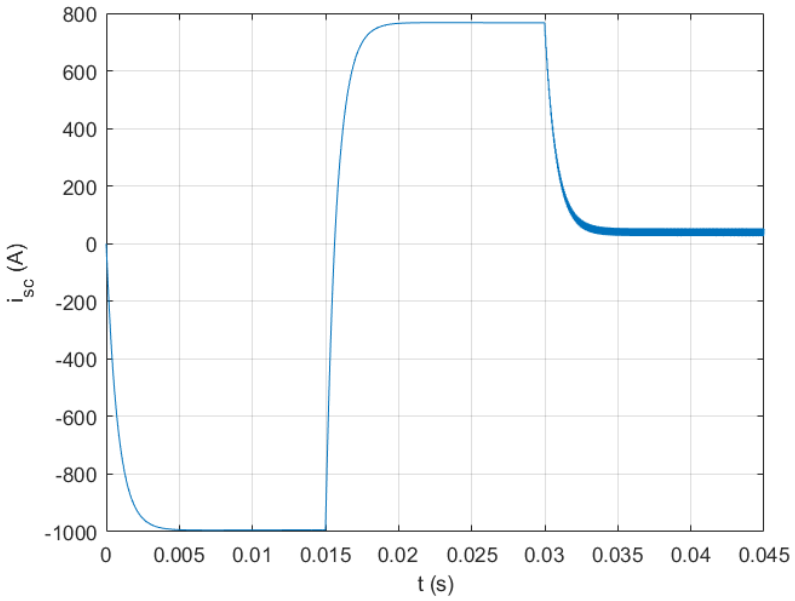

Figure 4.3: i_3 response ($t \in [0, 0.015) \rightarrow D_2 = 0$, $t \in [0.015, 0.03) \rightarrow D_2 = 1$, $t \in [0.03, 0.045) \rightarrow D_2 = 0.6$)

$$L_3 \frac{di_3}{dt} = -R_3 i_3 + V_{sc} - (1 - D_2) V_{bus} \tag{4.4}$$

When $D_2 = 0$, the derivative of the current is negative, so it will reach its minimum value at a certain time. When $D_2 = 1$ the current increase its value until it reaches its top. Finally, when $D_2 = 0.6$, the transistor is commuting and the current stays in the range formed by the previously reached peaks.

4.2 Control system design

4.2.1 State-space model generation

Once again, to be capable of designing controllers/observers by using LMIs, the state-space matrices of the dynamical model are necessary, so extracting them would be the first task.

The subsystem physical model can be recalled from Equation 4.2:

$$\begin{cases} L_3 \frac{di_3}{dt} = -R_3 i_3 + V_{sc} - V_{u2} \\ C_{sc} \frac{dV_{sc}}{dt} = -i_3 \end{cases} \tag{4.5}$$

Despite at first sight it seems to be proper to design a second order controller, as the system has two states, this procedure would lead to control problems. In practice, the dynamic equation for the supercapacitor voltage drop is neglected in the design, as this voltage will be measured. Therefore, a variable change is needed again: $V'' = V_{sc} - V_{u2}$.

Applying this change to the previous model, it can be presented in its state-space representation as in Equation 4.6 and Equation 4.7.

$$\dot{i_3} = \underbrace{\begin{bmatrix} -R_3/L_3 \end{bmatrix}}_{A_2} \begin{bmatrix} i_3 \end{bmatrix} + \underbrace{\begin{bmatrix} 1/L_3 \end{bmatrix}}_{B_2} V'' \tag{4.6}$$

$$y = \underbrace{\begin{bmatrix} 1 \end{bmatrix}}_{C_2} \begin{bmatrix} i_3 \end{bmatrix} + \underbrace{\begin{bmatrix} 0 \end{bmatrix}}_{D_2} V'' \tag{4.7}$$

And again, the continuous-time model needs to be discretized (using the FE approach with a sample time of 0.05 ms), finally reaching the discrete-time state-space model at Equations 4.8 and 4.9.

$$i_{3_{k+1}} = \underbrace{\begin{bmatrix} 1 - Ts \cdot R_3/L_3 \end{bmatrix}}_{A_{k_2}} \begin{bmatrix} i_{3_k} \end{bmatrix} + \underbrace{\begin{bmatrix} Ts/L_3 \end{bmatrix}}_{B_{k_2}} V_k'' \tag{4.8}$$

$$y_k = \underbrace{\begin{bmatrix} 1 \end{bmatrix}}_{C_{k_2}} \begin{bmatrix} i_{3_k} \end{bmatrix} + \underbrace{\begin{bmatrix} 0 \end{bmatrix}}_{D_{k_2}} V_k'' \tag{4.9}$$

4.2.2 Controller design

Theoretical framework

The theoretical basis for the controller design process by means of LMIs for the SC subsystem is the same than the one previously used for the PEMFC subsystem, so the mathematical developments can be found in **Chapter 3 - Section 3.2 - Subsection 3.2.2**.

Application to design

From Equation 4.8, and recalling the uncertainty representation shown at Equation 3.20, the space-state matrices can be expressed as:

$$A_{k_2} = \left[1 - Ts \cdot \frac{R_3+\delta_{R_3}}{L_3+\delta_{L_3}}\right] \quad B_{k_2} = \left[\frac{Ts}{L_3+\delta_{L_3}}\right] \tag{4.10}$$

And the uncertainties ranges being: $\delta_{R_3} \in [0.0326, 0.0526]\Omega$ and $\delta_{L_3} \in [30.87, 37.73]\mu H$.

For the controller gain K obtaining, the $\mathbb{D}_{q,r}$ - LMI parameters r and q are set to 0.1 and -0.8 respectively, targeting to reach relatively fast dynamics.

Therefore, for these settings, K is obtained as:

$$K = \left[0.0918\right] \tag{4.11}$$

To check that the $\mathbb{D}$-stabilization problem requirements have been fulfilled, as for the PEMFC system, the maximum among the absolute values for the different possible closed-loop poles is computed. It is located at 0.8086, so the design is valid at least from the theoretical point of view.

Despite in the previous chapter the control design was tested before including the observer, it was mainly done to show the disturbance rejection property of the latter, so the demonstration will not be repeated at this chapter. Therefore, the k^* would not be computed for the system without observer.

4.2.3 Observer design

Theoretical framework

For the observer design, the theoretical concepts were also explained in previous chapters, concretely in **Chapter 3 - Section 3.2 - Subsection 3.2.3**, so they will not be repeated here.

Application to design

Regarding the resultant parameters from the design, setting the LMI $\mathbb{D}$-stabilization parameters r and q to 0.1 and -0.7 respectively (so that the observer dynamics are faster than the previous ones), the observer gain is obtained as:

$$L^T = \begin{bmatrix} 0.0677 & 0.5293 \end{bmatrix} \tag{4.12}$$

And again the maximum absolute value among the observer poles is 0.7023, checking the accomplishment of the requisites.

The k^* value is computed as explained in the observer design theoretical framework of the previous chapter, obtaining that: $k^* = 0.1444$.

Simulation

Once the controller/observer pair has been computed, the validity of this design must be checked again, first using the averaged model of the plant, which has been implemented in Simulink® as is appears in Figure 4.4.

The controller subsystem is the only different, as the observer block is internally equal to the one used for the PEMFC system. It is presented in Figure 4.5.

It can be seen how the controller structure is quite similar, but the variable change is different.

For the simulation, the reference pattern has been set to: 0 A from 0 to 0.3 s; 10 A from 0.3 to 0.65 s; and 5 A from 0.65 to 1 s. The results can be found in Figure 4.6. The SC subsystem response is so fast that it overlaps the reference, resulting in an excellent performance.

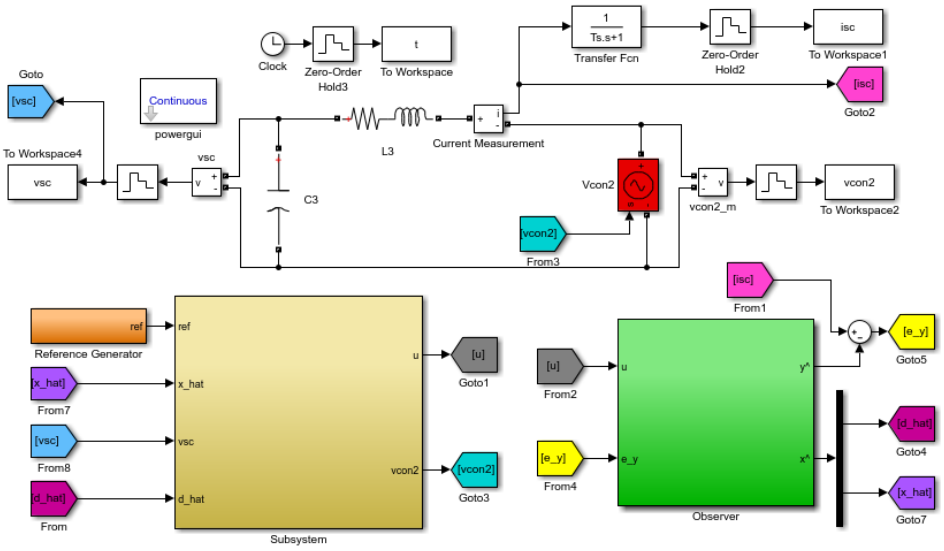

Figure 4.4: SC controlled system (controller/observer)

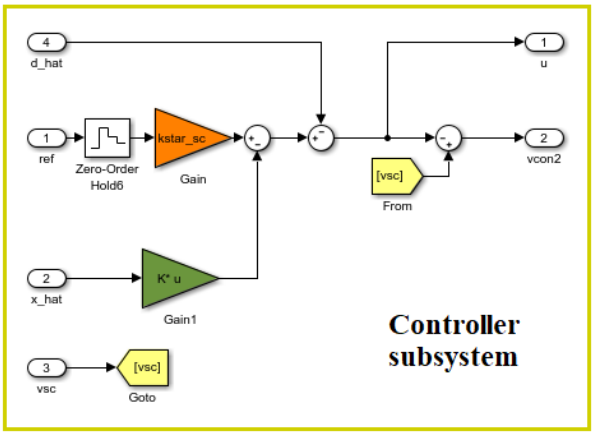

Figure 4.5: SC controlled system (controller subsystem)

4.2.4 Testing with the switched system

Finally, the last test must be carried out by using the switched model to implement a more precise representation of the real plant.

As it was stated in the subsystem introduction, in this case, there are two IGBTs instead of one, although only one duty cycle must be computed, as the PWM feeding each one of them has the

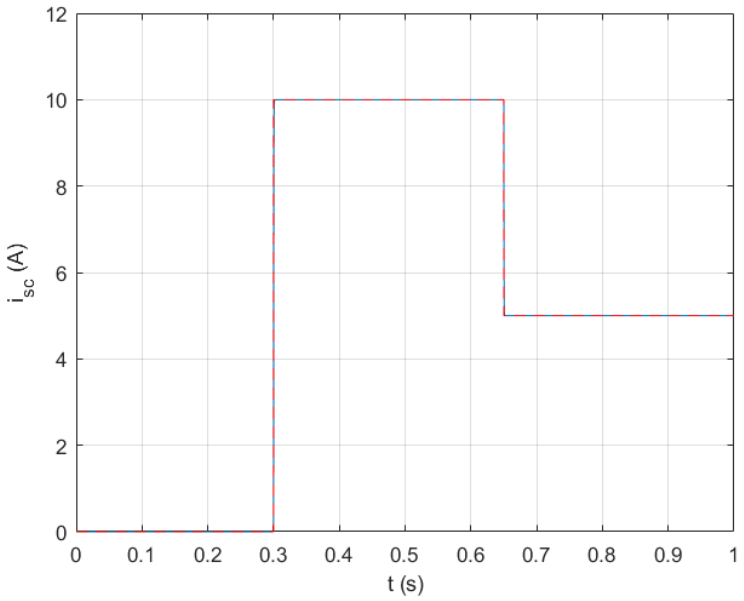

Figure 4.6: SC controlled system (controller/observer) - i_3 output

opposite duty cycle of the other.

Again, that voltage V_{u2} needs to be converted to the duty cycle, and as it was defined as $V_{u2} = (1 - D_2)V_{bus}$, the value of D_2 is obtained with the same transformation. Hence, the PWM generator block will be equal to the one of the PEMFC subsystem, with the only difference that in this case both outputs from the PWM generator (2-level) are utilized. The bus voltage will be constant for these simulations.

The Simulink® model can be found in Figure 4.7. The subsystems (controller, PWM generator and observer) will not be displayed this time, as they are almost the same than the ones previously shown.

Another reference pattern is used to feed the system: initially, a current of 0 A is asked, but it is changed at 0.35 s to 30 A. Then, at time 0.65 s, the current reference is decreased to 10 A, and ends at this value. The performance for this reference signals can be found in Figure 4.8.

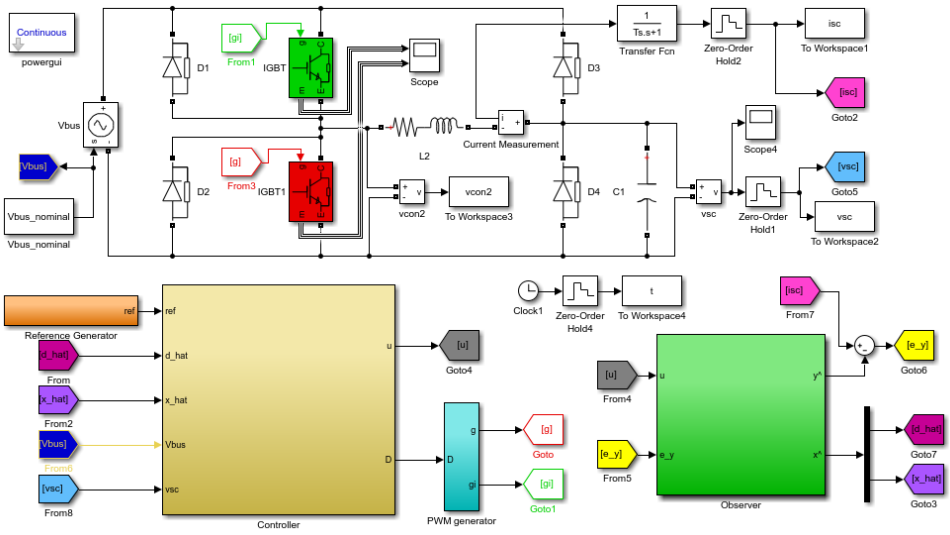

Figure 4.7: SC controlled system (switched model)

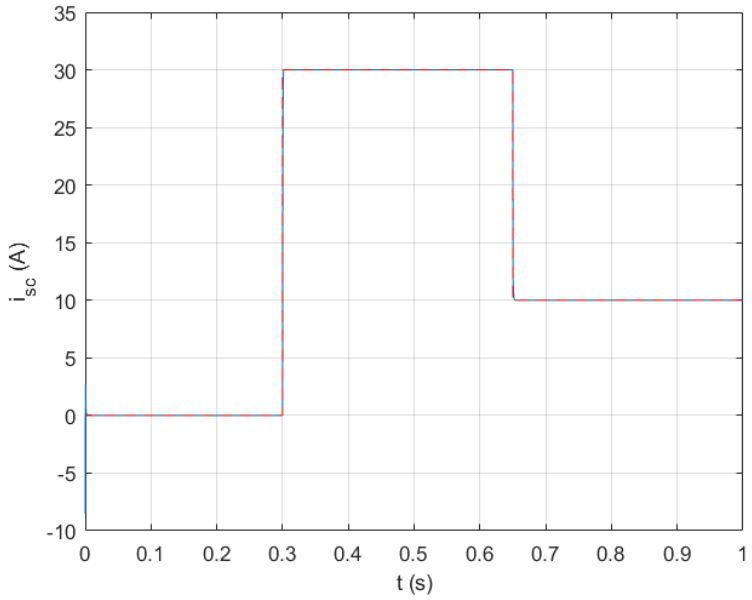

Figure 4.8: SC controlled system (switched) - i_3 output

It can be appreciated how the response is pretty similar to the one of the averaged model, although in this case the initialization of the system has some effects which are present at the very beginning of the simulation.

4.3 In Closing

In this chapter, a controller/observer pair has been designed for the DC-DC converter of the SC subsystem, so that the supercapacitor current could be controlled, and the procedure has been similar to the one used before for the PEMFC subsystem, so some theoretical developments had been skipped.

The performance has been contrasted using the averaged and switched models, obtaining quite good and similar results in both cases. This suitable response will allow a proper control of the bus voltage in the following chapter, where the same system analysis and control design will be carried out but for the complete system, joining these previous two subsystems.

Chapter 5

Complete system analysis and control design

5.1 Complete system description

Once both subsystems have been studied, analysed, and controllers have been designed for them, a new control system must be generated, so that the bus voltage V_{bus} can be set to a certain value, which is maintained despite disturbances that might affect the system.
As it was done previously for the subsystems, the electrical circuit is studied to understand its dynamics, obtaining the dynamical equations which represent the behaviour of the system.
A simplified diagram of the PEMFC subsystem can be found in Figure 5.1.

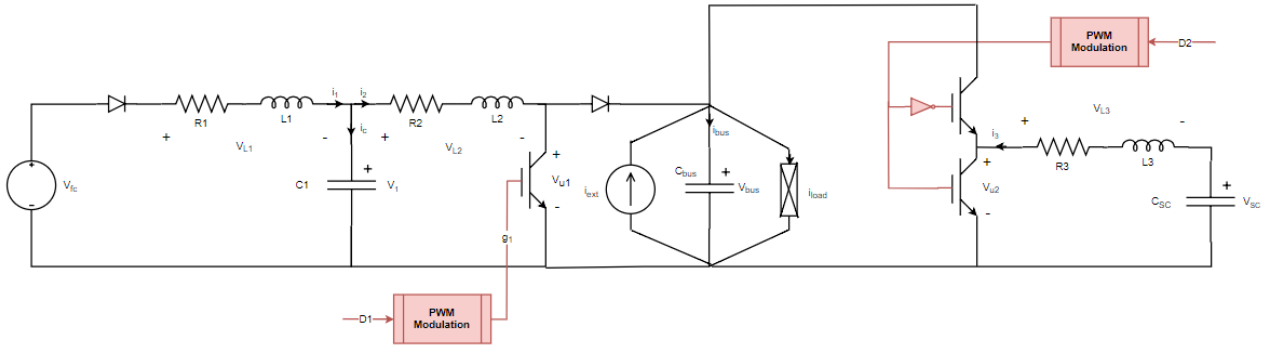

Figure 5.1: Complete system electrical diagram

Most of the variables involved in this circuit are known due to their explanation in previous chapters, so only the new ones are enumerated:

- $\boldsymbol{i_{bus}}$ → current at the bus.
- $\boldsymbol{i_{ext}}$ → current that can enter the system and act as an extra source.
- $\boldsymbol{i_{load}}$ → current that may leave the system.

Regarding the circuit parameters, only the bus capacitor has been introduced. It has a capacitance value of **2.72 mF**.

Analysis of the dynamical system

The complete system behaviour is defined by its dynamical equations, which are presented at Equation 5.1.

$$\begin{cases} L_1 \frac{di_1}{dt} + R_1 i_1 = V_{fc} - V_1 \\ L_2 \frac{di_2}{dt} + R_2 i_2 = V_1 - V_{u1} \\ C_1 \frac{dV_1}{dt} = i_1 - i_2 \\ L_3 \frac{di_3}{dt} = -R_3 i_3 + V_{sc} - V_{u2} \\ C_{sc} \frac{dV_{sc}}{dt} = -i_3 \\ i_{bus} = C_{bus} \frac{dV_{bus}}{dt} = i_2(1 - D_1) + i_3(1 - D_2) + i_{ext} - i_{load} \end{cases} \tag{5.1}$$

For its later usage, the last equation of the system is modified, so that a new variable Δi_{load} is created as $\Delta i_{load} = i_{ext} - i_{load}$, as well as the duty cycle related components, $1 - D_1$ and $1 - D_2$ are substituted by $\frac{V_{u1}}{V_{bus}}$ and $\frac{V_{u2}}{V_{bus}}$ respectively; by using Equation 3.3 and Equation 4.3. The final system can be found at Equation 5.2.

$$\begin{cases} L_1 \frac{di_1}{dt} + R_1 i_1 = V_{fc} - V_1 \\ L_2 \frac{di_2}{dt} + R_2 i_2 = V_1 - V_{u1} \\ C_1 \frac{dV_1}{dt} = i_1 - i_2 \\ L_3 \frac{di_3}{dt} = -R_3 i_3 + V_{sc} - V_{u2} \\ C_{sc} \frac{dV_{sc}}{dt} = -i_3 \\ C_{bus} \frac{dV_{bus}}{dt} = i_2 \frac{V_{u1}}{V_{bus}} + i_3 \frac{V_{u2}}{V_{bus}} + \Delta i_{load} \end{cases} \tag{5.2}$$

Some of these equations would be used and explained later in detail. Besides, opposite to the process followed for the previous chapters, the complete system would not be analysed by

simulation, as the individual behaviours of the subsystems which conform it have been studied in previous chapters.

5.2 Control system design

5.2.1 State-space model generation

In order to be capable of controlling the system using a state-feedback approach, as it was done previously, the state-space matrices that represent the system need to be obtained.
From previous sections, the state-space representations of the two subsystems which form the complete one are taken:

- First, the DC-DC converter for the PEMFC system:

$$\begin{bmatrix} \dot{i_2} \\ \dot{i_1} \\ \dot{V_{dif}} \end{bmatrix} = \underbrace{\begin{bmatrix} -R_2/L_2 & 0 & -1/L_2 \\ 0 & 0 & 1/L_1 \\ 1/C_1 & -1/C_1 & 0 \end{bmatrix}}_{A_1} \begin{bmatrix} i_2 \\ i_1 \\ V_{dif} \end{bmatrix} + \underbrace{\begin{bmatrix} 1/L_2 \\ 0 \\ 0 \end{bmatrix}}_{B_1} V' \tag{5.3}$$

$$y = \underbrace{\begin{bmatrix} 1 & 0 & 0 \end{bmatrix}}_{C_1} \begin{bmatrix} i_2 \\ i_1 \\ V_{dif} \end{bmatrix} + \underbrace{\begin{bmatrix} 0 \end{bmatrix}}_{D_1} V' \tag{5.4}$$

  Regarding that $V' = V_{fc} - V_{u1}$ and $V_{dif} = V_{fc} - V_1$.

- Then, the supercapacitor DC-DC converter subsystem:

$$\dot{i_3} = \underbrace{\begin{bmatrix} -R_3/L_3 \end{bmatrix}}_{A_2} \begin{bmatrix} i_3 \end{bmatrix} + \underbrace{\begin{bmatrix} 1/L_3 \end{bmatrix}}_{B_2} V'' \tag{5.5}$$

$$y = \underbrace{\begin{bmatrix} 1 \end{bmatrix}}_{C_2} \begin{bmatrix} i_3 \end{bmatrix} + \underbrace{\begin{bmatrix} 0 \end{bmatrix}}_{D_2} V'' \tag{5.6}$$

  Taking into consideration that $V'' = V_{sc} - V_{u2}$.

Before starting to use those equations and the control results obtained in the two previous chapters, a brief explanation of the theoretical context for the generation of the complete system space-state representation must be carried out.

Theoretical analysis: general case

As it was stated in the aforementioned Chapters 3 and 4, the implemented state-feedback control strategy includes the utilization of a disturbance rejection observer, so that a null steady-state error is reached. In order to comprehend how to reach the complete closed-loop form of both system for this analysis, the theoretical derivations would be carried out using a system as the following:

$$\begin{cases} \dot{x} = Ax + Bu + Bd \\ y = Cx + Du \end{cases} \tag{5.7}$$

Being d an uncertain input disturbance (this method will also be useful to delete the steady-state error provoked by uncertainty in the state-space matrices).
This disturbance must be included in the controller (or plant), so the system order increase will depend on the disturbance nature. For this case, a step generator would be considered, so its state-space representation could be expressed as:

$$\begin{cases} \dot{x^d} = 0 \\ d = x^d \end{cases} \tag{5.8}$$

Nevertheless, as the state-space models were discretized in both subsystems control design processes, this discretization effects must be taken into account for the analysis and for setting the complete closed-loop system, being necessary to discretize the previous equations (the forward Euler (FE) method will be used for this process as it was done in prior chapters):

- In the case of the system model, making the FE substitution :

$$\begin{cases} \frac{x_{k+1}-x_k}{T_s} = Ax_k + Bu_k + Bd_k \\ y_k = Cx_k + Du_k \end{cases} \tag{5.9}$$

  Manipulating the equations, the discrete state-space model is obtained as well as its ma-

trices:

$$\begin{cases} x_{k+1} = \underbrace{(I + T_s A)}_{A_k} x_k + \underbrace{T_s B}_{B_k} u_k + \underbrace{T_s B}_{B_k} d_k \\ y_k = \underbrace{C}_{C_k} x_k + \underbrace{D}_{D_k} u_k \end{cases} \tag{5.10}$$

- For the step disturbance model the process is analogous:

$$\begin{cases} \frac{x^d_{k+1} - x^d_k}{T_s} = 0 \\ d_k = x^d_k \end{cases} \tag{5.11}$$

Finally reaching its discrete state-space form:

$$\begin{cases} x^d_{k+1} = x^d_k \\ d_k = x^d_k \end{cases} \tag{5.12}$$

And the corresponding state-space matrices:

$$\begin{cases} A^d_k = 1; B^d_k = 0 \\ C^d_k = 1; D^d_k = 0 \end{cases} \tag{5.13}$$

These two separate systems can be merged into a bigger new system as follows:

$$x^t_{k+1} = \begin{bmatrix} x^d_{k+1} \\ x_{k+1} \end{bmatrix} = \underbrace{\begin{bmatrix} A^d_k & 0 \\ B_k C^d_k & A_k \end{bmatrix}}_{A^t_k} \begin{bmatrix} x^d_k \\ x_k \end{bmatrix} + \underbrace{\begin{bmatrix} 0 \\ B_k \end{bmatrix}}_{B^t_k} u_k \tag{5.14}$$

$$y_k = \underbrace{\begin{bmatrix} 0 & C_k \end{bmatrix}}_{C^t_k} \begin{bmatrix} x^d_k \\ x_k \end{bmatrix} + \underbrace{\begin{bmatrix} D_k \end{bmatrix}}_{D^t_k} u_k \tag{5.15}$$

Now, regarding (A^t_k, C^t_k) is observable, an observer is designed to obtain $\hat{x}^t_k$:

$$\hat{x}^t_{k+1} = A^t_k \hat{x}^t_k + B^t_k u_k + L^t_k (y_k - \hat{y}_k) = (A^t_k - L^t_k C^t_k)\hat{x}^t_k + B^t_k u_k + L^t_k y_k \tag{5.16}$$

And with this observer, the following control law can be defined:

$$u_k = -K_k^t \hat{x}_k^t + k^* y_k^{ref} = -K_k \hat{x}_k - C_k^d \hat{x}_k^d + k^* y_k^{ref} \tag{5.17}$$

By substituting this control law into the system equation:

$$x_{k+1} = A_k x_k + B_k u_k + B_k d_k = A_k x_k + B_k d_k - B_k K_k \hat{x}_k - B_k C_k^d \hat{x}_k^d + B_k k^* y_k^{ref} \tag{5.18}$$

Regarding that $d_k = C_k^d x_k^d$, as well as $e_{x_k} = x_k - \hat{x}_k$ and $e_{x_k^d} = x_k^d - \hat{x}_k^d$:

$$x_{k+1} = A_k x_k + B_k C_k^d x_k^d - B_k K_k (x_k - e_{x_k}) - B_k C_k^d (x_k^d - e_{x_k^d}) + B_k k^* y_k^{ref} \tag{5.19}$$

Manipulating the equation, the following result is reached:

$$x_{k+1} = (A_k - B_k K_k) x_k + B_k K_k e_{x_k} + B_k C_k^d e_{x_k^d} + B_k k^* y_k^{ref} \tag{5.20}$$

Now, as e_{x_k} and $e_{x_k^d}$ need to be defined as states of the complete closed-loop system, the next analysis must be carried out:

$$e_{x_{k+1}^t} = x_{k+1}^t - \hat{x}_{k+1}^t = A_k^t x_k^t + B_k^t u_k - (A_k^t - L_k^t C_k^t) \hat{x}_k^t - B_k^t u_k - L_k^t y_k \tag{5.21}$$

Again, manipulating the terms and regarding $y_k = C_k^t x_k^t$:

$$e_{x_{k+1}^t} = (A_k^t - L_k^t C_k^t) x_k^t - (A_k^t - L_k^t C_k^t) \hat{x}_k^t = (A_k^t - L_k^t C_k^t) e_{x_k^t} \tag{5.22}$$

And this last result can be separated into the two errors as follows:

$$\begin{bmatrix} e_{x_{k+1}^d} \\ e_{x_{k+1}} \end{bmatrix} = \left(\begin{bmatrix} A_k^d & 0 \\ B_k C_k^d & A_k \end{bmatrix} - \begin{bmatrix} L_k^d \\ L_k \end{bmatrix} \begin{bmatrix} 0 & C_k \end{bmatrix} \right) \begin{bmatrix} e_{x_k^d} \\ e_{x_k} \end{bmatrix} = \begin{bmatrix} A_k^d & -L_k^d C_k \\ B_k C_k^d & A_k - L_k C_k \end{bmatrix} \begin{bmatrix} e_{x_k^d} \\ e_{x_k} \end{bmatrix} \tag{5.23}$$

To conclude, from this last matrix equation and from previous results, the system of state equations for the complete closed loop system end being the following:

$$\begin{cases} x_{k+1} = (A_k - B_k K_k)x_k + B_k K_k e_{x_k} + B_k C_k^d e_{x_k^d} + B_k k^* y_k^{ref} \\ e_{x_{k+1}} = (A_k - L_k C_k)e_{x_k} + B_k C_k^d e_{x_k^d} \\ e_{x_{k+1}^d} = A_k^d e_{x_k^d} - L_k^d C_k e_{x_k} \end{cases} \tag{5.24}$$

PEMFC system

From the beginning of this chapter, the definition of the system formed by the DC-DC converter connected to the PEMFC is recalled, but adding an extra term to represent the possible disturbances (as it was included in the previous analysis).
Again, regarding that $V' = V_{fc} - V_{u1}$ and $V_{dif} = V_{fc} - V_1$:

$$\begin{bmatrix} \dot{i_2} \\ \dot{i_1} \\ \dot{V_{dif}} \end{bmatrix} = \underbrace{\begin{bmatrix} -R_2/L_2 & 0 & -1/L_2 \\ 0 & 0 & 1/L_1 \\ 1/C_1 & -1/C_1 & 0 \end{bmatrix}}_{A_1} \begin{bmatrix} i_2 \\ i_1 \\ V_{dif} \end{bmatrix} + \underbrace{\begin{bmatrix} 1/L_2 \\ 0 \\ 0 \end{bmatrix}}_{B_1} V' + \underbrace{\begin{bmatrix} 1/L_2 \\ 0 \\ 0 \end{bmatrix}}_{B_1} d_1 \tag{5.25}$$

$$y = \underbrace{\begin{bmatrix} 1 & 0 & 0 \end{bmatrix}}_{C_1} \begin{bmatrix} i_2 \\ i_1 \\ V_{dif} \end{bmatrix} + \underbrace{\begin{bmatrix} 0 \end{bmatrix}}_{D_1} V' \tag{5.26}$$

First, the model is discretized so that the aforementioned procedure can be replicated. Using FE method, the next state-space representation is reached:

$$\begin{bmatrix} i_{2_{k+1}} \\ i_{1_{k+1}} \\ V_{dif_{k+1}} \end{bmatrix} = \underbrace{\begin{bmatrix} 1 - Ts \cdot R_2/L_2 & 0 & -Ts/L_2 \\ 0 & 1 & Ts/L_1 \\ Ts/C_1 & -Ts/C_1 & 1 \end{bmatrix}}_{A_{k1}} \begin{bmatrix} i_{2_k} \\ i_{1_k} \\ V_{dif_k} \end{bmatrix} + \underbrace{\begin{bmatrix} Ts/L_2 \\ 0 \\ 0 \end{bmatrix}}_{B_{k1}} V'_k + \underbrace{\begin{bmatrix} Ts/L_2 \\ 0 \\ 0 \end{bmatrix}}_{B_{k1}} d_{1k} \tag{5.27}$$

$$y_k = \underbrace{\begin{bmatrix}1 & 0 & 0\end{bmatrix}}_{C_{k1}} \begin{bmatrix} i_{2_k} \\ i_{1_k} \\ V_{dif_k} \end{bmatrix} + \underbrace{\begin{bmatrix}0\end{bmatrix}}_{D_{k1}} V'_k \tag{5.28}$$

From this model, Equation 5.18 can be used to obtain the first set of discrete dynamic equations for the complete closed-loop system (for the states of the PEMFC subsystem in this case):

$$\begin{aligned}
\underbrace{\begin{bmatrix} i_{2_{k+1}} \\ i_{1_{k+1}} \\ V_{dif_{k+1}} \end{bmatrix}}_{x_{k+1}} &= \underbrace{\left(\begin{bmatrix} 1 - Ts \cdot R_2/L_2 & 0 & -Ts/L_2 \\ 0 & 1 & Ts/L_1 \\ Ts/C_1 & -Ts/C_1 & 1 \end{bmatrix} - \begin{bmatrix} Ts/L_2 \\ 0 \\ 0 \end{bmatrix} \begin{bmatrix} K_1 & K_2 & K_3 \end{bmatrix} \right) \begin{bmatrix} i_{2_k} \\ i_{1_k} \\ V_{dif_k} \end{bmatrix}}_{(A_{k1} - B_{k1}K)x_k} + \\
&+ \underbrace{\begin{bmatrix} Ts/L_2 \\ 0 \\ 0 \end{bmatrix} \begin{bmatrix} K_1 & K_2 & K_3 \end{bmatrix} \begin{bmatrix} e_{i_{2_k}} \\ e_{i_{1_k}} \\ e_{V_{dif_k}} \end{bmatrix}}_{B_{k1}Ke_{x_k}} + \underbrace{\begin{bmatrix} Ts/L_2 \\ 0 \\ 0 \end{bmatrix} e_{x^d_{1k}}}_{B_{k1}e_{x^d_k}} + \underbrace{\begin{bmatrix} Ts/L_2 \\ 0 \\ 0 \end{bmatrix} k^*_{PEMFC} i^{ref}_{2_k}}_{B_{k1}k^* y^{ref}_k} = \\
&= \begin{bmatrix} 1 - \frac{Ts \cdot R_2}{L_2} - \frac{Ts \cdot K_1}{L_2} & -\frac{Ts \cdot K_2}{L_2} & -\frac{Ts}{L_2} - \frac{Ts \cdot K_3}{L_2} \\ 0 & 1 & Ts/L_1 \\ Ts/C_1 & -Ts/C_1 & 1 \end{bmatrix} \begin{bmatrix} i_{2_k} \\ i_{1_k} \\ V_{dif_k} \end{bmatrix} + \begin{bmatrix} \frac{Ts \cdot K_1}{L_2} & \frac{Ts \cdot K_2}{L_2} & \frac{Ts \cdot K_3}{L_2} \\ 0 & 0 & 0 \\ 0 & 0 & 0 \end{bmatrix} \begin{bmatrix} e_{i_{2_k}} \\ e_{i_{1_k}} \\ e_{V_{dif_k}} \end{bmatrix} + \\
&+ \begin{bmatrix} Ts/L_2 \\ 0 \\ 0 \end{bmatrix} e_{x^d_{1k}} + \begin{bmatrix} Ts/L_2 \\ 0 \\ 0 \end{bmatrix} k^*_{PEMFC} i^{ref}_{2_k}
\end{aligned} \tag{5.29}$$

Giving room to the following system of equations:

$$\begin{cases}
i_{2_{k+1}} = (1 - \frac{Ts(R_2+K_1)}{L_2}) i_{2_k} - \frac{Ts \cdot K_2}{L_2} i_{1_k} - \frac{Ts(1+K_3)}{L_2} V_{dif_k} + \frac{Ts \cdot K_1}{L_2} e_{i_{2_k}} + \frac{Ts \cdot K_2}{L_2} e_{i_{1_k}} + \frac{Ts \cdot K_3}{L_2} e_{V_{dif_k}} + \\
+ \frac{Ts}{L_2} e_{x^d_{1k}} + \frac{Ts}{L_2} k^*_{PEMFC} i^{ref}_{2_k} \\
i_{1_{k+1}} = i_{1_k} + \frac{Ts}{L_1} V_{dif_k} \\
V_{dif_{k+1}} = \frac{Ts}{C_1} i_{2_k} - \frac{Ts}{C_1} i_{1_k} + V_{dif_k}
\end{cases} \tag{5.30}$$

Then, the states formed by the different errors need to be defined by employing the Equation 5.21:

$$\underbrace{\begin{bmatrix} e_{i_{2_{k+1}}} \\ e_{i_{1_{k+1}}} \\ e_{V_{dif_{k+1}}} \end{bmatrix}}_{e_{x_{k+1}}} = \underbrace{\left(\begin{bmatrix} 1 - Ts \cdot R_2/L_2 & 0 & -Ts/L_2 \\ 0 & 1 & Ts/L_1 \\ Ts/C_1 & -Ts/C_1 & 1 \end{bmatrix} - \begin{bmatrix} L_{obs_2} & L_{obs_3} & L_{obs_4} \end{bmatrix} \begin{bmatrix} 1 \\ 0 \\ 0 \end{bmatrix} \right) \begin{bmatrix} e_{i_{2_k}} \\ e_{i_{1_k}} \\ e_{V_{dif_k}} \end{bmatrix}}_{(A_{k1} - L_{obs} C_{k1}) e_{x_k}} +$$

$$+ \underbrace{\begin{bmatrix} Ts/L_2 \\ 0 \\ 0 \end{bmatrix} e_{x^d_{1k}}}_{B_{k1} C^d_{k1} e_{x^d_k}} = \begin{bmatrix} 1 - Ts \cdot R_2/L_2 - L_{obs_2} & 0 & -Ts/L_2 \\ -L_{obs_3} & 1 & Ts/L_1 \\ Ts/C_1 - L_{obs_4} & -Ts/C_1 & 1 \end{bmatrix} \begin{bmatrix} e_{i_{2_k}} \\ e_{i_{1_k}} \\ e_{V_{dif_k}} \end{bmatrix} + \begin{bmatrix} Ts/L_2 \\ 0 \\ 0 \end{bmatrix} e_{x^d_{1k}} \tag{5.31}$$

Ending in the last system of equations of the PEMFC subsystem:

$$\begin{cases} e_{i_{2_{k+1}}} = (1 - \frac{Ts \cdot R_2}{L_2} - L_{obs_2}) e_{i_{2_k}} - \frac{Ts}{L_2} e_{V_{dif_k}} + \frac{Ts}{L_2} e_{x^d_{1k}} \\ e_{i_{1_{k+1}}} = -L_{obs_3} e_{i_{2_k}} + e_{i_{1_k}} + \frac{Ts}{L_1} e_{V_{dif_k}} \\ e_{V_{dif_{k+1}}} = (\frac{Ts}{C_1} - L_{obs_4}) e_{i_{2_k}} - \frac{Ts}{C_1} e_{i_{1_k}} + e_{V_{dif_k}} \\ e_{x^d_{1k+1}} = e_{x^d_{1k}} - L_{obs_1} e_{i_{2_k}} \end{cases} \tag{5.32}$$

SC system

As it was carried out before for the PEMFC subsystem, the definition of the model that represents the DC-DC converter system connected to the supercapacitor is recalled here, adding the term that symbolizes the disturbance (regarding that $V'' = V_{sc} - V_{u2}$):

$$\dot{i_3} = \underbrace{\left[-R_3/L_3\right]}_{A_2} \left[i_3\right] + \underbrace{\left[1/L_3\right]}_{B_2} V'' + \underbrace{\left[1/L_3\right]}_{B_2} d_2 \tag{5.33}$$

$$y = \underbrace{\left[1\right]}_{C_2} \left[i_3\right] + \underbrace{\left[0\right]}_{D_2} V'' \tag{5.34}$$

Repeating the process, the model is discretized using the FE approach, giving room to the following state-space representation:

$$i_{3_{k+1}} = \underbrace{\left[1 - Ts \cdot R_3/L_3\right]}_{A_{2_k}} \left[i_{3_k}\right] + \underbrace{\left[Ts/L_3\right]}_{B_{2_k}} V_k'' + \underbrace{\left[Ts/L_3\right]}_{B_{2_k}} d_{2_k} \tag{5.35}$$

$$y_k = \underbrace{\left[1\right]}_{C_{2_k}} \left[i_{3_k}\right] + \underbrace{\left[0\right]}_{D_{2_k}} V_k'' \tag{5.36}$$

So by employing this model and recalling Equation 5.18 again, the first equation for this new system is obtained:

$$\underbrace{i_{3_{k+1}}}_{x_{k+1}} = \underbrace{\left(1 - \frac{Ts}{L_3}(R_3 + K_{sc})\right) i_{3_k}}_{(A_{k2} - B_{k2}K)x_k} + \underbrace{\frac{Ts}{L_3} K_{sc} e_{i_{3_k}}}_{B_{k2}Ke_{x_k}} + \underbrace{\frac{Ts}{L_3} e_{x_{2_k}^d}}_{B_{k2}C_{k2}^d e_{x_k^2}} + \underbrace{\frac{Ts}{L_3} k_{sc}^* i_{3_k}^{ref}}_{B_{k2}k^* y_k^{ref}} \tag{5.37}$$

In the same way, the errors need to be included as states, so their dynamical equations must be obtained. It is done by using Equation 5.21:

$$\underbrace{e_{i_{3_{k+1}}}}_{e_{x_{k+1}}} = \underbrace{\left(1 - \frac{Ts \cdot R_3}{L_3} - L_{obs_{sc_2}}\right) e_{i_{3_k}}}_{(A_{k2} - L_{obs}C_{k2})e_{x_k}} + \underbrace{\frac{Ts}{L_3} e_{x_{2_k}^d}}_{B_{k2}C_{k2}^d e_{x_k^d}} \tag{5.38}$$

$$\underbrace{e_{x_{2_{k+1}}^d}}_{e_{x_{k+1}^d}} = \underbrace{e_{x_{2_k}^d}}_{e_{x_k^d}} - \underbrace{L_{obs_{sc_1}} e_{i_{3_k}}}_{L_{obs_k}^d C_k 2 e_{x_k}} \tag{5.39}$$

State-space models for both systems

From the equations derived in the previous subsections, two state-space representations can be obtained:

- For the PEMFC subsystem, the state space matrices are:

$$A_{PEMFC} = \begin{bmatrix} 1-\frac{Ts(R_2+K_1)}{L_2} & -\frac{Ts\cdot K_2}{L_2} & -\frac{Ts(1+K_3)}{L_2} & \frac{Ts\cdot K_1}{L_2} & \frac{Ts\cdot K_2}{L_2} & \frac{Ts\cdot K_3}{L_2} & \frac{Ts}{L_2} \\ 0 & 1 & \frac{Ts}{L_1} & 0 & 0 & 0 & 0 \\ \frac{Ts}{C_1} & -\frac{Ts}{C_1} & 1 & 0 & 0 & 0 & 0 \\ 0 & 0 & 0 & 1-\frac{Ts\cdot R_2}{L_2}-L_{obs_2} & 0 & -\frac{Ts}{L_2} & \frac{Ts}{L_2} \\ 0 & 0 & 0 & -L_{obs_3} & 1 & \frac{Ts}{L_1} & 0 \\ 0 & 0 & 0 & \frac{Ts}{C_1}-L_{obs_4} & -\frac{Ts}{C_1} & 1 & 0 \\ 0 & 0 & 0 & 0 & 0 & 0 & 1 \end{bmatrix}$$

$$B_{PEMFC} = \begin{bmatrix} \frac{Ts\cdot k^*_{PEMFC}}{L_2} \\ 0 \\ 0 \\ 0 \\ 0 \\ 0 \\ 0 \end{bmatrix} \quad C_{PEMFC} = \begin{bmatrix} 1 & 0 & 0 & 0 & 0 & 0 & 0 \end{bmatrix} \quad D_{PEMFC} = \begin{bmatrix} 0 \end{bmatrix} \tag{5.40}$$

- For the SC subsystem, the state space matrices would be:

$$A_{SC} = \begin{bmatrix} 1-\frac{Ts(R_3+K_{sc})}{L_3} & \frac{Ts\cdot K_{sc}}{L_3} & \frac{Ts}{L_3} \\ 0 & 1-\frac{Ts\cdot R_3}{L_3}-L_{obs_{sc_2}} & \frac{Ts}{L_3} \\ 0 & -L_{obs_{sc_1}} & 1 \end{bmatrix}$$

$$B_{SC} = \begin{bmatrix} \frac{Ts\cdot k^*_{SC}}{L_3} \\ 0 \\ 0 \end{bmatrix} \quad C_{SC} = \begin{bmatrix} 1 & 0 & 0 \end{bmatrix} \quad D_{SC} = \begin{bmatrix} 0 \end{bmatrix} \tag{5.41}$$

Models order reduction

Once both models for the two subsystems in closed-loop are derived, in order to simplify the control design and reduce the controller order, the state-space representations of both systems will be reduced, by employing implicit balancing techniques regarding the Hankel singular values [26], so that the states with relatively small Hankel SV can be safely discarded [7]. To implement this functionality, MATLAB® has been used, concretely the **balred** [6] function.

It basically needs as inputs the model to reduce and the target order, so for our systems, after carrying out some experiments, it has been chosen an order of 3 states for the PEMFC subsystem, and a first order for the supercapacitor system.

The following models are obtained:

- For the PEMFC system (regarding that still $y_{PEMFC_k} = i_{2_k}$):

$$\begin{bmatrix} x_{1_{k+1}} \\ x_{2_{k+1}} \\ x_{3_{k+1}} \end{bmatrix} = \underbrace{\begin{bmatrix} 0.9863 & -0.0008 & 0.1066 \\ -0.0068 & 1.0287 & -0.2641 \\ 0.0294 & 0.0783 & 0.7810 \end{bmatrix}}_{A^r_{PEMFC}} \begin{bmatrix} x_{1_k} \\ x_{2_k} \\ x_{3_k} \end{bmatrix} + \underbrace{\begin{bmatrix} 0.1557 \\ -0.0179 \\ -0.1736 \end{bmatrix}}_{B^r_{PEMFC}} i^{ref}_{2_k} \tag{5.42}$$

$$y_{PEMFC_k} = \underbrace{\begin{bmatrix} 0.1664 & -0.0191 & -0.1856 \end{bmatrix}}_{C^r_{PEMFC}} \begin{bmatrix} x_{1_k} \\ x_{2_k} \\ x_{3_k} \end{bmatrix} + \underbrace{\begin{bmatrix} 0 \end{bmatrix}}_{D^r PEMFC} i^{ref}_{2_k} \tag{5.43}$$

- For the SC system (taking into consideration that $y_{SC_k} = i_{3_k}$):

$$\begin{bmatrix} x_{4_{k+1}} \end{bmatrix} = \underbrace{\begin{bmatrix} 0.8041 \end{bmatrix}}_{A^r_{SC}} \begin{bmatrix} x_{4_k} \end{bmatrix} + \underbrace{\begin{bmatrix} 0.2105 \end{bmatrix}}_{B^r_{SC}} i^{ref}_{3_k} \tag{5.44}$$

$$y_{SC_k} = \underbrace{\begin{bmatrix} 1 \end{bmatrix}}_{C^r_{SC}} \begin{bmatrix} x_{4_k} \end{bmatrix} + \underbrace{\begin{bmatrix} 0 \end{bmatrix}}_{D^r SC} i^{ref}_{3_k} \tag{5.45}$$

By substituting the corresponding values of the parameters of the SC model state-space matrices at 5.41, it stands out that $x_{4_k} = i_{3_k}$, as the values obtained for the reduced model match the ones located at the corresponding column/row for i_{3_k} at the SC model matrices.

In order to check the goodness of the approximation made by using the reduced models, the frequency response of the original system is compared with the frequency response of the reduced model (Figure 5.2), for each one of the subsystems).

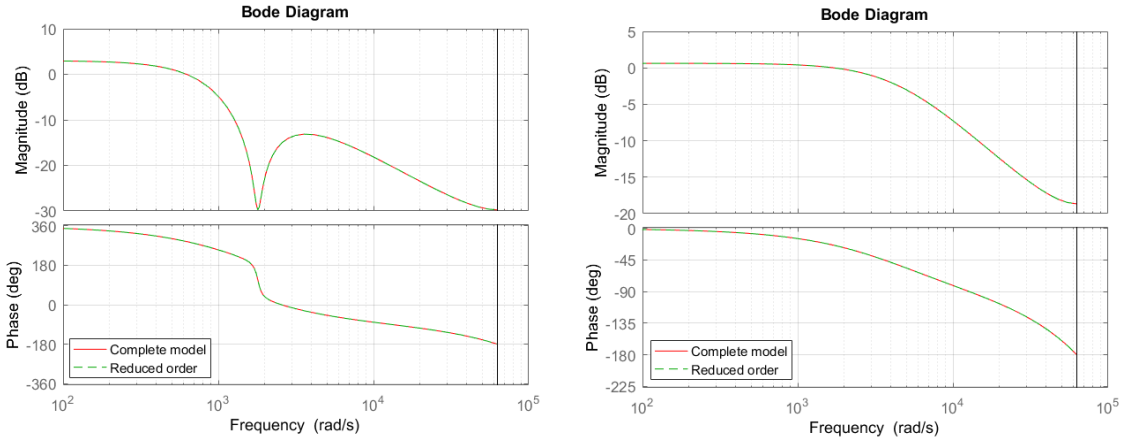

Figure 5.2: Frequency response of the comparions between original/reduced models (PEMFC subsystem at the left - SC at the right)

Bus voltage dynamic equation

From the theoretical insight about the complete system given at Section 5.1, the dynamic equation for the bus voltage can be derived from the previous subsystems and their respective relation with the bus, as well as from the insertion of a term which reflects the difference between the entering and outgoing currents:

$$\dot{V_{bus}} = \frac{1}{C_{bus}}\left(i_2\frac{V_{u1}}{V_{bus}} + i_3\frac{V_{u2}}{V_{bus}}\right) - \Delta i_{load} \tag{5.46}$$

It could be discretized as before, giving room to the following equation:

$$V_{bus_{k+1}} = V_{bus_k} + \frac{Ts}{C_{bus}}\left(i_{2_k}\frac{V_{u1}}{V_{bus_k}} + i_{3_k}\frac{V_{u2}}{V_{bus_k}}\right) - \Delta i_{load_k} \tag{5.47}$$

As it can be appreciated, this relation among the bus voltage drop and the currents of both subsystems presents several non-linear terms involving products of these variables.
To handle this situation, an important approximation is carried out: each on of the terms $\frac{V_{u1}}{V_{bus_k}}$ and $\frac{V_{u2}}{V_{bus_k}}$ is considered as a parameter, c_{con1} and c_{con2} respectively.
Taking this into account, these two values will be considered as variable inside a studied range, so the control parameters (controller gain, observer gain, k^* and even the state-space model matrix A_k) become dependent of c_{con1} and c_{con2}. In this way, we are defining the polytope to employ the LPV (Linear Varying Parameters) [33] technique to the control of V_{bus_k}.
For this case, these parameters are ranged from 0.35 to 0.6 for c_{con1}, and from 0.35 to 0.65 for

c_{con2}, obtaining these values by observation of the minimums and maximums reached by these two at several experiments.

It must be pointed out that due to the LPV internal loops (the parameters values are needed to get the control elements to carry a simulation to get the values), both parameters need to be initialized. The selected values are 0.4063 ($\frac{32.5}{80}$) for c_{con1} and 0.4375 ($\frac{35}{80}$) for c_{con2}, achieving them by using the nominal values in the parameters formula.

Moreover, the term which represents the difference between entering and outgoing currents (Δi_{load}) will be considered as a disturbance for the control system design, so the bus voltage dynamic equation employed to set the complete system results as follows:

$$V_{bus_{k+1}} = V_{bus_k} + \frac{Ts}{C_{bus}}\Big(i_{2_k} c_{con1} + i_{3_k} c_{con2}\Big) \tag{5.48}$$

And regarding the model reduction previously explained, the equation can be represented using the new state variables by employing the relations at 5.43 and 5.45 respectively:

$$V_{bus_{k+1}} = V_{bus_k} + \frac{Ts}{C_{bus}}\Big(Cr^r_{PEMFC}(1) x_{1_k} c_{con1} + Cr^r_{PEMFC}(2) x_{2_k} c_{con1} + Cr^r_{PEMFC}(3) x_{3_k} c_{con1} + \\ + Cr^r_{SC} x_{4_k} c_{con2}\Big) \tag{5.49}$$

Complete system

From 5.42, 5.43, 5.44, 5.45 and 5.49, a model for the complete system, composed by both subsystems (PEMFC and SC) and the bus voltage equation relating them, can be obtained. Its matrices are presented at Equation 5.50.

$$A^c = \begin{bmatrix} A^r_{PEMFC}(1,1) & A^r_{PEMFC}(1,2) & A^r_{PEMFC}(1,3) & 0 & 0 \\ A^r_{PEMFC}(2,1) & A^r_{PEMFC}(2,2) & A^r_{PEMFC}(2,3) & 0 & 0 \\ A^r_{PEMFC}(3,1) & A^r_{PEMFC}(3,2) & A^r_{PEMFC}(3,3) & 0 & 0 \\ 0 & 0 & 0 & A^r_{SC} & 0 \\ \frac{Ts}{Cbus}c_{con1}C^r_{PEMFC}(1) & \frac{Ts}{Cbus}c_{con1}C^r_{PEMFC}(2) & \frac{Ts}{Cbus}c_{con1}C^r_{PEMFC}(3) & \frac{Ts}{Cbus}c_{con2}C^r_{SC} & 1 \end{bmatrix}$$

$$B^c = \begin{bmatrix} B^r_{PEMFC}(1) & 0 \\ B^r_{PEMFC}(2) & 0 \\ B^r_{PEMFC}(3) & 0 \\ 0 & B^r_{SC} \\ 0 & 0 \end{bmatrix} \quad C^c = \begin{bmatrix} 0 & 0 & 0 & 0 & 1 \end{bmatrix} \quad D^c = \begin{bmatrix} 0 & 0 \end{bmatrix} \tag{5.50}$$

For this complete model, the output y_{c_k} is V_{bus_k}, as it is the variable to control.

5.2.2 Controller design

Theoretical framework

The mathematical developments used to explain the controller design process can be found in **Chapter 3 - Section 3.2 - Subsection 3.2.2**, as it is an analogue design.

Nevertheless, for this case, due to the inclusion of LPV in the V_{bus_k} control, the main features of this technique must be explained.

Opposite to the process for obtaining a robust controller against uncertainties (used in the aforementioned section) in which one LMI is solved involving four constraints (besides $P > 0$) to get a controller that is valid at the extreme cases (so it is also robust for uncertainties whose value belongs to the ranges defined by those extreme cases); when using LPV (regarding there are only two considered parameters as at this problem), four LMIs are solved, one for each extreme case of the polytope, so that the control elements adapt their values depending on the parameters.

That is, instead of computing only one K (the observer parameters, as well as k^*, face the

same issue but they will be commented at Section 4.2 - Subsection 4.2.3), four values for each design parameter are calculated, so the actual one is worked out as a proportion of the four aforementioned values, and the weights to compute this proportion come from the actual values of the LPV parameters (c_{con1} and c_{con2} in this case).

The main advantage of using LPV resides in the fact that the approximation which was employed during the state-space model about considering c_{con1} and c_{con2} as constants is reduced, and due to the LPV computation of the control parameters, for every combination of c_{con1} and c_{con2}, the control system would be approximately the one that could be obtained for those values of the LPV parameters.

Application to design

For the controller gain K obtaining, the $\mathbb{D}_{q,r}$ - LMI parameters r and q are set to 0.09 and -0.9 respectively, so that the V_{bus} control dynamics are faster than the ones for the V_{sc} (that will be explained in Section 5.2.5.

Before presenting the results, it is worth to mention that for these four values of K (for the extreme cases in the polytope) and the rest of the control parameters, the combination of values (minimum or maximum) for the LPV parameters is $(c_{con1}^{max}, c_{con2}^{min})$ for the first presented set of values, $(c_{con1}^{min}, c_{con2}^{min})$ for the second, $(c_{con1}^{max}, c_{con2}^{max})$ for the third and $(c_{con1}^{min}, c_{con2}^{max})$ for the fourth and last one.

For these settings, the four values of K are obtained as:

$$
\begin{aligned}
K\{1\} &= \begin{bmatrix} 0.0319 & 0.0413 & -0.0438 & 0.0052 & 0.0618 \\ 0.0679 & 0.0157 & 0.0119 & -0.4068 & 0.9140 \end{bmatrix} \\
K\{2\} &= \begin{bmatrix} 0.0281 & 0.0398 & -0.0436 & 0.0032 & 0.0375 \\ 0.0412 & 0.0095 & 0.0072 & -0.4041 & 0.9475 \end{bmatrix} \\
K\{3\} &= \begin{bmatrix} 0.0276 & 0.0396 & -0.0433 & 0.0024 & 0.0190 \\ 0.0391 & 0.0089 & 0.0062 & -0.4079 & 0.5442 \end{bmatrix} \\
K\{4\} &= \begin{bmatrix} 0.0265 & 0.0392 & -0.0432 & 0.0014 & 0.0112 \\ 0.0230 & 0.0052 & 0.0037 & -0.4075 & 0.5483 \end{bmatrix}
\end{aligned}
\tag{5.51}
$$

In the LPV case, it is necessary to check that the $\mathbb{D}$-stabilization problem requirements have been accomplished for the four extreme cases of the polytope. As it was carried out in previous

sections, the maximum absolute value of the closed-loop poles would be checked, so that it resides in the unitary circle:

$$\begin{aligned} CL_{pole}^{max}\{1\} = 0.9864 \quad CL_{pole}^{max}\{2\} = 0.9866 \\ CL_{pole}^{max}\{3\} = 0.9854 \quad CL_{pole}^{max}\{4\} = 0.9855 \end{aligned} \tag{5.52}$$

The resultant poles are located inside the area defined at the $\mathbb{D}$-stabilization problem, so the properness of the poles with respect to the design requisites is checked.
The control system without observer is not simulated here, and neither the k^* is computed for this system. The simulations will be carried out at the next subsection.

5.2.3 Observer design

Theoretical framework

The more general concepts of the observer design using LMIs were also explained in previous chapters, concretely in **Chapter 3 - Section 3.2 - Subsection 3.2.3**, so they will not be repeated here again.
Regarding some issues about the inclusion of LPV to manage the variation of the parameters c_{con1} and c_{con2}, it is important to remark that, as it was done for the controller gain K, the observer gain L, the scaling term k^* and even the state-space matrix A need to be scheduled during the simulation (or real system functioning) depending on the values of the LPV parameters. The mentioned A matrix is computed due to its use inside the observer block. However, if the LPV parameters had appeared in other state-space matrices, they would have been scheduled too.
About the scaling term k^*, it is not obtained as in the previous sections due to the nature of LPV. Instead of computing four values of this parameter and schedule it during the simulation, the k^* value at each simulation instant is computed using the theoretical concepts explained in the aforementioned section, inside the simulation loop, obtaining more precise value at the cost of a computationally heavier simulation.

Application to design

For the observer case for the V_{bus} control system design, the $\mathbb{D}$-stabilization parameters r and q are set to 0.9999 and 0 respectively. Therefore, the LMI will only assure stability (poles inside the unitary circle) for the observer, but we will not impose dynamics to it, because it causes

some stability problems.

The resulting observer gain L results as follows (using the template presented for the controller gain K in the previous section, and regarding the combinations of LPV parameters values explained there too):

$$\begin{aligned} L^T\{1\} &= \begin{bmatrix} 0.0015 & 0.4305 & 0.0177 & -0.0101 & -0.0001 & 0.4250 & 0.9800 \end{bmatrix} \\ L^T\{2\} &= \begin{bmatrix} 0.0009 & 0.4310 & 0.0103 & -0.0059 & -0.0000 & 0.4255 & 0.9800 \end{bmatrix} \\ L^T\{3\} &= \begin{bmatrix} 0.0014 & 0.4357 & 0.0161 & -0.0086 & 0.0001 & 0.4310 & 0.9854 \end{bmatrix} \\ L^T\{4\} &= \begin{bmatrix} 0.0008 & 0.4360 & 0.0094 & -0.0050 & 0.0001 & 0.4313 & 0.9854 \end{bmatrix} \end{aligned} \tag{5.53}$$

To check that the stability requirement of having the poles inside the unitary circle is fulfilled, the method employed alongside this document is recalled, obtaining the following maximum closed loop poles for each one of the polytope points:

$$\begin{aligned} CL_{pole}^{max}\{1\} = 0.9970 \quad CL_{pole}^{max}\{2\} = 0.9969 \\ CL_{pole}^{max}\{3\} = 0.9943 \quad CL_{pole}^{max}\{4\} = 0.9943 \end{aligned} \tag{5.54}$$

Simulation

Recalling the methodology followed in previous chapters, the averaged system is tested before carrying out the final checking with the switched model.

However, from this point on, the averaged model will not be used anymore, as it has been only a middle-point test bench utilized until a sufficiently proper control was reached, or to debug the controllers when they were not suitable for the switched one yet.

The following Simulink® model was employed to carry out the simulations for the tests.

The implemented system emulating the plant is at the left of Figure 5.3: at the top the PEMFC subsystem can be found (as it was depicted in Chapter 3), at the bottom it is presented the SC subsystem (the same but for Chapter 4), and at between them there is a representation of the bus by using the bus capacitor (from which the bus voltage is measured) and a current source whose value is defined by the last equation in Equation 5.1, computed using the pink block located at the bottom right corner of the image (it also generates the LPV scheduling parameters c_{con1} and c_{con2}), showed in detail at Figure 5.4.

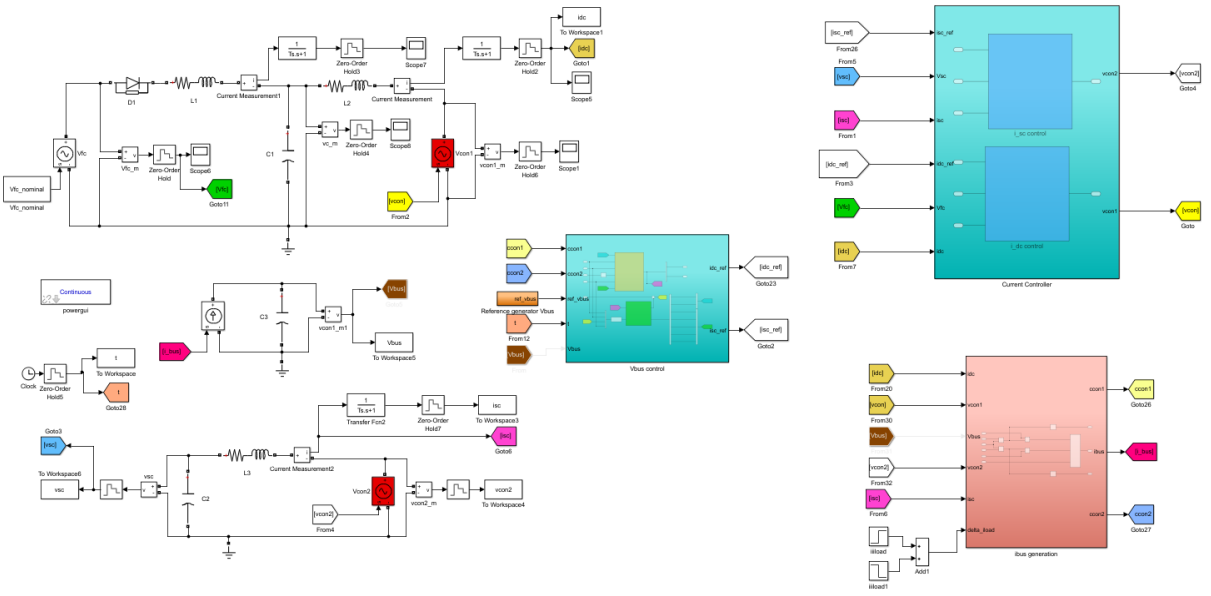

Figure 5.3: Averaged model of the complete system

Regarding the two blue blocks, they are the system controllers: the one at the centre of the picture acts as the V_{bus} controller (Figure 5.5), while the other is storing the currents (i_2 and i_3) controllers (Figure 5.6). It is interesting how the computation of K, L and k^* is carried out using functions instead of gains (these functions are the scheduling algorithms).

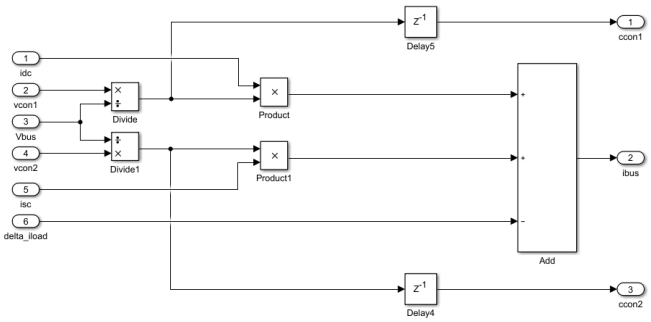

Figure 5.4: i_{bus} and LPV scheduling parameters generator

For the currents control system block showed in the aforementioned figure, the controller/observer blocks are not repeated because they are the same than the ones presented in Figure 3.9 and Figure 4.5. However, it is important to comment the use of a saturation (min. 0 A - max. 50 A for i_2 / min. -50 A - max. 50 A for i_3) and its associated anti-windup [1] structure to avoid the controller accumulating error.

For the simulation, the reference signal profile for V_{bus} is shown in Table 5.1.

Time period (s)	**Setpoint value (V)**
$t \in [0, 0.2)$	80
$t \in [0.2, 0.4)$	85
$t \in [0.4, 0.6)$	80
$t \in [0.6, 0.8)$	75
$t \in [0.8, 1)$	80

Table 5.1: Reference profile for the switched system with one reference simulation

There is also a disturbance in the current of the bus of -1 A at t = 0.5 s, and it disappears at t = 0.7 s. The results are presented at Figure 5.7.

It can be appreciated how the overall functioning of the control system is quite good: the output reaches the reference with no steady-state error, with a proper performance and the aforementioned disturbances are perfectly rejected (the control system responds increasing i_3 and i_2 when there is a extraction of current in t = 0.5 s, so that V_{bus} does not end falling; and vice versa at t = 0.7 s).

However, at the initial stage of the simulation, V_{bus} falls because i_2 does not behave completely in the proper manner.

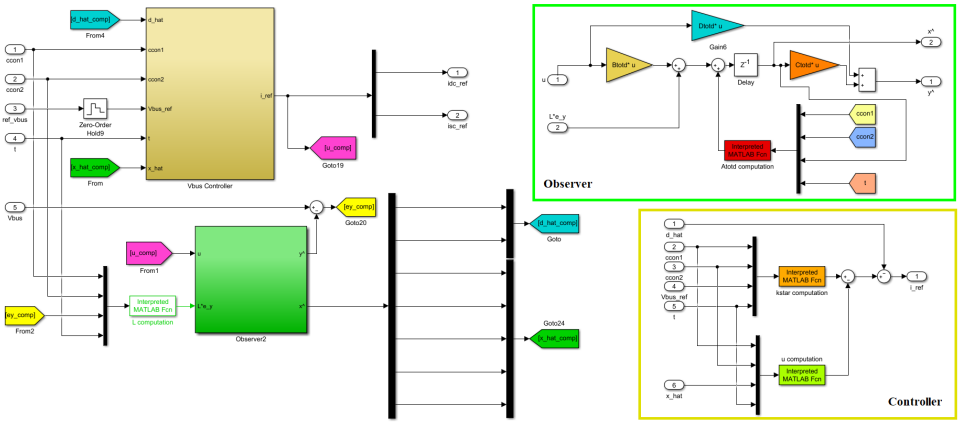

Figure 5.5: V_{bus} control system

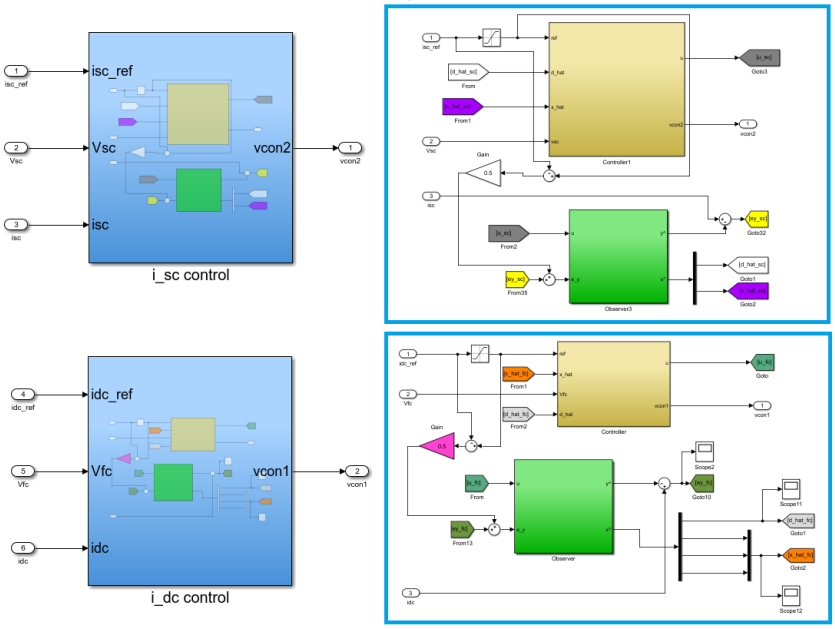

Figure 5.6: i_2 and i_3 control systems

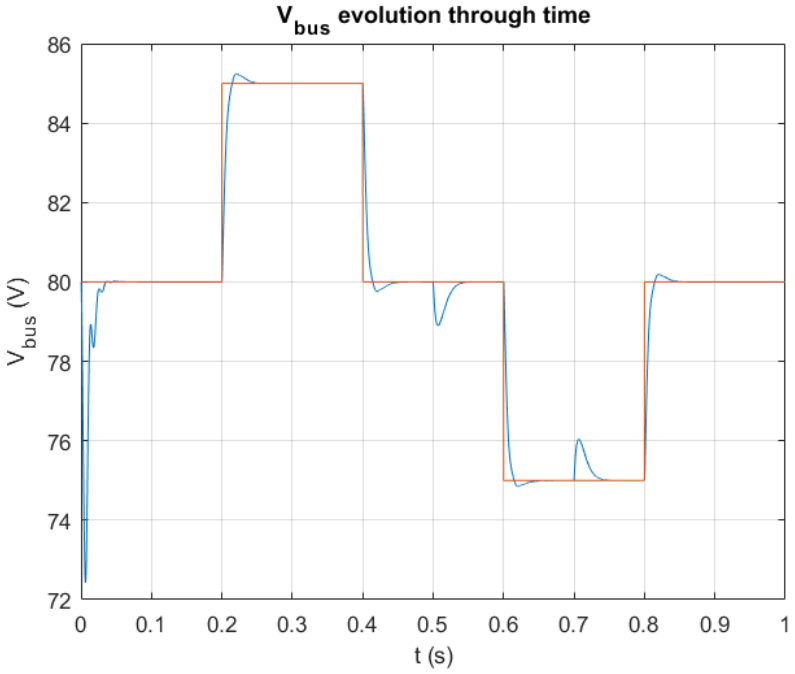

Figure 5.7: V_{bus} (averaged system)

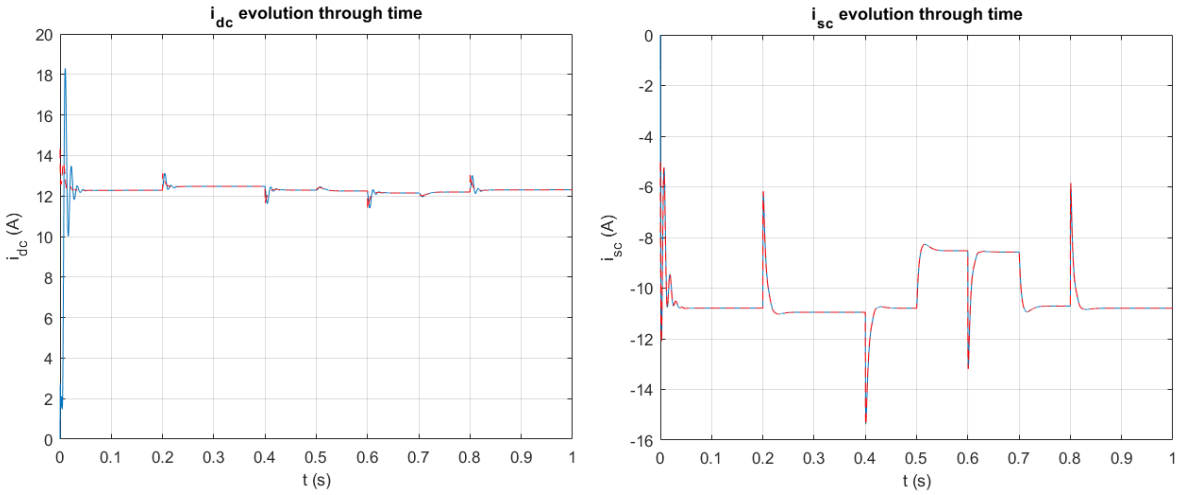

Figure 5.8: i_2 and i_3 (averaged system)

5.2.4 Testing with the switched model

The same simulation must be carried out using the more realistic switched model, so that the similarities between this virtual plant and the real system allow us to be sure about the controllers goodness before testing them.

Some changes are necessary in the Simulink® in order to adapt the one used for the averaged model to the switched one. It can be found in Figure 5.9.

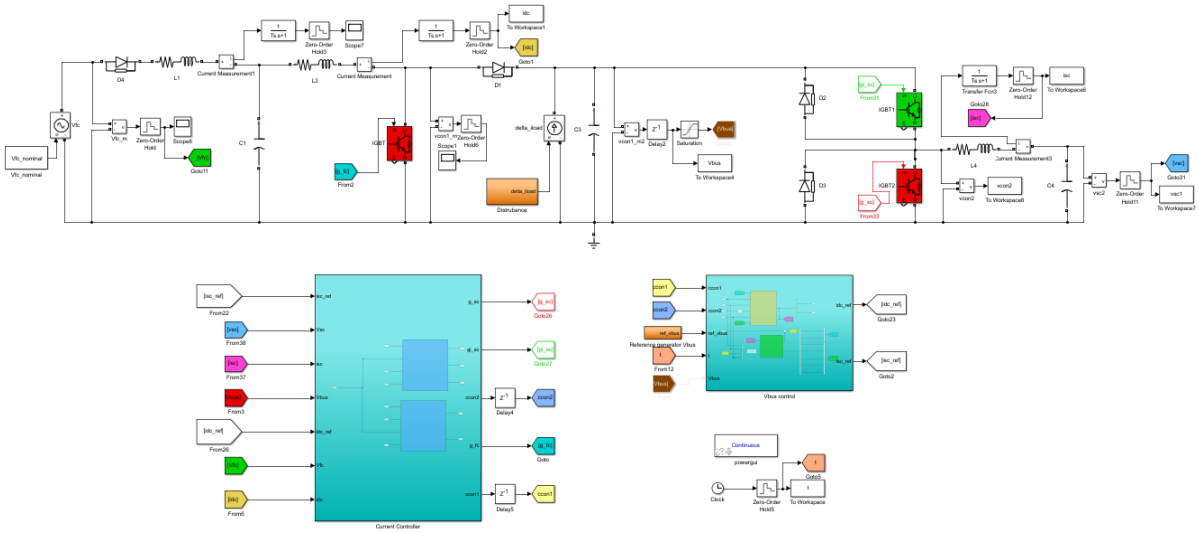

Figure 5.9: Switched model of the complete system

The virtual plant is not splitted: both PEMFC and SC subsystems are electrically connected by means of the DC bus. Therefore, the pink block at Figure 5.3 is not used anymore, as it was used to implement the bus dynamic equation, which for the switched model is implemented by construction.

About the controller subsystems, the only difference is the utilization of the PWM-generator of Figure 3.12, as well as its associated controller subsystems (with the proper conversion of the control signals V_{u1} and V_{u2} to D_1 and D_2 respectively). This generation of the PWM outputs is done inside the two blue blocks.

By implementing the same reference profile for the bus voltage than the one presented in Table 5.1, the results are presented at Figure 5.10 and Figure 5.11.

In this case, the disturbance profile is the opposite: an inlet current of 1 A enters the system at $t = 0.5s$, and it disappears in $t = 0.7s$.

Despite the performance is quite similar for the bus voltage, the reference tracking is not properly working in i_2. Due to the increase in complexity which arises when computing a reference signal for each one of the currents; and taking into consideration these results, it is decided to change the control system so that a reference signal for both currents is computed, and then it is divided for each one of them by means of a discrete filter [5], taking advantage of the fact that the PEMFC should be working only at low frequencies.

The main results of this new control structure are presented in the next subsections.

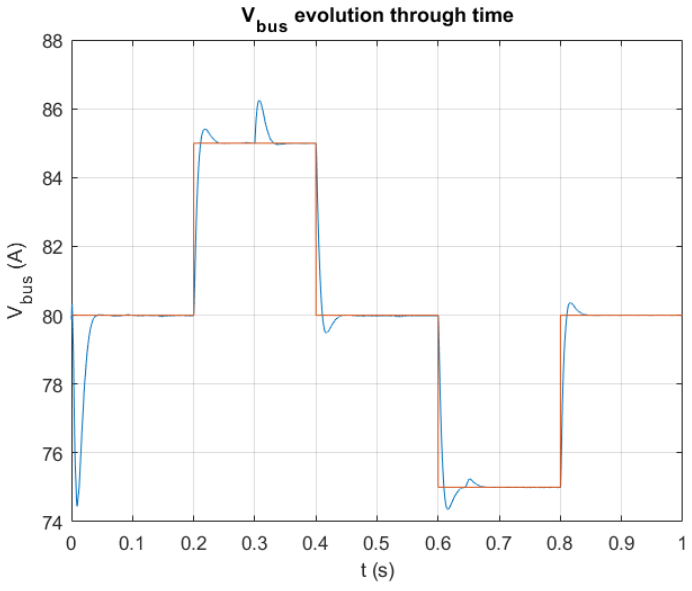

Figure 5.10: V_{bus} (switched system)

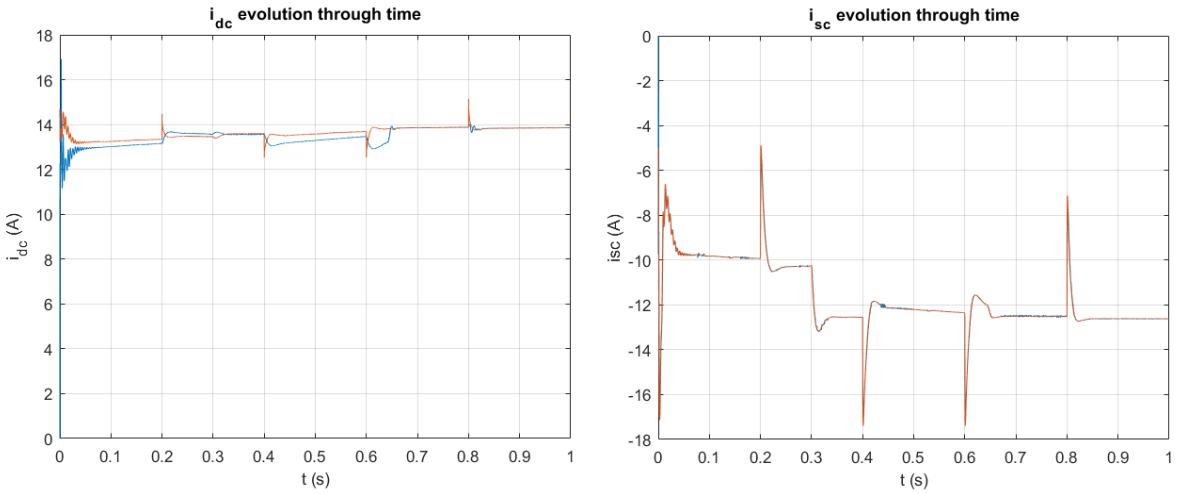

Figure 5.11: i_2 and i_3 (switched system)

Complete system: one reference signal

The state-space model presented at Equation 5.50 is modified to represent a system in which there is only one current reference input (the same for both i_2 and i_3) called i^{ref}:

$$A^c = \begin{bmatrix} A^r_{PEMFC}(1,1) & A^r_{PEMFC}(1,2) & A^r_{PEMFC}(1,3) & 0 & 0 \\ A^r_{PEMFC}(2,1) & A^r_{PEMFC}(2,2) & A^r_{PEMFC}(2,3) & 0 & 0 \\ A^r_{PEMFC}(3,1) & A^r_{PEMFC}(3,2) & A^r_{PEMFC}(3,3) & 0 & 0 \\ 0 & 0 & 0 & A^r_{SC} & 0 \\ \frac{Ts}{Cbus} c_{con1} C^r_{PEMFC}(1) & \frac{Ts}{Cbus} c_{con1} C^r_{PEMFC}(2) & \frac{Ts}{Cbus} c_{con1} C^r_{PEMFC}(3) & \frac{Ts}{Cbus} c_{con2} C^r_{SC} & 1 \end{bmatrix}$$

$$B^c = \begin{bmatrix} B^r_{PEMFC}(1) \\ B^r_{PEMFC}(2) \\ B^r_{PEMFC}(3) \\ B^r_{SC} \\ 0 \end{bmatrix} \quad C^c = \begin{bmatrix} 0 & 0 & 0 & 0 & 1 \end{bmatrix} \quad D^c = \begin{bmatrix} 0 \end{bmatrix} \tag{5.55}$$

Again, the output is V_{bus_k}.

Controller design: application

For the controller gain K obtaining, the $\mathbb{D}_{q,r}$ - LMI parameters r and q are set to 0.09 and -0.875 respectively, looking for even faster dynamics than before.
For these settings, the four values of K are obtained as:

$$\begin{aligned} K\{1\} &= \begin{bmatrix} 0.6100 & 0.2286 & -0.0094 & 0.1802 & 6.3334 \end{bmatrix} \\ K\{2\} &= \begin{bmatrix} 0.5048 & 0.1852 & 0.0020 & 0.2647 & 8.9068 \end{bmatrix} \\ K\{3\} &= \begin{bmatrix} 0.4866 & 0.1788 & 0.0030 & 0.2758 & 4.9839 \end{bmatrix} \\ K\{4\} &= \begin{bmatrix} 0.3740 & 0.1320 & 0.0156 & 0.3664 & 6.4702 \end{bmatrix} \end{aligned} \tag{5.56}$$

The properness of the obtained controller gains to get stable closed-loop systems that fulfil the requirements is evaluated as previously:

$$\begin{aligned} CL_{pole}^{max}\{1\} = 0.9454 \quad CL_{pole}^{max}\{2\} = 0.9456 \\ CL_{pole}^{max}\{3\} = 0.9456 \quad CL_{pole}^{max}\{4\} = 0.9457 \end{aligned} \tag{5.57}$$

The resultant poles are located inside the area defined at the $\mathbb{D}$-stabilization problem, so the properness of the poles with respect to the design requisites is checked.

Observer design: application

For the observer case, the $\mathbb{D}$-stabilization parameters r and q are set to 0.999 and 0 respectively. Therefore, the LMI assures stability (poles inside the unitary circle) for the observer, as well as dynamics slightly faster than the previous ones.
The resulting observer gain L results as follows:

$$\begin{aligned} L^T\{1\} &= \begin{bmatrix} 0.6665 & 3.6230 & -0.0069 & -0.0654 & 0.7236 & 1.0476 \end{bmatrix} \\ L^T\{2\} &= \begin{bmatrix} 0.6656 & 3.7461 & -0.1287 & -0.0941 & 0.7212 & 1.0335 \end{bmatrix} \\ L^T\{3\} &= \begin{bmatrix} 0.6789 & 3.2812 & 0.2276 & -0.0429 & 0.7360 & 1.0586 \end{bmatrix} \\ L^T\{4\} &= \begin{bmatrix} 0.6845 & 3.4064 & 0.1365 & -0.0641 & 0.7403 & 1.0486 \end{bmatrix} \end{aligned} \tag{5.58}$$

The stability requirement is checked to be fulfilled, obtaining:

$$\begin{aligned} CL_{pole}^{max}\{1\} = 0.9833 \quad CL_{pole}^{max}\{2\} = 0.9889 \\ CL_{pole}^{max}\{3\} = 0.9764 \quad CL_{pole}^{max}\{4\} = 0.9839 \end{aligned} \tag{5.59}$$

Simulation

The Simulink® model in Figure 5.9 is slightly modified to use the new control structure. However, this modifications only affect some multiplexors, the LPV scheduling functions and the output of the V_{bus} controller, so the scheme is not quite different from the one at Figure 5.9 (this modifications will be present in the schemes of the next section).
However, before presenting the results of the performance, the filter used to adapt the reference for the PEMFC current from the computed reference for both subsystems is presented in Figure 5.12. It is a Butterworth filter [2] of second order, generated using the *Filter Designer Application* tool [8] from MATLAB®.

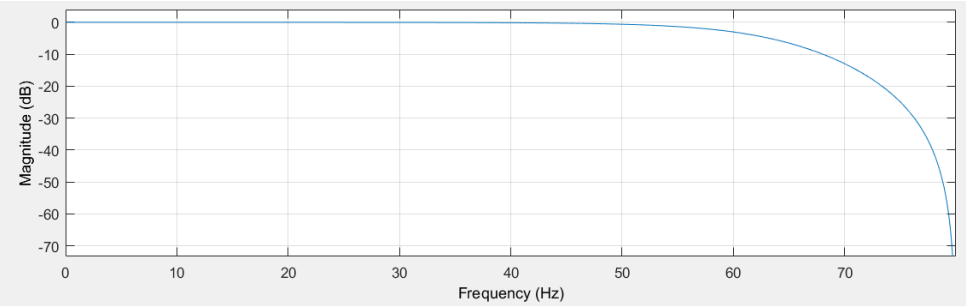

Figure 5.12: Low-pass filter for i_2^{ref}

By means of it, the frequencies higher than approximately 80 Hz (it should be between 10 Hz and 100 Hz) are neglected. The results for the new control structure are presented in Figure 5.13 and Figure 5.14. The setpoint for V_{bus} is again the one presented at Table 5.1.
Moreover, the initial instants of the reference signal are generated with a ramp, to start using simulation conditions similar to the reality. Due to this, for this simulation, the bus voltage initial value has been set to 40 V, so that at the beginning, the control system needs to manage a more complex situation. The disturbance profile is the last employed: a disturbance of 1 A enters the system at $t = 0.5s$ and it stops at $t = 0.7s$.
It can be appreciated how the performance for the bus voltage control has been improved, so that the new control structure gives better results than the previous one.

Moreover, the change in the dynamics of the controller has been adjusted to avoid surpassing the current limitations imposed to the two system currents: 50 A for i_2 (the lower limit is imposed because it is not feasible to introduce current to the PEMFC) and -50 A and 50 A for i_3.

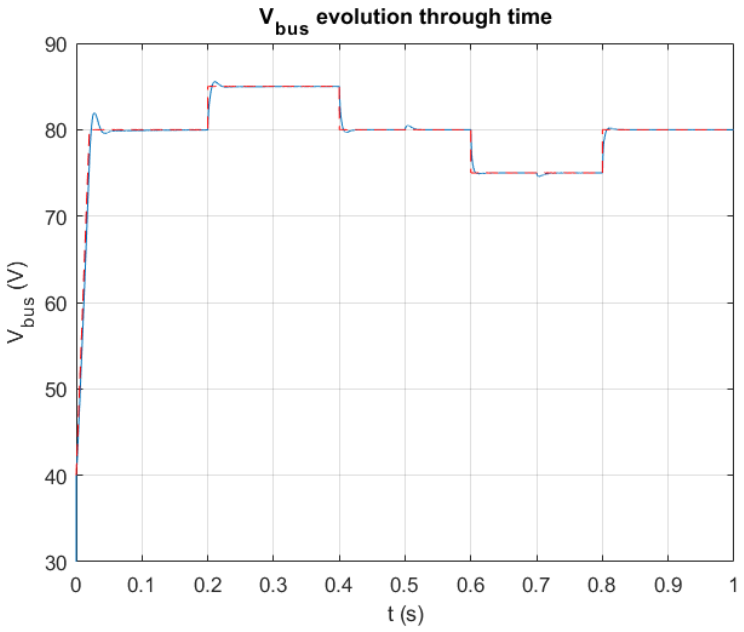

Figure 5.13: V_{bus} (switched system - one input)

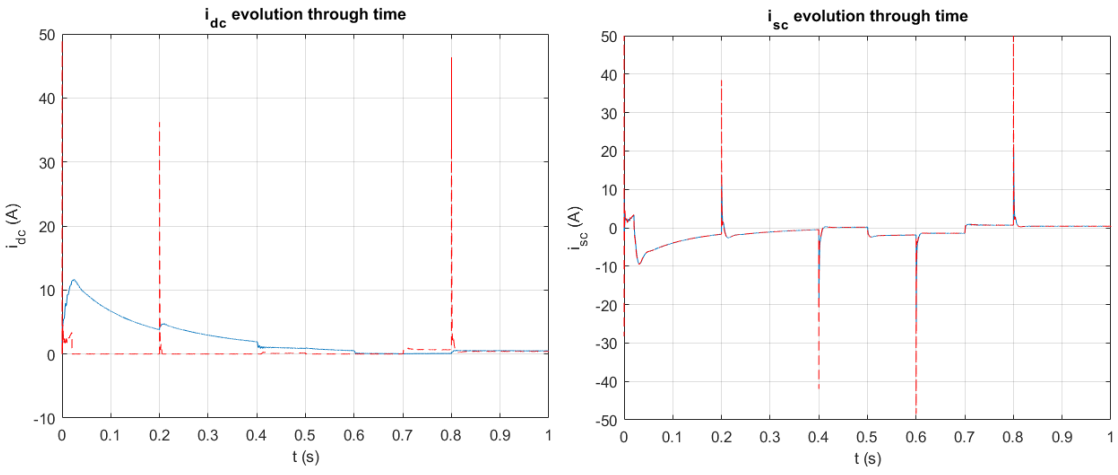

Figure 5.14: i_2 and i_3 (switched system - one input)

5.2.5 Control of the supercapacitors voltage

For several applications of the PEMFCs it would be interesting not only to manage the voltage at the bus, but also the voltage at the supercapacitors. As they store energy to supply it when it is necessary, this control will allow us to optimize the utilization of the energetic resources, even widening the PEMFC lifetime, due to its more intelligent usage.

Up to now, the designed and validated in simulation control structure can be summarised in Figure 5.15 (some of the controllers need extra data as V_{bus}, V_{fc},... They are not depicted to preserve simplicity and understandability).

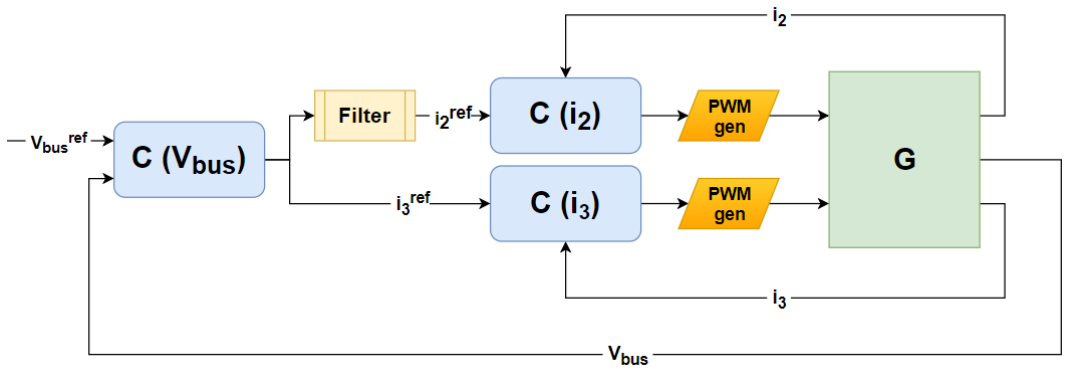

Figure 5.15: Control system general overview (only V_{bus} control)

To achieve the aforementioned advantages, a control structure for the management of the supercapacitors voltage has been developed (as it was mentioned in Chapter 2 - Section 2.2), computing a trade-off between the control of V_{bus} and V_{sc}.

State-space model generation

For the derivation of this state-space representation, the reduced models of the PEMFC and SC subsystems are recalled from Chapter 5 - Section 5.2 - Subsection 5.2.1.

For this case, instead of completing the state-space model employing the bus dynamic equation, the equation that relates the current at the supercapacitors with the derivative of its voltage is employed (Equation 5.60).

$$\frac{dV_{sc}}{dt} = -\frac{i_3}{C_{sc}} \tag{5.60}$$

By discretizing it using the FE approach, Equation 5.61 is achieved (recalling from 5.45 the

relation between the output i_{3_k} and the states in the SC subsystem).

$$V_{sc_{k+1}} = V_{sc_k} - \frac{T_s i_{3_k}}{C_{sc}} = V_{sc_k} - \frac{T_s C^r_{SC} x_{4_k}}{C_{sc}} \tag{5.61}$$

Finally, the state-space representation generated for the V_{sc} control system design is presented at Equation 5.62 and 5.63

$$\begin{bmatrix} x_{1_{k+1}} \\ x_{2_{k+1}} \\ x_{3_{k+1}} \\ x_{4_{k+1}} \\ V_{sc_{k+1}} \end{bmatrix} = \underbrace{\begin{bmatrix} A^r_{PEMFC}(1,1) & A^r_{PEMFC}(1,2) & A^r_{PEMFC}(1,3) & 0 & 0 \\ A^r_{PEMFC}(2,1) & A^r_{PEMFC}(2,2) & A^r_{PEMFC}(2,3) & 0 & 0 \\ A^r_{PEMFC}(3,1) & A^r_{PEMFC}(3,2) & A^r_{PEMFC}(3,3) & 0 & 0 \\ 0 & 0 & 0 & A^r_{SC} & 0 \\ 0 & 0 & 0 & -\frac{Ts}{C_{sc}} C^r_{SC} & 1 \end{bmatrix}}_{A^c_{sc}} \begin{bmatrix} x_{1_k} \\ x_{2_k} \\ x_{3_k} \\ x_{4_k} \\ V_{sc_k} \end{bmatrix} + \underbrace{\begin{bmatrix} B^r_{PEMFC}(1) & 0 \\ B^r_{PEMFC}(2) & 0 \\ B^r_{PEMFC}(3) & 0 \\ 0 & B^r_{SC} \\ 0 & 0 \end{bmatrix}}_{B^c_{sc}} \begin{bmatrix} i^{ref}_{2_k} \\ i^{ref}_{3_k} \end{bmatrix} \tag{5.62}$$

$$y_{c_k} = \underbrace{\begin{bmatrix} 0 & 0 & 0 & 0 & 1 \end{bmatrix}}_{C^c_{sc}} \begin{bmatrix} x_{1_k} \\ x_{2_k} \\ x_{3_k} \\ x_{4_k} \\ V_{sc_k} \end{bmatrix} + \underbrace{\begin{bmatrix} 0 & 0 \end{bmatrix}}_{D^c_{sc}} \begin{bmatrix} i^{ref}_{2_k} \\ i^{ref}_{3_k} \end{bmatrix} \tag{5.63}$$

Controller design

As it has been done at previous sections, the theoretical framework will not be repeated.

To achieve a suitable value for the controller gain K, the $\mathbb{D}_{q,r}$ - LMI parameters r and q are set to 0.0009 and -0.999 respectively, trying to obtain the slowest dynamics as possible. This is interesting because due to the own supercapacitors dynamics (their capacitance value is so high that the changes in the capacitors voltage are incredibly slow in comparison with the rest

of electrical variables in the system), and because it would be desirable that the V_{bus} control, which is the main task of this project, results the least affected as possible by the V_{sc} control. The obtained value of K is:

$$K_{V_{sc}} = \begin{bmatrix} -0.1804 & -0.4398 & 1.0411 & 0.0000 & 0.0000 \\ 0.0000 & 0.0000 & 0.0000 & -0.9253 & -1.9493 \end{bmatrix} \tag{5.64}$$

Checking the slowest pole of the closed loop system, it is located at:

$$CL_{pole}^{max} = 0.9999 \tag{5.65}$$

So the objective of achieving slow dynamics seems to be fulfilled.

Observer design

Again, the theoretical framework will not be repeated.
For the observer, the $\mathbb{D}$-stabilization parameters r and q are set to 0.999 and 0 respectively, like in previous cases. Hence, the observer dynamics would be slightly faster than the previous ones. The following value of observer gain L is obtained:

$$L_{V_{sc}}^{T} = \begin{bmatrix} 0.0000 & -3314.0 & 0.0000 & 0.0000 & 0.0000 & -3560.7 & 0.0013 \end{bmatrix} \tag{5.66}$$

And the slowest pole of the observer results to be:

$$CL_{pole_{obs}}^{max} = 0.9992 \tag{5.67}$$

Therefore, our control requirements are fulfilled in design.

Reference signal distribution

As it was introduced in Chapter 2 - Section 2.2), the currents reference generated by both the V_{sc} and V_{bus} controls would be different, so it is not possible to perfectly control both variables at the same time.
Due to this fact, a trade-off in their control must be done, giving priority to one of them over the other, and choosing the proportion of this provided importance.
To develop this idea, a parameter called α is defined as distributive parameter, being the responsible of setting the aforementioned proportion.

The algorithm used to carry out the division is the one presented at Equation 5.68 (it has been explained in previous sections the usage of the filter, so for the equations understanding, the filtered current reference signal coming from the V_{bus} control would be called $i_{V_{bus}}^{ref^{filt}}$).

$$\begin{cases} i_2^{ref} = \alpha i_{V_{bus}}^{ref^{filt}} + (1-\alpha) i_{2_{V_{sc}}}^{ref} \\ i_3^{ref} = \alpha i_{V_{bus}}^{ref} + (1-\alpha) i_{3_{V_{sc}}}^{ref} \end{cases} \tag{5.68}$$

Opposite to what was done for the V_{bus} control, it can be appreciated how for the V_{sc} control, a reference signal for each one of the currents is generated. In this case, the calculation of these two different setpoints does not deteriorate the performance, as it happened when designing the V_{bus} controller. Hence, there is not necessity for another filter to divide the reference for the two currents.

In this way, the general overview of the control structure presented in Figure 5.15 is updated with this new control loop, resulting in the diagram at Figure 5.16

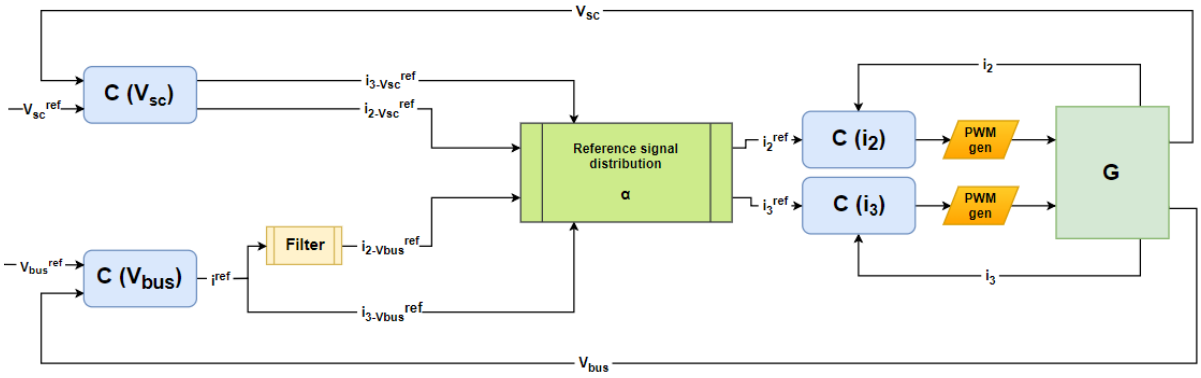

Figure 5.16: Control system general overview (V_{bus} and V_{sc} control)

Testing in the switched model

For the final validations in simulation, a new Simulink® is generated using the previous ones as a template. It can be observed in Figure 5.17.

The main difference lies in the inclusion of the V_{sc} control block (see Figure 5.18), connected alongside the V_{bus} control block to the red block (see Figure 5.19), which takes the two references and makes a trade-off between them, providing to the currents control block the references for i_2 and i_3.

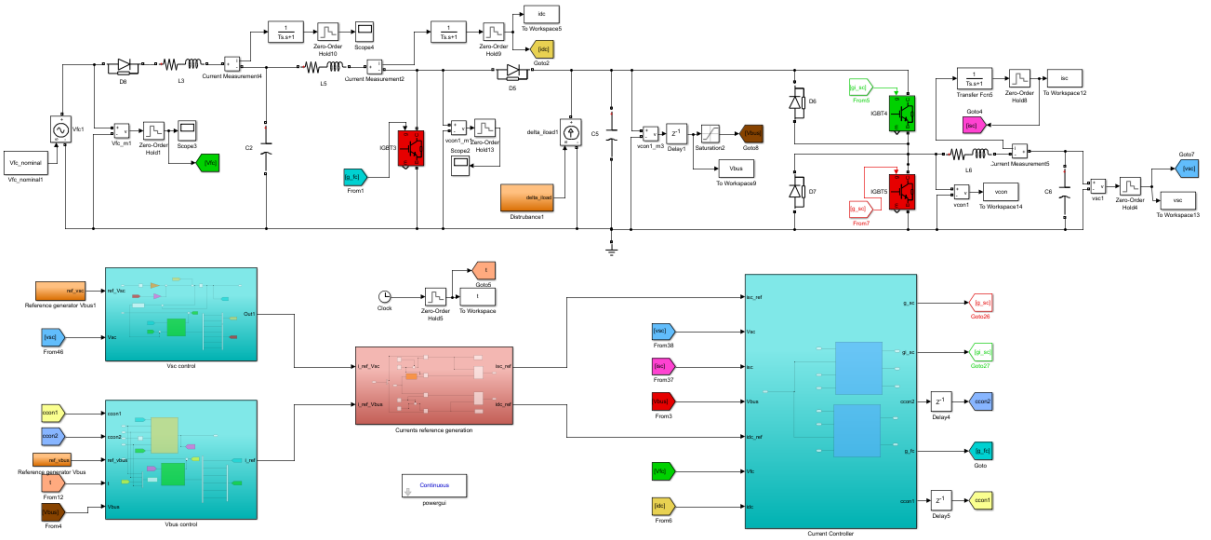

Figure 5.17: Simulink® model of the complete control structure

The utilization of a saturation with its corresponding anti-windup structure (in this case, instead of employing a gain to implement it, the own state-space model employed to design the control system has been used. This increases the complexitiy but assures stability) can be appreciated in Figure 5.18). It is necessary to avoid that the V_{sc} control interferes too much with the V_{bus} control.

For the first experiment, the setpoint for V_{bus} is again the one presented at Table 5.1, and the initial ramp is also employed. The disturbance profile is also the last utilized: a disturbance of 1 A enters the system at $t = 0.5s$ and it stops at $t = 0.7s$. Moreover, from $t = 0s$ to $t = 1s$, the parameter α is set to 0.8, giving much more importance to the V_{bus} control for the first stage of the experiment.

For the second stage, when the V_{sc} control is tested, α is set to 0.5; and the reference for the voltage at the supercapacitors follows a constant profile of 35.05 V (a initial value of 34.95 V is given to the capacitor for the tests).

Before presenting the results, it is important to comment that despite the supercapacitors capacitance value is $C_{sc} = 165F$, for these tests, its value has been set to $20F$, because the huge capacitance value of the real supercapacitors make the change of its voltage value incredibly slow, forcing to run a quite long simulation. In this way, by using a lower capacitance value, the effects of the V_{sc} control will be clearer.

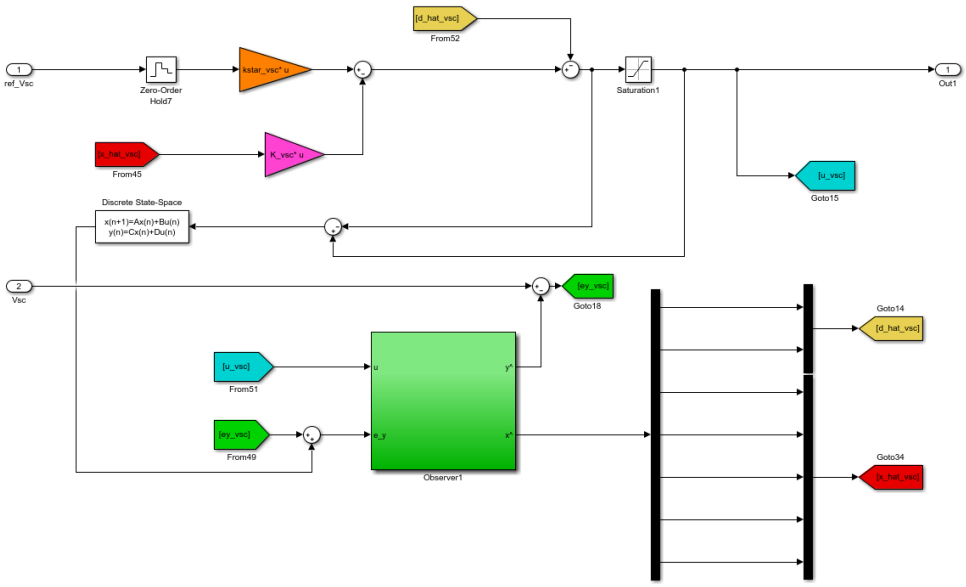

Figure 5.18: V_{sc} control subsystem

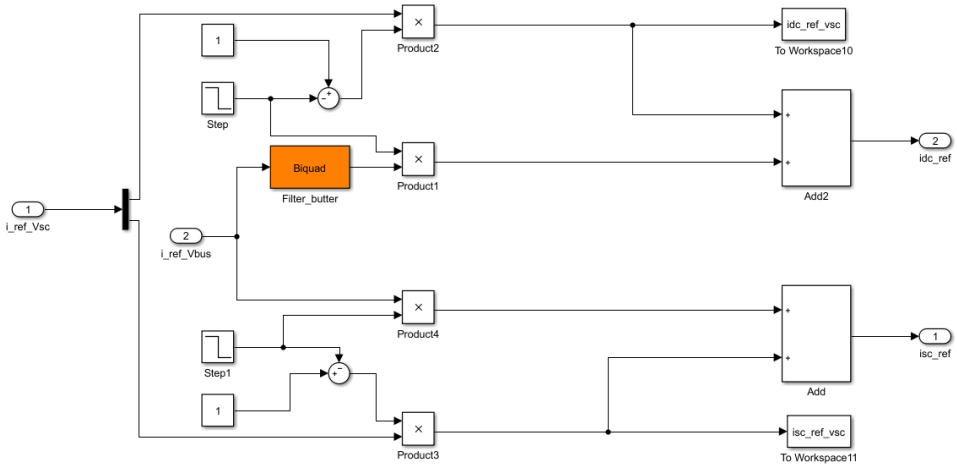

Figure 5.19: Reference signal distrubution subsystem

The results of the presented experiment can be found at Figure 5.20 for the V_{sc},Figure 5.21 for the V_{bus} evolution, and at Figures 5.22 for i_2 and 5.23 for i_3.

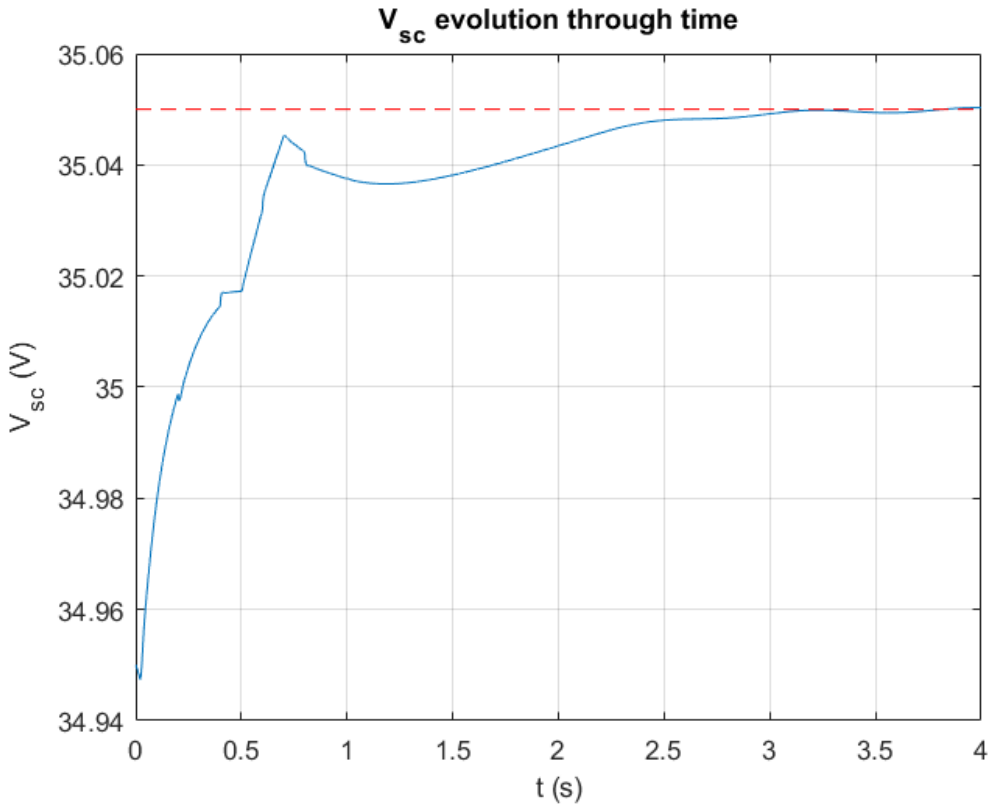

Figure 5.20: Evolution of V_{sc}

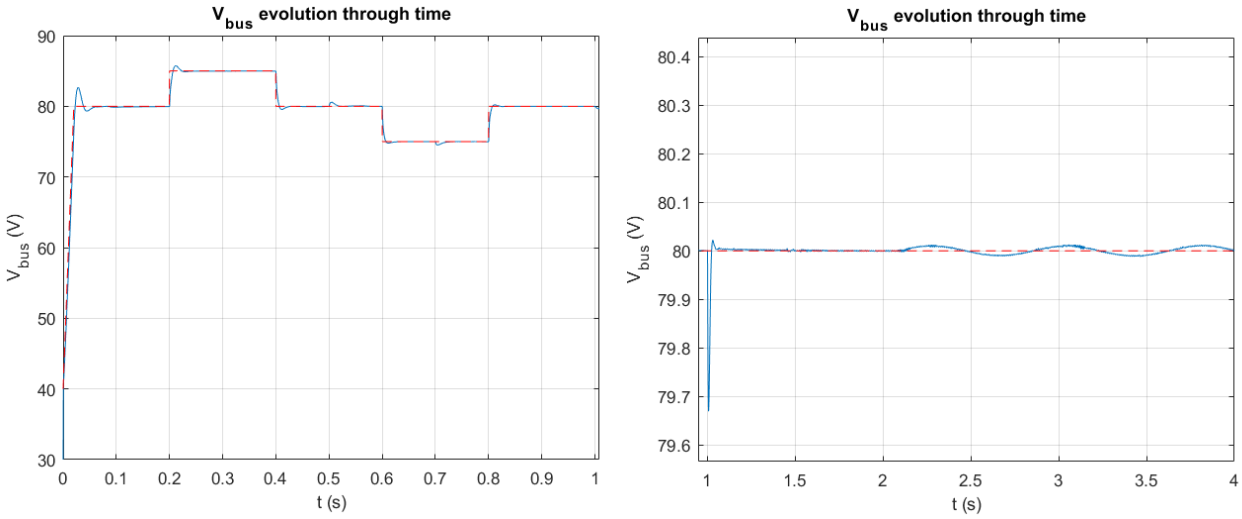

Figure 5.21: Evolution of V_{bus}

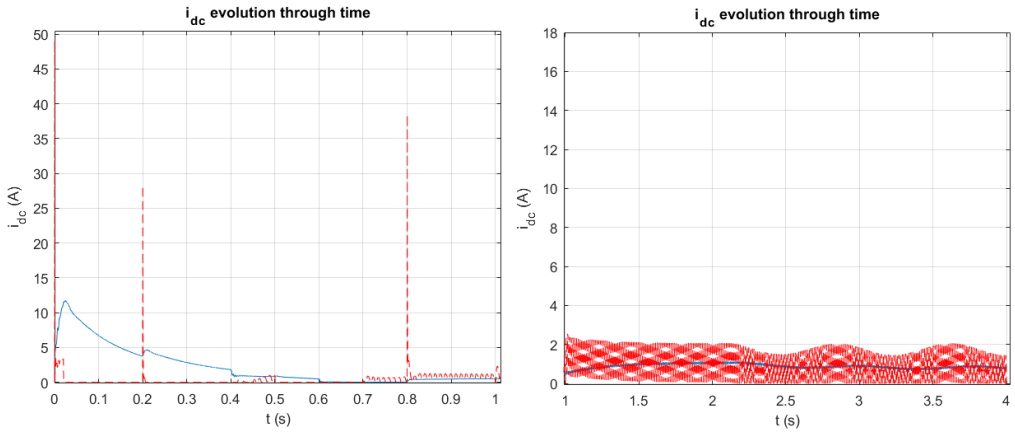

Figure 5.22: Evolution of i_2

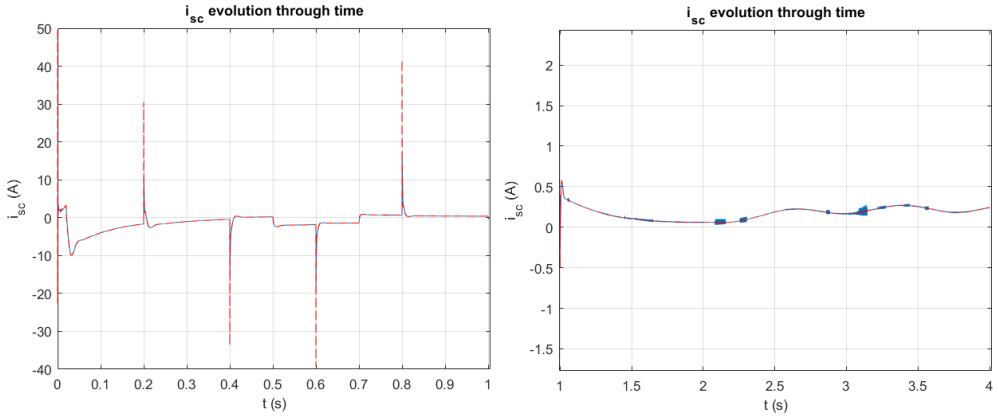

Figure 5.23: Evolution of i_3

5.3 In Closing

With these experiments, the developed control structure has been tested in simulation, giving quite good results.

The performance in the control of the bus voltage is really precise, tracking the reference with ease and rejecting the disturbances without problems.

Moreover, the supercapacitors voltage is also regulated so that its value tracks the given setpoint. The aforementioned trade-off is present, and it can be changed by modifying the parameter α.

Hence, all the main and secondary control aims have been accomplished, and the control system has been validated, at least in simulation. The real implementation can be found in Chapter 6.

Chapter 6

Implementation

Once the control system design has been validated in simulation, it has to be tested in the real system in order to be sure that all the structure is working as it should.
Going from simulation to implementation tends to be a complex task, due to the intrinsic difficulties that arise when dealing with physical systems.
To carry out the control of the plant in the real world (described in Chapter 2 - Section 2.1), which is located at IRI, a device called cRIO-9035 [4] is employed.
It is an embedded controller for control and monitoring tasks, which has a FPGA (Xilinx® [15] Kintex-770T concretely) and a real-time processor. These two elements confer the cRIO an incredibly wide range of possibilities when facing a control problem.

6.1 FPGA programming

For our application, the FPGA is going to be programmed to be in charge of the management of the control loops, due to its parallel processing capabilities and its high processing speed.
The Xilinx® FPGAs are programmed using bitstreams normally generated using their propetary software, creating programs in a language called VHDL (there are other possibilities as Verilog). The VHDL is a hardware programming language, that is, when generating codes with it, the program consist in a direct management of hardware resources, and the programmation is made bit to bit. For the FPGAs of the Kintex family, the recommended software is Vivado Design Suite [14].
In this case, as the cRIO is a National Instruments hardware product, it is prepared to work with their propetary software LabView® [9], which allows to introduce programs into the FPGA

without the necessity of coding in VHDL: it convert the Labview® code to HDL and to the bitstream file.

To carry out this programming, several possibilities have been covered.

6.1.1 VHDL generation from MATLAB®

MATLAB® and XilinxMATLAB® have worked together for years to offer their users a wide range of tools to complement the ones of the other, and have optimized the cooperation among their softwares.

Regarding the use of Vivado®, for the MATLAB® version R2016b, it must be used the 2017.4 version. In this case, through the tool *System Generator 2017.4*, Simulink® blocks can be directly converted to VHDL code (if they meet some requirements).

It is also necessary to take into account that the FPGA is working with fixed-point [34] operations, so the MATLAB® *Fixed-Point Tool* is previously employed.

This possibility is the most attractive due to the option of creating an IP block in LabView where the HDL code is introduced, and that carries out all the controller functions without the necessity of programming them again.

HDL Workflow Advisor

The HDL Workflow Advisor [10] is a MATLAB® tool which allows to produce VHDL projects from designs by employing a HDL installed software.

By following several steps that define the project properties, the Simulink® block is converted to HDL code and even to a bitstream file that can be directly introduced into de FPGA.

This method was one of the first attempts to produce the necessary HDL code, but its connection to LabView was not possible due to problems with the software versions and the OS.

Xilinx® Blockset for Simulink®

It is a group of blocks created by Xilinx®, so that by creating Simulink® models with these blocks, and using an extra element called *System Generator Block*, the VHDL code and the project containing it could be generated without the utilization of the HDL Workflow Advisor.

It was also tested, but the same problem arose, making clear that the problem was located in the LabView IP block, used to introduce external VHDL programs.

6.1.2 VHDL generation from LabView®

Once the previous possibilities were discarded, the control structure was directly programmed employing LabView®.

Programming in the local host

At first, the control loops for i_2, i_3 and V_{bus} were coded (the V_{sc} control was not translated into LabView® due to time constraints) in the local host, in order to assure the LabView® codification was right before testing it into the real plant.
The resultant schemes are the ones present at Figures 6.1, 6.2 and 6.3.

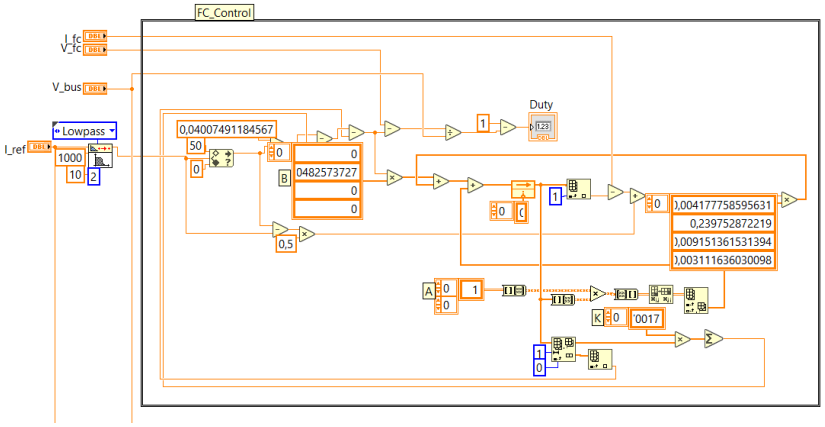

Figure 6.1: LabView® program for the control of i_2 - Local host

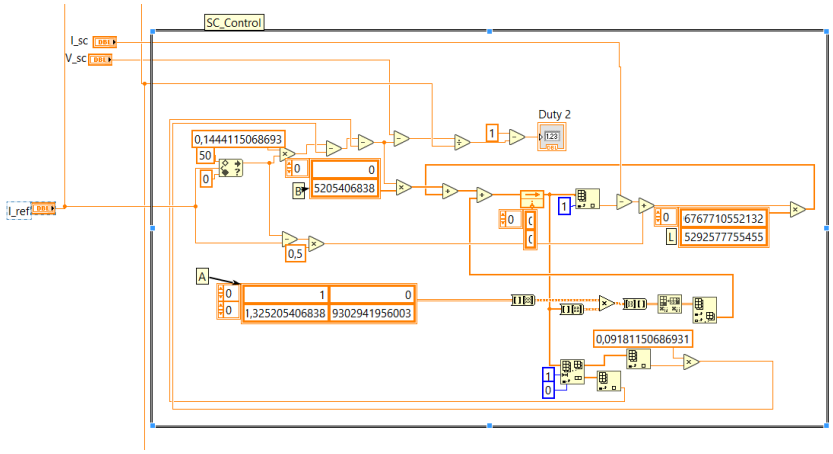

Figure 6.2: LabView® program for the control of i_3 - Local host

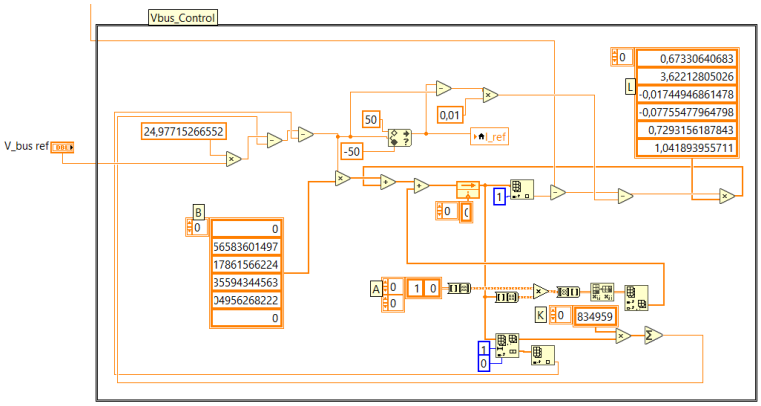

Figure 6.3: LabView® program for the control of V_{bus} - Local host

They were tested separately (there was no model to test the controllers in LabView®) by means of the following methodology: giving changes to the difference between the reference and the measures value, the controller, if it is properly working, must try to compensate this difference by changing the value of the duty cycle. These tests were satisfactory in a qualitative way, which was our aim for these experiments, so the next step was started.

Programming into the FPGA

The previous control structures were adapted to be implemented into the FPGA, being the biggest problem the use of matrices and the multiplications among them: despite the LabView® block libraries offer a matrix multiplication function [3], its usage is not clear; so many problems were faced using the provided block. Hence, the matrix multiplication was directly programmed using common LabView® blocks (summations, scalar multiplications and a switch case structure inside a for loop to go through the matrix).

Apart from that, it was also necessary to convert the data types of all the operations and connections to suitable ones, due to the use of fixed-point operations in the FPGA being more efficient. The selection of the fixed-point representation for every node in the scheme was based on the maximum and minimum values that those nodes reach in a Simulink® simulation of the controlled system.

As LabView® is a user friendly software, it allows to create interfaces quite similar to a SCADAs [16]. To implement the controllers here presented, a previous program from other tests was reused, employing its user interface (see Figure 6.4).

Figure 6.4: LabView® User Interface for the tests

Once the utilized environment has been presented, the different experiments that were carried out must be explained. For this demonstrations, instead of employing the actual PEMFC (it was not recommendable to use it with a control that, at that moment, was not tested), a voltage source was utilized. Also there was the possibility of including a source/sink to test the rejection of the disturbances, so that they can emulate inlet and outlet currents.

Regarding the control structure, the final one tested in simulation is not implemented here, due to the presence of the LPV technique highly increasing the complexity of this implementation. It is also important to remark that the control parameters were recalculated because the capacitance of the bus capacitor in the real plant is 4.92 mF.

- For the test of the i_2 control, the structure was implemented as shown in Figure 6.5. Two changes were made to the control structure designed in simulation:
  - The low-pass filter cut-off frequency was modified from its original value to 1 Hz, due to the previous successful utilization of the last for other similar control systems.
  - A saturation for the duty cycle was added (in simulation, it was included in the block that generates the PWM signal), with its corresponding anti-windup structure, to avoid the duty cycle reaching unfeasible values.

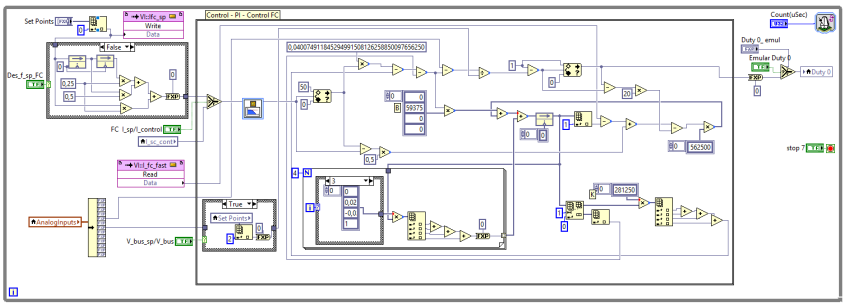

Figure 6.5: LabView® program for the control of i_2 - FPGA

The experiment is presented at Figure 6.6. The red line is the output of i_2. At first, the setpoint value was progressively increased in several steps, until reaching an approximate value of 8 A. For these values, a oscillation in the signal is present, but the control system is able to manage it. Then the setpoint is set to 0 A, and finally to 5 A. The final value can be appreciated in the blue box.

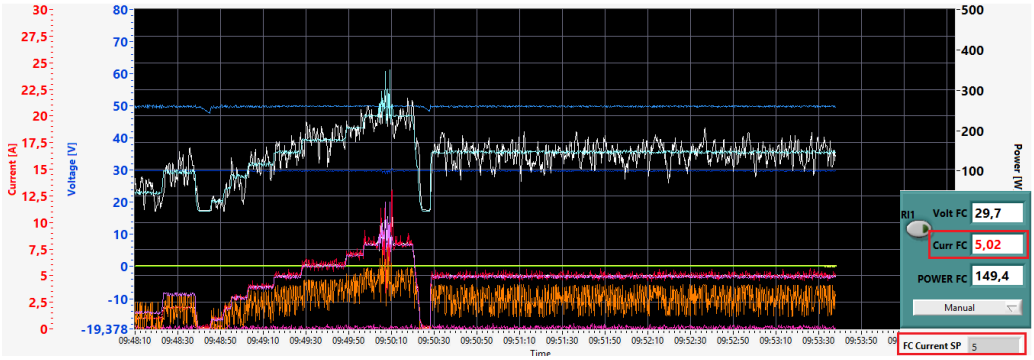

Figure 6.6: Control experiment results - i_2

From these results, it is concluded that the i_2 control has been properly designed as it is capable of tracking the provided reference, though it can be improved

- Then, the i_3 control was implemented, giving room to the scheme presented ar Figure 6.7.

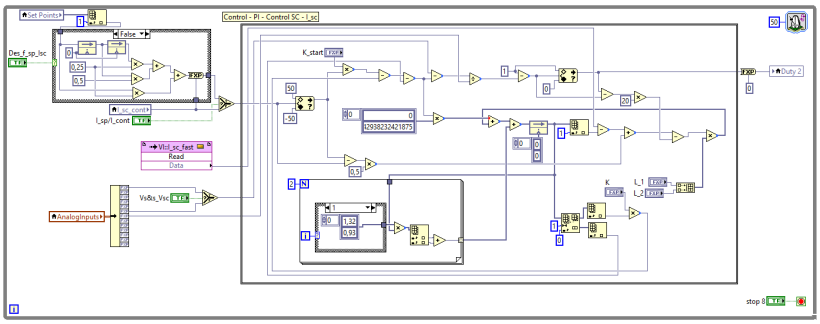

Figure 6.7: LabView® program for the control of i_3 - FPGA

Again, the saturation (and the associated anti-windup) were added to the original design, as it can be appreciated.

At first, the previous i_2 control and this one were tested working simultaneously. However, it did not provide good results due to a hardware problem: as for these tests the voltage at the bus was not controlled but set directly using a source, the one which was used for this task does not have the sufficient stability in the given voltage value. As both current control structures employ the V_{bus} value to make the calculations, the tests did not provide proper results.

Therefore, the hardware settings were changed so that instead of using the aforementioned source to generate V_{bus}, the one previously utilized to supply i_2 was the source employed to generate the bus voltage in this case, testing only if the control of i_3 was functioning in a proper manner. Therefore, for this experiment, i_2 was not tested.

The results are presented in Figure 6.8. The reference of i_3 was first set to zero for a while, starting then to increase its value little by little. The setpoint was set suddenly to zero again, providing this time decreasing values, to end setting zero as reference again.

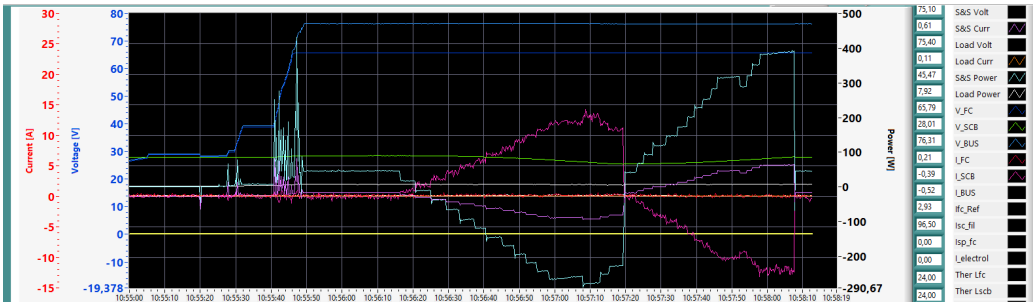

Figure 6.8: Control experiment results - i_3

It can be seen how the supercapacitors current is tracking the reference, but it is not providing a totally constant and stable value. Hence, to test its validity, the experiment was redesigned: the bus voltage, instead of being provided by the source, was controlled using a PI structure from a previous project, which generates the setpoint profile for i_3. As the supercapacitors were already charged, the test in this experiment was to check if the control system of i_3 was able to use the references supplied by the PI V_{bus} control to maintain this voltage.

The results of the experiment can be seen in Figure 6.9. The bus voltage is the light blue line, as remarked in the legend at the right, while the pink one is the supercapacitors current. The V_{bus} reference is set to 70 V, but first there exists a ramp to reach this value.

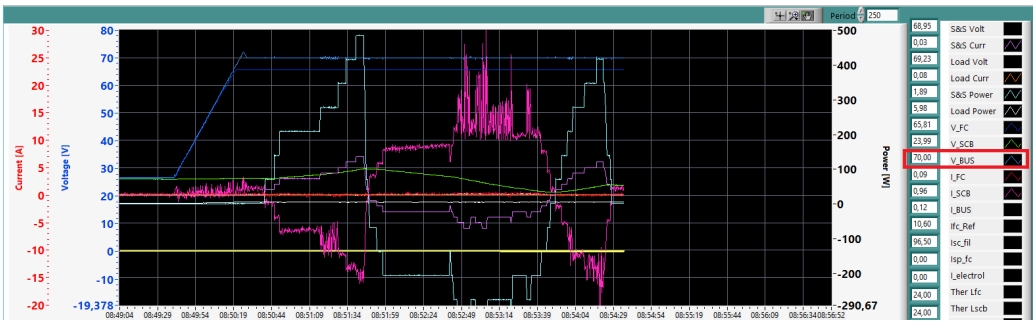

Figure 6.9: Control experiment results - i_3 with PI V_{bus} control

It is concluded that the control structure is working despite it has excessive oscillations when surpassing certain values. The changes in the value of i_3 are provoked by the inclusion of external current disturbances, first introducing current at the bus, and then demanding it. It is observed how the i_3 control system manages to charged the supercapacitors with the extra introduced current at first, and then it makes these supercapacitors supply the demanded current to the bus. Due to this desirable behaviour, it is appreciated how the V_{bus} is perfectly controlled and it is not affected by the disturbances.

- Once both current control structures had been tested, it was necessary to check the properness of the designed V_{bus} control. A saturation for the minimum and maximum current references generated by this control was included (alongside the required anti-windup structure). The programmed control is presented at Figure 6.10.

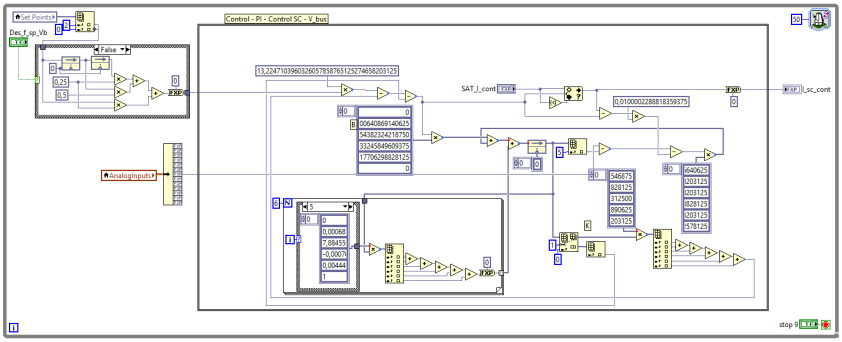

Figure 6.10: LabView® program for the control of V_{bus} - FPGA

This scheme substituted the previously employed one using PIs, so that for this experiment all the control structures were designed in this project. However, the i_2 control was not employed again: this experiment was to test if the designed V_{bus} control could manage to perform as the previously used one.

The result at the LabView® user interface can be appreciated in Figure 6.11. The reference value for this experiment is 75 V.

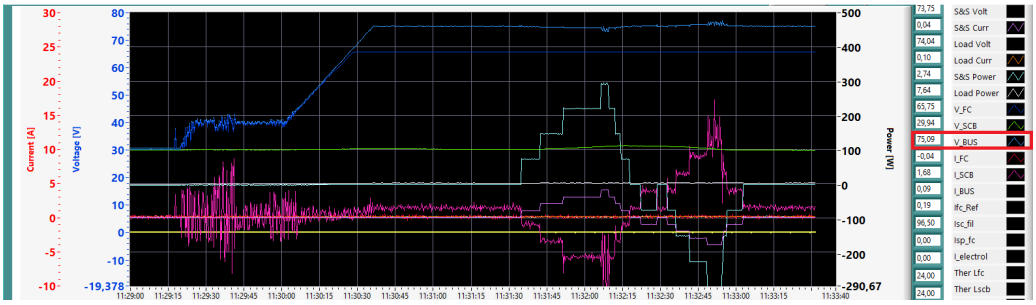

Figure 6.11: Control experiment results - V_{bus}

For low values of the bus voltage, the control system does not perform as well as for the normal or nominal values of V_{bus}. It can be appreciated how the control system is capable of tracking the reference and even reject the disturbances, although this last functionality is not perfect.

- To connect the previous results, all the previous individually tested controllers were implemented together, working simultaneously to manage the whole system maintaining the bus voltage constant to the setpoint value.

The experiment development is presented in Figure 6.12.

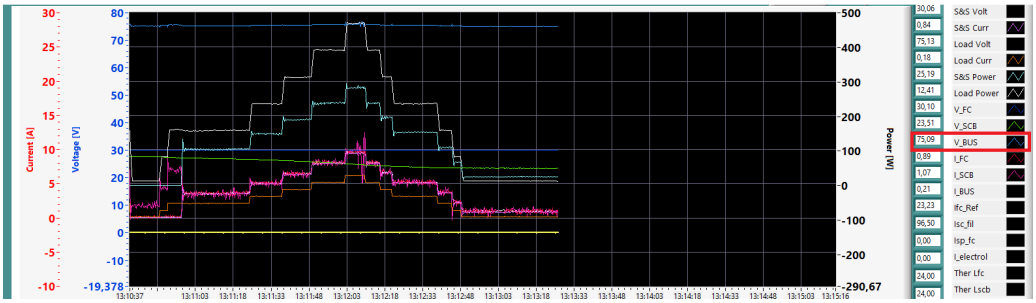

Figure 6.12: Control experiment results - V_{bus} managed by i_2 and i_3

It is concluded that the control structure is properly designed, due to it being able to provide a quite constant value of V_{bus} while rejecting the inlet and outlet currents to the bus. However, and opposite to what happened in simulation, the system response to the given references of current consists in using the PEMFC and SC currents in the same way, so the requirement of making the PEMFC work at low frequencies, using the supercapacitors to compensate fast changes of current in the bus, is not fulfilled.

- Finally, some changes were introduced in the last implemented control system in order to achieve the desired behaviour: the difference between the reference signal before and after being filtered was computed, becoming the setpoint for the supercapacitors current. The programs were changed as it can be observed in Figure 6.13 for i_2 and Figure 6.14 for i_3.

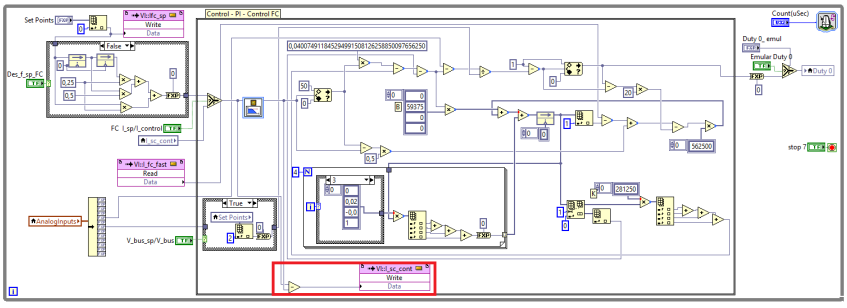

Figure 6.13: LabView® programs for the control of i_2 - second design

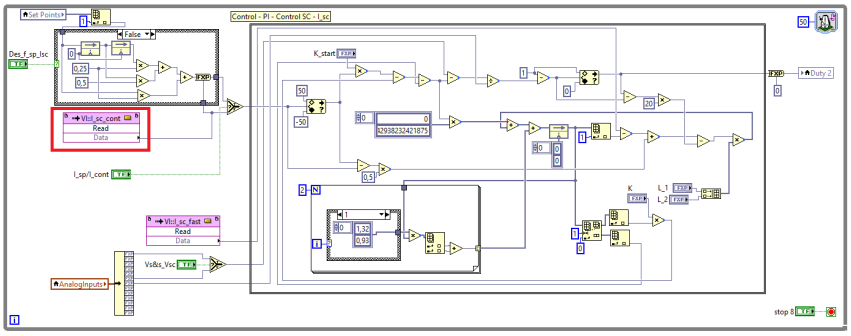

Figure 6.14: LabView® programs for the control of i_3 - second design

By using these new control structures, the results are the ones presented in Figure **??**

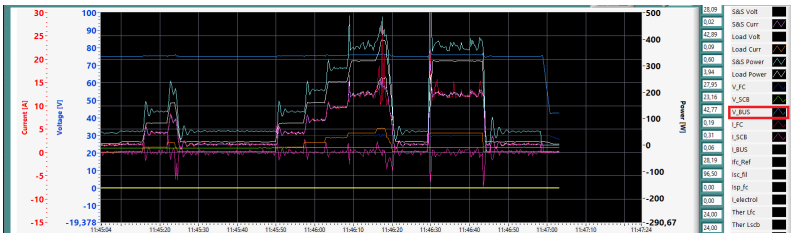

Figure 6.15: Control experiment results - V_{bus} managed by i_2 and i_3 - second design

The bus voltage (blue line at 75 V which is the setpoint) remains constant and the control system is able to reject efficiently the disturbances without making it oscillate, reaching a better result than before. The i_2 current is the red line, while the i_3 is the pink one near the zero. There is a detail of their evolution at Figure 6.16.

It can be observed how for the first three disturbances, the PEMFC current is providing the necessary energy regarding slow changes or low frequencies, while the supercapacitors compensate the fast changes by storing the excess of current. When reaching a certain value of current disturbance, the filter is not enough to make the distribution of the dynamics at the reference and the PEMFC sees some fast changes at i_2. However, it is remarkable how when drastically reducing the disturbance, so there is necessity of current at the bus, the supercapacitors are able to provide it (negative value of i_3) so that the PEMFC current decreases smoothly.

Therefore, the requirement that was not previously accomplished has been fulfilled by employing this structure, reaching an excellent result in the control of the bus voltage.

Moreover, the manner in which the currents control is managed allows to reduce fast changes in the required current at the PEMFC, so there is much less degradation and corrosion due to these fast dynamics.

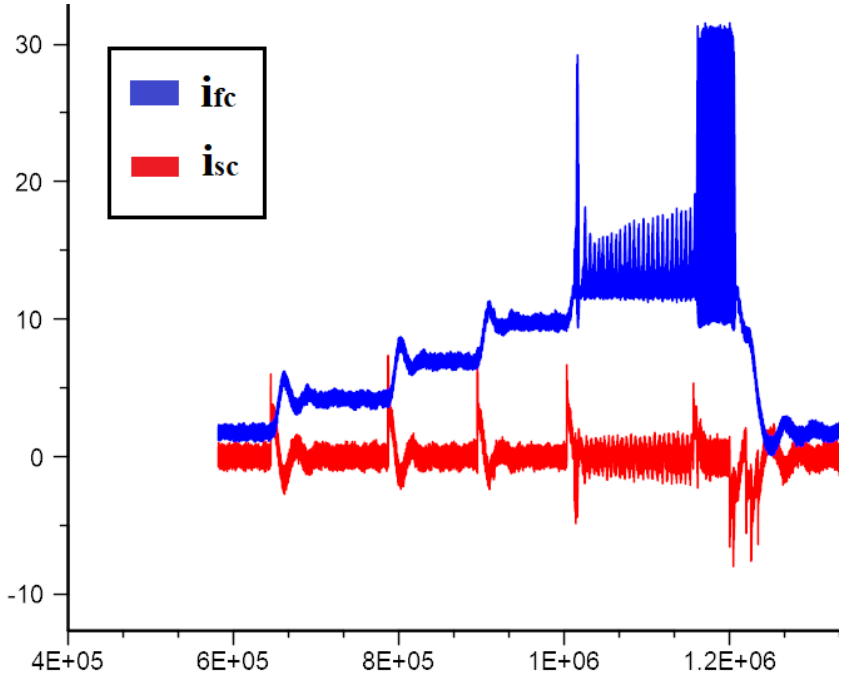

Figure 6.16: Control experiment results - Detail of i_2 and i_3 - second design

Chapter 7

Planning and scheduling

In this chapter, all the previous contents are chronologically distributed, as well as the developed activities for the composition of this project are enumerated and briefly described.

7.1 Activities related with the project execution

7.1.1 Related information and projects search

During the first week approximately (January 29th - February 4 th), the main task consisted in the search and study of information regarding the field of the project, in order to get some insights about how to deal with the different elements of the work to carry out.
The main focus of this research phase was at [28], [38] and [27], due to their previous work in the PEMFCs field.

7.1.2 Control design and simulation

This stage was the largest in the project, due to the inherent difficulty of the design of advanced control systems.

Controller design for the PEMFC and SC subsystems

The analysis of the physical systems and their dynamical equations, as well as the design and validation by simulation of the controllers for these subsystems lasted around four weeks (February 5 th - March 5th).

There were some difficulties during the process, related to the concepts explained at their respective chapters: necessary variable changes, selection of a proper discretization approach, difficulties arising during the simulation with the switched model...

Controller design for the bus voltage management

Due to an increase in the theoretical and mathematical complexity at this step (it can be appreciated along the corresponding chapter), it was one of the longest parts of the project covering approximately seven weeks March 6th - April 22 nd).
Indeed, this period includes the development of the control system from scratch to the moment it was functional and suitable, although it was constantly improved and tested until the end of the project, due to its high importance.

Controller design for the supercapacitors voltage management

Once the bus voltage controller was designed and validated, the process for generating a complementary control structure that allows to manage the voltage of the supercapacitors was started, and this stage lasted around five weeks (April 22 nd - May 27 th), although this control system design was not the only task carried out during this period but the main.

7.1.3 Implementation

The implementation of the control system lasted from May 28th to the end of the project, alongside other different tasks that needed to be carried out.

7.2 Activities related with the project writing

Regarding the composition of this document, it started at the stage of "Controller design for the bus controller", due to the necessity of developing the mathematical concepts for the models generation. All these demonstrations were written at first, and from this moment to the end of the project, the process of making this document was constant in time, intensifying at the final stages.

Chapter 8

Budget

8.1 Budget for the development of this project

During the process of making this project, considering it as a real engineering problem, there were some associated costs that are detailed below:

8.1.1 Human resources cost

Student

As an engineer developing a project (but regarding that I have not finished the Master degree yet), I will consider my position as junior engineer. From a research, the minimal salary of a junior engineer in a factory in Spain is 40.000 €/year, so converting it to salary per hour (considering 8 hours of work per day) it would be approximately 14 €/h.
About the number of hours, the associated amount of time for the number of credits of this project, 12, will be considered, despite surely this number of hours has been surpassed.
In that case, the total cost of the engineer for this project can be computed as follows:

$$Cost_{TOTAL_{Engineer}} = Salary_{byhour} \cdot Hours = 14€/h \cdot 360h = 5040€ \tag{8.1}$$

Supervisor

Due to the supervisor work helping and solving doubts about the project, this cost must be included in the budget.

Having a mean of two meetings every three weeks, lasting also a mean of one hour each one, and setting a cost per hour of 60 € due to his expertise in the field, the associated cost would be:

$$Cost_{TOTAL_{Supervisor}} = Salary_{byhour} \cdot Hours = 60€/h \cdot \frac{16weeks}{1.5hours/week} = 640€ \tag{8.2}$$

8.1.2 Materials costs

Regarding the different elements employed during the project that may be considered as costs, the following can be stood out:

Computer

The computer used to develop the whole project formatted just before starting it, and a new hard drive was installed. The folder where all the components of this Master thesis are stored occupies 1,61 GB.
About its value, the computer cost 1300 € and it was bought two years ago. Considering a lifetime of 5 years for the computer, and that the project has lasted around 4 months (1/3 of a year), it will lead to:

$$Cost_{TOTAL_{Computer}} = Price_{Computer} \cdot Usage_{years} \cdot \frac{1}{Lifetime_{Years}} = 1300€ \cdot \frac{1}{3}year \cdot \frac{1}{15years} = 86.67€ \tag{8.3}$$

Software

For this project, different softwares were employed:

- MATLAB®/Simulink®: the student version has a licensing cost of 85 €, and it lasts 1 year, but the project has lasted 4 months.
- Latex (TextStudio) and Vivado 2017.4 have not had a cost for this project.
- LabView® will not be considered because it was not only installed and used for this project.

Therefore, the total cost due to the softwares is:

$$Cost_{TOTAL_{Software}} = Price_{Year_{MATLAB®}} \cdot Usage_{years} = 85€/year \cdot \frac{1}{3}year = 28.33€ \tag{8.4}$$

8.1.3 Transport

The transporting costs will be considered, as the route between my residence and the university is covered by metro. Considering two journeys every three weeks, and taking into account the cost of a 10-trips ticket for the metro:

$$Cost_{TOTAL_{Transport}} = \frac{Cost_{10-trips}}{10} \cdot Trips_{byweek} \cdot Weeks_{duringtheproject} = \\ = 1.02€ \cdot 1.5 trips/week \cdot 16 weeks = 24.5€ \tag{8.5}$$

8.1.4 Energy

Neglecting costs like bulbs lights, the main focus of energy consumption for the project was the computer. As it was used approximately a 95% of the time, an estimation of 0.1 kW for the computer can be made, and the cost of the electrical energy is 0.1302 $\frac{€}{kWh}$, the total cost associated to the electricity would be:

$$Cost_{TOTAL_{Energy}} = Usage \cdot Energy_{consumption} \cdot Cost_{energy} = \\ = 0.95 \cdot 360h \cdot 0.1kW \cdot 0.1302 \frac{€}{kWh} = 4.45€ \tag{8.6}$$

Total cost

Adding all the previous terms (other minor costs as paper have been neglected), the result at Table 8.1 about the costs is obtained:

Concept	**Cost (€)**
Student	5040
Supervisor	640
Computer	86.67
Software	28.33
Transport	24.5
Energy	4.45
TOTAL	**5823.95**

Table 8.1: Budget to carry out the project

Chapter 9

Environmental impact

First, a brief description of the impact of the development of this project in the environment is carried out, to end the chapter remarking the environmental advantages of using hydrogen-based fuel cells for the generation of energy.

9.1 Environmental impact of the development of the project

Regarding the process to create this project from scratch, the main (although it can not be considered an important factor indeed) impact in environment might be the constant use of electrical energy to charge on the computer in which the project has been developed.
However, regarding other issues, the project can be considered to have a minimal impact on the environment:

- About the paper consumption, it has been negligible: it was only used for the mathematical developments, so at most, 20 pages of a notebook have been used. Even this notebook was an old one from a previous subject which still had some blank pages, so it was no necessary to get a new one.
- Regarding the transport, it was always managed using the metro or by walking, and never a private car, impacting minimally on the environment.

9.2 Environmental impact of the contents of the project

One of the most important parts of this project consists of using PEMFCs, which as an alternative source of energy helps to reduce the degree of pollution generated by the usage of oil-based energy

sources.

Despite they can have some contaminants, as fuel impurities like CO, CO_2, H_2S or NH_3 [21], in proportion to the total emission, for hydrogen-based fuel cells derived from renewable sources, it will be nothing but water vapour. Hence, there is a huge difference in the pollution generated by this source and the competence, regarding current possibilities.

The usage of fuel cells is highly recommendable for applications that need features like [35]:

- High power reliability, as computer or communication facilities, data processing centers...
- Reduced or non-existing polluting emissions: cars, buses, airports...
- Limited access to the electrical grid, as rural areas or zones where the maximum grid capacity is reached.
- Biological waste gases are available, like waste treatment plants.

Therefore, the proper control of the driving system of this PEMFCs is extremely important, extending the lifetime of the fuel cells and reducing possible contaminants derived from a wrong or poor use of them.

Conclusions

Once the content of the project has been covered, it is important to summarise its main points, extracting conclusions about the work done, the obtained results...
To end, some general conclusions about the project development and aims accomplishment are presented.

9.3 Currents control design and validation

Regarding the PEMFC and SC subsystems separately, the initial goal was completely accomplished: for both plants, a proper control design was developed to manage the currents that enter the DC-DC converters, tracking the provided references without steady-state errors, good performance and rejecting possible disturbances. This control systems were even prepared to work without problems if the system electrical parameters values were different from the nominal ones but inside a defined range.

9.4 DC bus voltage control design and validation

About the voltage V_{bus}, a new control structure was developed to make the most of the ones designed for the currents, that is, by supplying setpoints for the bus voltage, this controller converts the given value into a reference for the previously defined control structures for the currents at the PEMFC side and the supercapacitors side.
Advanced control techniques were employed for this design, being the most important one the Linear Varying Parameters, improving the capabilities of this controller and avoiding the issues that arise from the non-linearities present at the dynamical equation which models the behaviour at the bus.
Again, fantastic results for the performance of the control system were achieved, tracking setpoints and minimizing the effects of external current flows on the bus voltage value.

9.5 Supercapacitors voltage control design and validation

To complete the previous control structure, the last step was to include a way of managing the voltage at the supercapacitors. This is a quite important stage, because for most of the applications, the usage of these capacitors stored energy instead of the PEMFC one, at concrete moments of the system functioning, will decrease the fuel cell fast changes of demanded current and will make its durability grow.
Hence, a complementary control structure was developed to control this voltage value while also managing V_{bus}, by means of a trade-off between the two control objectives.
The validation of the complete system was quite successful, giving room to a control structure capable of handling the simultaneous management of the required electrical variables with a great performance.

9.6 Implementation in the real plant

For the last step of this project, a more limited but complete version of the control system (without LPV and without the V_{sc} control) was converted from Simulink® (the simulation environment) to LabView® (the implementation environment). Using the last, the control structure can be programmed by means of blocks like in Simulink® , but it can also be translated into a bitstream that is finally programmed into a FPGA.
From the results for this stage (presented at Chapter 6), it can be concluded that the designed control structure is suitable and fulfils the requirements imposed at the beginning of the project: achieving a constant value of bus voltage (tracking the setpoint) and rejecting the possible inlet and outlet current disturbances that enter the bus.

9.7 General conclusions

In closing, and taking into account the overall developed work and achieved results, I consider this project has reached most of the initial objective, providing suitable and interesting solution to the problems that have been arising during its realization.
It studies a different approach to the control of hybrid energy stations management systems, while being useful to open future lines of work.

Acknowledgements

I want to express my acknowledgements to all the people that have helped me to make this project possible.

First, to my family, which support me unquestioningly, bear my complaints and celebrate my successes. In my best and worst moments, they are always there for me, and despite the distance, I keep them in my mind and my heart everyday.

Second, to the people that has directly helped me to develop this project. To Ramón Costa, my mentor, whose wisdom, dedication and patience are worthy of all my respect, being the maximum responsible of the good result I think this project consists in. Besides, to Vicente Roda, responsible of the Fuel Cells Laboratory technical area, whose help on the implementation stage has been incredible, making possible to test the controllers in the real plant in such a little amount of time. It would have been impossible without him.

Finally, to the IRI, because the plant employed for the implementation is their property, to the UPC, and to all the teachers I have had the pleasure to be a student of. In my opinion, their work and effort to instil knowledge in us is not appreciated enough.

Bibliography

[1] Anti-windup - Feedback Control Systems - MIT. https://ocw.mit.edu/courses/aeronautics-and-astronautics/16-30-feedback-control-systems-fall-2010/lecture-notes/MIT16_30F10_lec23.pdf.

[2] Butterworth Filter Design. https://www.electronics-tutorials.ws/filter/filter_8.html.

[3] Configuring the Matrix Size and Interface of the Linear Algebra Matrix Multiply Function (FPGA Module). http://zone.ni.com/reference/en-XX/help/371599J-01/lvfpgaconcepts/linearalgebra_configure_mm/.

[4] cRIO-9035 Official Web Page - National Instruments. http://www.ni.com/es-es/support/model.crio-9035.html.

[5] Design of Digital Filters. https://web.eecs.umich.edu/~fessler/course/451/l/pdf/c8.pdf.

[6] *balred* - MathWorks® Help. https://es.mathworks.com/help/control/ref/balred.html.

[7] Hankel Optimal Model Reduction - MIT. http://web.mit.edu/6.242/www/images/lec10_6242_2004.pdf.

[8] Introduction to Filter Design - MathWorks®. https://es.mathworks.com/help/signal/examples/introduction-to-filter-designer.html.

[9] LabView® Official Web Page - National Instruments. http://www.ni.com/es-es/shop/labview.html.

[10] MATLAB® HDL Workflow Advisor Tutorial. https://es.mathworks.com/help/hdlcoder/examples/basic-hdl-code-generation-with-the-workflow-advisor.html.

[11] SeDuMi Web Site. http://sedumi.ie.lehigh.edu/.

[12] Simscape - MathWorks® Help. https://es.mathworks.com/help/physmod/simscape/.

[13] State Observers and State Feedback - Electrical Engineering and Computer Science course. https://ocw.mit.edu/courses/electrical-engineering-and-computer-science/6-011-introduction-to-communication-control-and-signal-processing-spring-2010/readings/MIT6_011S10_chap06.pdf.

[14] Vivado® Design Suite - Xilinx®. https://www.xilinx.com/products/design-tools/vivado.html.

[15] Xilinx® Official Web Page. https://www.xilinx.com/.

[16] SCADA: SUPERVISORY CONTROL AND DATA ACQUISITION. *International Journal Of Engineering And Computer Science* (2014).

[17] Albarbar, A., and Alrweq, M. *Proton Exchange Membrane Fuel Cells*. 2018.

[18] BALLARD. *Nexa^{TM} Power Module's User Manual*, 2005.

[19] Boyd, S., El-Ghaoui, L., Feron, E., and Balakrishnan, V. *Linear Matrix Inequalities in System and Control Theory*. 1994, ch. 1.

[20] Chapman, S. *Electric Machinery Fundamentals*. 2001, pp. 189–195.

[21] Chen, X., and Shi, Z. A review of PEM hydrogen fuel cell contamination: Impacts, mechanisms, and mitigation.

[22] Daud, W., Rosli, R., Majlan, E., Hamid, S., and Mohamed, R. PEM fuell cell system control: A review.

[23] Duan, G.-R., and Yu, H.-H. *LMIs in Control Systems*. 2013.

[24] Löfberg, J. YALMIP : A toolbox for modelling and optimization in MATLAB.

[25] M. S. Dresselhaus, I. L. T. Alternative energy technologies.

[26] Moore, B. C. Principal Component Analysis in Linear Systems: Controllability, Observability, and Model Reduction.

[27] Moré, J. J. *Advanced control strategies for non-linear systems. Application to the control of Hybrid systems of energy generation based on fuel cells.* PhD thesis, 2014.

[28] Paredes, J. F. Control of an Hybrid Station for the energy management of a PFC based system, 2015.

[29] Rowell, D. State-Space Representation of LTI Systems. `http://web.mit.edu/2.14/www/Handouts/StateSpace.pdf`.

[30] SEMIKRON. *SEMISTACK - IGBT.*

[31] SEMIKRON. *SEMiX 251GD126HDs IGBT datasheet.*

[32] SEMIKRON. *SKHI 20opA datasheet.*

[33] Sename, O. Linear Parameter Varying systems: from modelling to control. `https://www.gipsa-lab.grenoble-inp.fr/~o.sename/docs/LPVcourse.pdf`.

[34] So, H. Fixed-Point Introduction. `http://www-inst.eecs.berkeley.edu/~cs61c/sp06/handout/fixedpt.html`.

[35] Stambouli, A. B., and Traversa, E. Fuel cells, an alternative to standard sources of energy.

[36] ström, K. J. A., and Murray, R. M. *Feedback Systems: An Introduction for Scientists and Engineers.* 2009, ch. 6.

[37] ström, K. J. A., and Murray, R. M. *Feedback Systems: An Introduction for Scientists and Engineers.* 2009, p. 207.

[38] Talpone, J. I. Development of a Hybrid System for energy generation based on PEM Fuel Cells and capacitors, 2014.

[39] Zeltkevic, M. Forward and Backward Euler Methods. `http://web.mit.edu/10.001/Web/Course_Notes/Differential_Equations_Notes/node3.html`.